EVALUATING SNO+ BACKGROUNDS THROUGH ^{222}RN ASSAYS AND THE SIMULATION OF ^{13}C$(\alpha, n)^{16}$O REACTIONS DURING WATER PHASE

by

Janet <u>Rumleskie</u>

A thesis submitted in partial fulfillment of the requirements for the degree of Master of Science (MSc) in Physics

The Faculty of Graduate Studies
Laurentian University
Sudbury, Ontario, Canada

THESIS DEFENCE COMMITTEE/COMITÉ DE SOUTENANCE DE THÈSE
Laurentian Université/Université Laurentienne
Faculty of Graduate Studies/Faculté des études supérieures

Title of Thesis
Titre de la thèse   EVALUATING SNO+ BACKGROUNDS THROUGH 222RN ASSAYS AND
                           THE SIMULATION OF 13C(_, n)16O REACTIONS DURING WATER PHASE

Name of Candidate
Nom du candidat   Rumleskie, Janet

Degree
Diplôme   Master of Science

Department/Program   Date of Defence
Département/Programme   Physics   Date de la soutenance October 14, 2015

APPROVED/APPROUVÉ

Thesis Examiners/Examinateurs de thèse:

Dr. Christine Kraus
(Supervisor/Directeur(trice) de thèse)

Dr. Richard Ford
(Committee member/Membre du comité)

Dr. Clarence Virtue
(Committee member/Membre du comité)

Approved for the Faculty of Graduate Studies
Approuvé pour la Faculté des études supérieures
Dr. David Lesbarrères
Monsieur David Lesbarrères

Dr. Gilles Gerbier   Acting Dean, Faculty of Graduate Studies
(External Examiner/Examinateur externe)   Doyen intérimaire, Faculté des études supérieures

ACCESSIBILITY CLAUSE AND PERMISSION TO USE

Abstract

SNO+ is a large multipurpose neutrino detector searching for rare interactions. Some backgrounds come from naturally occurring ^{222}Rn and its daughters within the ^{238}U chain. Under development are cryogenic trapping assay systems which will monitor the ^{222}Rn levels within scintillator, water, N$_2$ cover gas, and small detector materials. These systems can measure concentrations up to 8×10^{-5} Rn atoms/L (1.6×10^{-17} g ^{238}U/g LAB) within scintillator, and 4.75×10^{-15} g ^{238}U/g H$_2$O in water. The status of the assay systems are discussed within. ^{13}C(α,n)^{16}O reactions occur from ^{222}Rn's progeny ^{210}Po, but Monte Carlo simulations predict < 0.4 events within the SNO+ fiducial volume of 5.5 m and 5 - 9 MeV region of interest over a 9 month running period within water.

Keywords: SNO+, neutrino detection, radon assay, decay chain

Acknowledgements

I would first like to thank my supervisor, Dr. Christine Kraus, for her patience, guidance, and continuous support throughout my time at Laurentian University. She was always there to ensure I stayed on track with my thesis and created many opportunities for me to advance my professional career. I would like to thank Dr. Clarence Virtue and Dr. Richard Ford, both of whom were instrumental guiding forces with deep knowledge and expertise in their areas of research. I also thank Dr. Gilles Gerbier, for his presence during the final steps of my thesis.

Special thanks to Dr. Alex Wright, Dr. Valentina Lozza, and Dr. Eric Vazquez-Jauregui, for all the informative discussions, emails, and phone calls regarding my many projects. Thanks to all SNOLAB personnel, as their quick responses and support ensured my work was always moving forward. I am sincerely thankful to everyone I've worked shifts with underground, there are too many names to mention but you know who you are - thank you for making service work fun. I thank all of the SNO+ collaborators, especially those at Laurentian University, for making me an integral part of the team. I would like to thank my fellow office mates Caitlyn Darrach, Colin Bruulsema, and Stéphane Venne, without whom it would have been an extremely dry and lonely two years.

I also thank my family, for their presence not only in these past two years, but throughout my entire life. Your unwavering love and support has always encouraged me to follow my dreams, even if it leads me far away from you. Sean Graham, I believe you know that last sentence applies to you too.

Contents

List of Figures

List of Tables

List of Abbreviations and Symbols

Ag	Silver
atm	Atmospheric pressure
AV	12 m diameter acrylic vessel
C-300	Gas-stripping (degasser) column
CP	Charge-parity
cpd	counts per day
DOS	Disk operating system
FV	Fiducial volume
GEANT4	GEometry ANd Tracking toolkit developed by CERN
GV	Gate valve
HCl	Hydrochloric acid
L	Lepton number, or Litre
LAB	Linear alkylbenzene (liquid organic scintillator)
LC	Lucas cell
LPM	Liters per minute
LS	Liquid scintillator (LAB+PPO)
MCA	Multichannel analyzer
MCB	Multichannel buffer
MDG	Monitor degasser
MeV	Mega-electronvolt (unit of energy/mass)
MSS	Metal scavengers
NTP	National Pipe Thread
OD	Outer diameter
P&ID	Piping and instrumentation diagram
PC	Personal computer
PDG	Process degasser
PMT	Photomultiplier tube
PPO	2,5-diphenyloxazole (wavelength shifter)
PSUP	17.5 m diameter PMT support structure
RAT	Reactor Analysis Tool (SNO+ Monte Carlo software)
ROI	Energy region of interest
ROOT	A modular scientific software toolkit
Rn	Radon
SB	Calibration source storage box
SRAS	Scintillator Radon Assay Skid
SOC	Start of counting
SN	Supernova
SNO	Sudbury Neutrino Observatory
SNO+	Successor experiment to SNO
STF	Surface transfer facility

Te	Tellurium
Te-LS	Tellurium and liquid scintillator cocktail
Th	Thorium
U	Uranium
UI	Universal interface
UPW	Ultrapure water
URM	Umbilical Retrieval Mechanism
UTF	Underground transfer facility
UVT	Ultraviolet transmitting
V	Volts
VCR	Variable compression ratio fittings
ZnS	Zinc sulfide
ZnS(Ag)	Zinc sulfide with silver activator (inorganic scintillator)
$\mathbf{0\nu\beta\beta}$	Neutrinoless double beta decay
$\mathbf{2\nu\beta\beta}$	Double beta decay

Chapter 1

Introduction

1.1   Historical Introduction to Neutrinos

On December 4, 1930, a famous letter was read to the attendees at the Gauverein meeting in Tübingen, Germany. Written by Wolfgang Pauli, who himself was too busy to attend the conference, the letter described a desperate "remedy" to explain the missing energy from beta decays. The remedy was a particle Pauli called the "neutron", which would have spin 1/2 and mass "of the same order of magnitude as the electron mass" [1], such that it was carrying away the unmeasured energy. In his journal, Pauli apologizes for his suggestion, adding in that he had proposed a particle that cannot be detected, which is "something no theorist should ever do" [2].

While another particle was discovered in the meantime and subsequently called the neutron [3], Pauli's theory persevered. Renamed the "neutrino" for "little neutral one" by E. Fermi, the first published references to this particle were in the Proceedings of the Solvay Conference on October 1933, when Fermi [4] and Perrin [5] both independently concluded that the neutrino could actually be massless. Beta decay processes were described by Fermi [6, 7], in which a nucleus of N neutrons and Z protons could undergo the following processes:

$$(N, Z) \rightarrow (N - 1, Z + 1) + e^- + \bar{\nu}_e \tag{1.1}$$

$$(N, Z) \rightarrow (N + 1, Z - 1) + e^+ + \nu_e \tag{1.2}$$

In 1935, a process called double beta decay $(2\nu\beta\beta)$ was suggested by Maria Goeppert-Mayer [8]:

$$(N, Z) \rightarrow (N - 2, Z + 2) + e^- + e^- + \bar{\nu}_e + \bar{\nu}_e \tag{1.3}$$
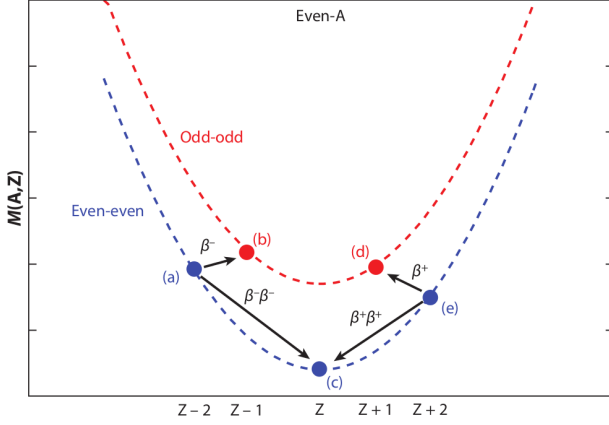
Figure 1.1: Mass parabola for isobaric nuclei with even atomic mass number A with Z protons, N neutrons [10]. Nuclear pair energy splits the diagram into two parabolas: (even, even) and (odd, odd). Single beta decay of some isotopes are forbidden (e.g. a to b) as the daughter energy level would be higher, but double beta decay is possible (e.g. a to c).

In opposition to single beta decay, the double beta decay process would be exceptionally rare, with a half-life on the order of 10^{17} years or longer. In this second order weak process, two electrons and two antineutrinos are emitted simultaneously along with the conversion of a nucleus of N neutrons and Z protons into a lighter nucleus with N-2, Z+2. This second order weak process can only occur with even-N, even-Z nuclei, and nature would provide an effective filter for this decay, since single beta decay (N-1, Z+1) for certain nuclei are forbidden due to the tight binding of the nuclear pairing force [8] (see Fig. 1.1). Thus, only about 3 dozen even-N, even-Z nuclei can undergo the double beta process, without the interference of single beta decay [9].

Not long after, Racah introduced the theory of a neutrinoless double beta ($0\nu\beta\beta$) decay process [11], in which the same nuclear conversion occurs, except only two electrons are emitted with no antineutrinos. At this time, the neutrino carried no charge or other quantum "label" which changed sign under particle-antiparticle conjugation, so in theory it was possible that $\nu_e \equiv \bar{\nu}_e$. This was motivated by Ettore Majorana, who was made famous by his namesake equation, the Majorana equation, in which the solution is a neutral particle which is its own antiparticle [12]. Such a "Majorana particle" differs from a Dirac particle, which is distinct from its antiparticle counterpart.

Furry made calculations on the possibility of neutrinoless double beta decay [13], of which the process would be two step:

$$(N, Z) \rightarrow (N - 1, Z + 1) + e^- + \bar{\nu}_e \equiv (N - 1, Z + 1) + e^- + \nu_e \tag{1.4}$$

followed by

$$(N-1, Z+1) + e^- + \nu_e \rightarrow (N-2, Z+2) + e^- + e^- \tag{1.5}$$

In condensed form, it is simply written as:

$$(N, Z) \rightarrow (N-2, Z+2) + e^- + e^- \tag{1.6}$$

The neutrinoless double beta decay process requires transitionary states via single beta decay, which is energetically forbidden for these isotopes, causing the intermediate neutrinos to be be virtual [13]. Figures of the $2\nu\beta\beta$ and $0\nu\beta\beta$ processes are in Figure 1.8 in § 1.3 below, as additional theories must still be explained below.

Counter and tracking experiments in the late 1940's and 1950's established lower bounds on the process of neutrinoless double beta decay, brought about by theoretical calculations predicting half-lives of 6×10^{14} years if the neutrinos were Majorana and 10^{24} years if neutrinos were Dirac [14]. A half-life between 4×10^{15} and 9×10^{15} years was reported for the double beta decay of ^{124}Sn by Fireman in 1949 [15], but was later refuted by more sensitive experiments, and a particular study in 1951 recorded lifetimes up to 2.4×10^{17} years [16]. Geochemical experiments further excluded the process of neutrinoless double beta decay: studies of an ancient tellurium ore measured ^{130}Xe content, the product of ^{130}Te $2\nu\beta\beta$ decay, and concluded a total double beta decay lifetime of $>1.4\times10^{21}$ years for ^{130}Te [14]. Radiochemical studies also established a lower bound of 6×10^{18} years for ^{238}U, a study which searched for the product ^{238}Pu in uranium decay [17]. All of these long half-lives were considered evidence against the possibility of a Majorana neutrino.

A major nail in the coffin for the neutrinoless double beta decay process occurred in 1953, when lepton number (L) and its conservation was introduced to explain some missing decay modes [18]. Now, leptons with lepton number L = +1 are particles, while leptons with L = -1 are antiparticles. This made neutrinos distinct from antineutrinos, and as $0\nu\beta\beta$ would change L by two units (producing two leptons but no antileptons), it was obviously forbidden. Double beta decay remained possible, as the two leptons and two antileptons produced would ensure L was conserved.

Although Pauli himself told his audience that his particle could not be detected, physicists tried anyway. And on June 14, 1956, nearly 26 years after the particle had been proposed, Pauli received a telegram from Frederick Reines and Clyde Cowan. Reines and Cowan had been determined to detect the neutrino, initially planning to use a nuclear bomb as their neutrino source. Yet after careful consideration it became clear that close proximity to a nuclear reactor coupled with a detector capable of recognizing delayed coincidence signals would suffice. Even so, their first attempt at detecting neutrinos at the Hanford reactor was swamped by

background and led to inconclusive evidence [19]. Undeterred, they improved on background discrimination and built a detector 12 meters underground and 11 meters away from the reactor core of the Savannah River Plant in Aiken, South Carolina [20]. This new detector was composed of two thin tanks filled with 200 L of water loaded with 40 kg of cadmium chloride, and sandwiched between tanks of liquid scintillator which were viewed by 55 light detectors known as photomultiplier tubes (PMTs). The hydrogen in the water interacted with antineutrinos under inverse beta decay:

$$\bar{\nu}_e + p \rightarrow n + e^+ \tag{1.7}$$

The positron then annihilated with an existing electron, producing two 0.51 MeV photons to be detected in coincidence by the PMTs. The neutrons, meanwhile, would slow down and were captured by the cadmium, producing light a few microseconds after the positron annihilation. Once certain of their results, they sent a telegram to Pauli, which said, "We are happy to inform you that we have definitely detected neutrinos" [21].

One year later it was concluded that parity is maximally violated in weak interactions such as beta decay [22]. This is in direct contrast with the other forces (electromagnetism, strong interactions, and gravity), which all conserve parity to date. Parity violation is a breaking of symmetry which indicates nature requires a specific coordinate system (left- or right-handed) on a fundamental level. In this case, only left-handed components of particles and right-handed components of antiparticles can participate in weak interactions. Even if neutrinos were Majorana and lepton number violation possible, this means neutrinos could actually be distinguished by their handedness. In the case of neutrinoless double beta decay, the neutrino produced from the first step has the wrong handedness to be absorbed in the next step:

$$(N, Z) \rightarrow (N - 1, Z + 1) + e^- + \nu_e^{RH} \nrightarrow (N - 2, Z + 2) + e^- + e^- \tag{1.8}$$

The muon neutrino (ν_μ) was discovered in 1962 at Brookhaven National Laboratory (BNL) [23] when physicists determined that neutrinos from muon interactions were different than those involved in electron interactions. This led to an adjustment of lepton numbers so that each lepton family has a different number. Motivated by the existence of two different neutrinos, in 1967 Pontecorvo presented a theory on two-neutrino flavour oscillations [24], which wasn't fully developed until 1975-76 [25]. Such a theory required the flavour states (e.g. ν_e and ν_μ) to be a linear combination of so-called mass states, such that a probability existed for ν_e to oscillate into ν_μ. Yet neutrinos were still believed massless at this time.

The Glashow-Weinberg-Salam Standard Model also incorporated the Higgs mechanism in 1967, allowing gauge bosons to acquire longitudinal degrees of freedom and the ever important explanation of mass [26].

Figure 1.2: Most complete table of Standard Model elementary particles, including the recently discovered Higgs boson which provides mass to "massive" particles (except the neutrinos) [27].

Significant effort had been invested in attempting to reconcile the four known forces: electromagnetic, gravitational, strong, and weak. A gauge theory was developed that combines the electromagnetic and weak theories into one electroweak theory. The massive gauge bosons W^+, W^-, and Z^0 were proposed to explain the range of weak interactions, yet symmetry breaking was required to allow these bosons their mass, while leaving the photon massless. The scalar Higgs field allowed for this spontaneous symmetry breaking, and thus the Higgs boson was theorized to give particles their mass.

The Standard Model was tested by searching for weak neutral current interactions, and affirmed in 1973 when the Gargamelle detector at CERN observed events in which neutral particles (namely neutrinos) produced hadrons (particles composed of quarks and/or antiquarks) [28]. As the present theory suggested, neutrinos were considered massless and the Standard Model was developed without incorporating neutrino mass as a property. Meanwhile, studies of quarks and gluons led to theories of the strong force through quantum chromodynamics (QCD). Combining QCD with the electroweak theory leads to the Standard Model as understood today, although the fourth force, gravity, has yet to be incorporated. Figure 1.2 is the most complete table listing particles within the Standard Model, including the Higgs boson which has only recently been confirmed [29, 30].

In 1975 the tau lepton was discovered, when researchers on the Mark I detector at the Stanford Linear Accelerator Center (SLAC) concluded that at least two additional particles were being produced in the

Stanford Positron Electron Asymmetric Rings (SPEAR) collider [31]. Soon after the discovery, the existence the tau neutrino (ν_τ) was inferred, but not confirmed until 2000 [32], when the DONUT experiment (Direct Observation of the Nu Tau) at Fermilab reported four events out of a total of 203 neutrino interactions were from tau decays, suggesting the production of tau neutrinos. While the tau neutrino was yet to be discovered, a controversial issue known as the solar neutrino problem (§ 1.2) was causing physicists to rethink the neutrino, and a solution would not be satisfactorily verified until the SNO experiment published their first results in 2001 [33].

1.2   The Solar Neutrino Problem and SNO

Models of the sun were formulated by assuming stars in the main sequence produce energy via fusion reactions similar to those assumed for terrestrial fusion models [34]. Before solar neutrino detectors, the only way to observe the sun was through photons emitted through the outermost layers of the sun. Deep within the dense solar core, photons take thousands of years to escape, yet the neutrinos, due to their weak interactions, have the capability to pass through unimpeded and have the potential to reach earthbound detectors around 8 minutes after their production. In 1968 Ray Davis Jr. developed the first solar neutrino detector to act as a probe into the inner workings of the sun, and test the solar model for the first time [34]. The 400 000 litre tank Davis designed was located a depth of 1500 m below surface in the Homestake Mine. Containing argon and chlorine molecules, his detector interacted with solar neutrinos via:

$$\nu_e + {}^{37}\mathrm{Cl} \leftrightarrow {}^{37}\mathrm{Ar} + e^- \tag{1.9}$$

Unfortunately, the experiment yielded approximately only one-third of the expected number of neutrinos [35]. Further experiments attempted to resolve the deficit: Kamiokande [36, 37] (which later upgraded to Super-Kamiokande [38]) searched for neutrino scattering with an electron in water, while SAGE [39] and GALLEX [40] (GALLEX then upgraded to GNO [41]) employed gallium which would undergo inverse beta decay with the electron neutrino: ${}^{71}\mathrm{Ga}(\nu_e, e){}^{71}\mathrm{Ge}$. Yet all off these experiments were missing various neutrino amounts (see Fig. 1.3).

Pontecorvo's theory of flavour oscillations had not been forgotten, and in 1985 Herbert Chen wrote a letter suggesting a large, heavy water (D_2O) Cherenkov detector to solve the solar neutrino problem [43]. This detecting medium was unique compared to all previous experiments, in that it could interact not only with electron neutrinos, but with all neutrino flavours (including the not-yet discovered tau neutrino). If Pontecorvo's theory was correct and neutrino flavour oscillation was possible, then it was entirely plausible
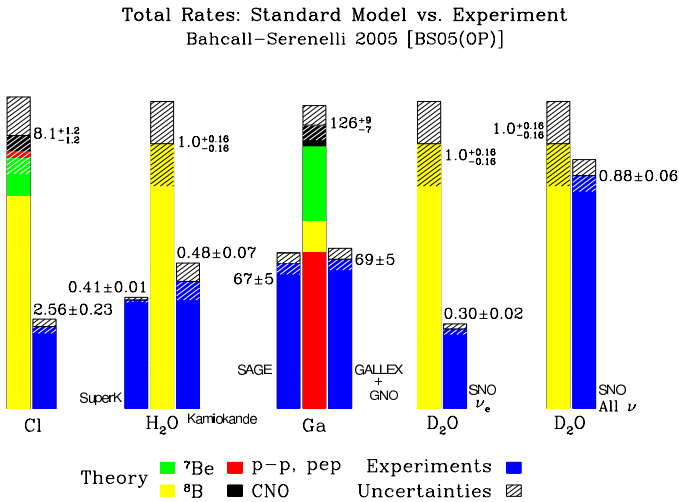
Figure 1.3: Neutrino rates from the solar model vs. observations of different experiments [42]. All experiments except for SNO reported a deficit of about 30 - 60 % in the number of solar neutrinos.

that the electron neutrinos produced in the sun were changing flavour along their way to the earth. As all previous detectors were only sensitive to electron neutrinos (ν_e), the deficit observed could possibly be explained by an increase in muon and tau neutrino (ν_μ and ν_τ) fluxes. An immediate consequence of flavour oscillation was that neutrinos had mass eigenstates, a property which the Higgs mechanism cannot explain. This would result in irrefutable evidence of physics beyond the Standard Model. By comparing the fluxes from the different types of reactions in the detector, the Sudbury Neutrino Observatory (SNO) experiment, which turned on in 1998, could once and for all determine if the solar neutrino deficit was due to an incorrect solar model, or if new physics was occurring.

The SNO detector is described in detail in Chapter 2, as most of the main hardware remains the same going forward to the successor experiment, SNO+ (see Fig. 1.4 for detector diagram). In general, SNO was one kilotonne of heavy water (D_2O) contained within a 12 meter diameter acrylic sphere, which the solar neutrinos would interact with. Such interactions produced relativistic charged particles that emitted Cherenkov light as they travelled faster than the speed of light through the water [44]. The light would then be detected by photomultiplier tubes, suspended on a 17.8 meter diameter structure surrounding the detecting medium, allowing for event reconstruction depending on which phase the detector was in. Each phase led to a different sensitivity of the neutral current reaction, which is listed, along with the other two reactions SNO was sensitive to, below.
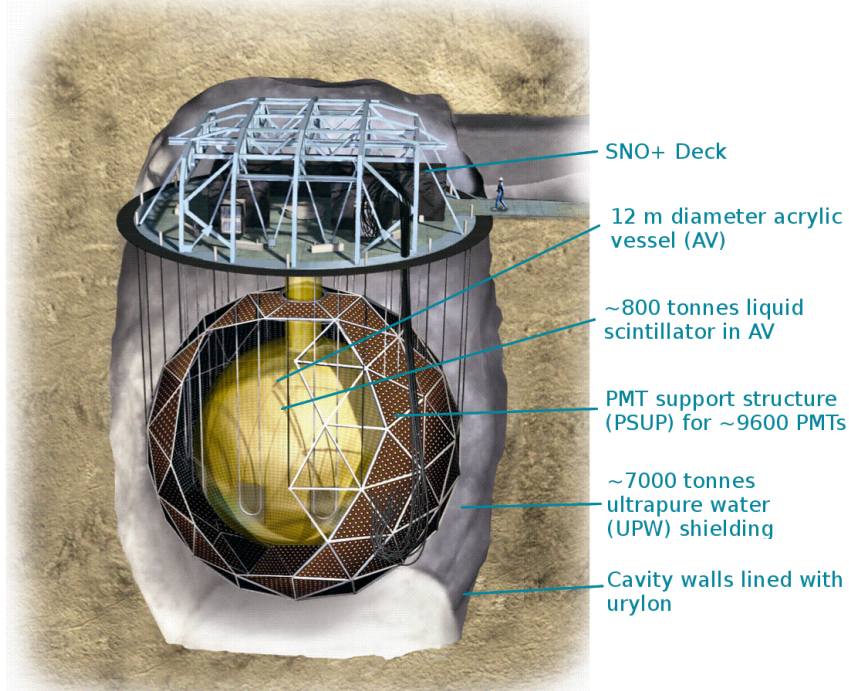
Figure 1.4: The SNO detector with major components, now refurbished for the SNO+ experiment. D_2O for SNO was located inside the AV, where the liquid scintillator is now shown. Missing (for SNO+) are the hold-down ropes. Figure modified from [45].

$$\text{ES:} \quad \nu_x + e^- \rightarrow \nu_x + e^- \tag{1.10}$$

$$\text{CC:} \quad \nu_e + d \rightarrow e^- + p + p \tag{1.11}$$

$$\text{NC:} \quad \nu_x + d \rightarrow \nu_x + n + p \tag{1.12}$$

The elastic scattering (ES) of neutrinos off electrons (Eq. 1.10) could occur with any active neutrino ($x = e$, μ, τ) energetic enough to cause the electron to travel faster than the speed of light in water, providing a Cherenkov light ring. This reaction is highly directional and within SNO allowed the sun to be established as the source of neutrinos, but is suppressed compared to the charged current reaction. Eq. 1.11 is a charged current reaction (CC) mediated by the W boson, and is sensitive only to electron neutrinos, which again produced a relativistic electron and a resulting Cherenkov ring in SNO. The last equation (Eq. 1.12) is a neutral current (NC) reaction mediated by the Z boson, and is equally sensitive to all types of neutrinos. The free resulting neutron in Eq. 1.12 captured on a nucleus in the detector, which depended greatly on the phase SNO was in (either pure heavy water, ^{35}Cl insertion, or ^{3}He counter insertion).

Even after the first phase of SNO the data clearly showed neutrino flavours oscillate [33], and the remaining phases allowed for improved systematic and statistical uncertainties. The data from SNO's latest

publication revealed ratios of CC to NC fluxes which demonstrated that approximately one-third of the anticipated electron neutrinos from the sun were oscillating into other active flavours, assumedly the muon and tau neutrinos [46]:

$$\frac{\phi_{cc}^{SNO}}{\phi_{NC}^{SNO}} = 0.301 \pm 0.033 \tag{1.13}$$

Solar neutrino flavour changes mostly occur due to matter induced oscillation known as the Mikheyev-Smirnov-Wolfenstein (MSW) resonance conversion effects within the sun [47].

1.3   Neutrino Mass and Double Beta Decay

With the groundbreaking work of SNO, flavour oscillation was inferred from the disappearance and appearance of different neutrinos, occurring when the small difference in mass leads to a large difference in phase. In addition to solar neutrinos, oscillation measurements of atmospheric neutrinos (from experiments such as Kamiokande [48] and Super-Kamiokande [49]) and long baseline detectors for reactor antineutrinos (e.g. KamLAND [50]) have been integral in studying the implications of neutrino oscillations. Since neutrinos change over time, they cannot be traveling at the speed of light, and at least one of the neutrino states must have non-zero mass, requiring physics beyond the Standard Model.

The mixing of flavour and mass eigenstates can be expressed as:

$$|\nu_k\rangle = \sum_k U_{\alpha k} |\nu_\alpha\rangle \tag{1.14}$$

where $|\nu_k\rangle$ are mass states ($k = 1, 2, 3$), $|\nu_\alpha\rangle$ represent flavour states ($\alpha = e, \mu, \tau$), and $U_{\alpha k}$ is the Pontecorvo–Maki–Nakagawa–Sakata (PMNS) mixing matrix. In some cases a two-neutrino mixing approximation results in the change in flavour state ($\nu_\alpha \rightarrow \nu_\beta$) probability as:

$$P_{\alpha \rightarrow \beta} = \sin^2(2\theta) \sin^2\left(\frac{\Delta m^2 L}{4E_\nu}\right) \tag{1.15}$$

The premise of solar and reactor neutrino experiments is through survival probability measurements (with L as the distance from the neutrino source and E as the particle's energy), providing values of mixing angles between phases (θ) and mass splittings (Δm) between pairs of neutrino mass states. Oscillation experiments indicate very small absolute mass splittings [52], but are limited as they do not provide any actual mass values (measuring mass differences instead), nor do they suggest a mass hierarchy of the neutrino mass states. Currently there exist two possibilities for the three light neutrino mass scheme: the normal and inverted hierarchies (see Fig. 1.5). The normal scheme simply suggests the likeliness to the lepton flavour
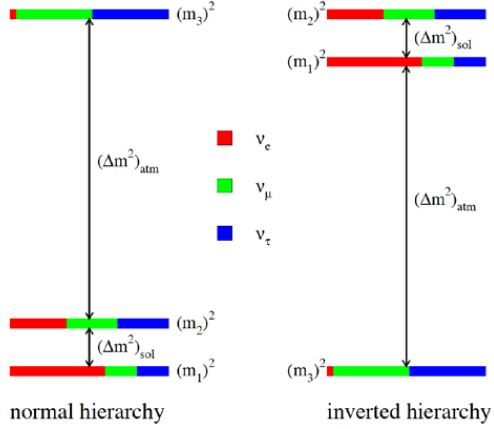
Figure 1.5: The two possible hierarchy schemes for neutrino masses: normal (left) and inverted (right) hierarchy [51]. Measurements of neutrino oscillations provide mass splitting values ($\Delta m_{sol}^2 = \Delta m_{21}^2$, $\Delta m_{atm}^2 = \Delta m_{32}^2$) and the flavour combination for each state, but not the actual mass values themselves, nor do they verify which hierarchy is correct.
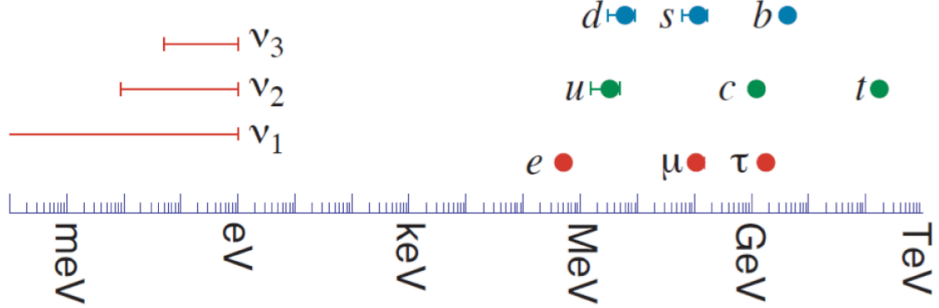
Figure 1.6: Mass scale of fermion particles [51]. Neutrinos are estimated to be orders of magnitude lighter than other leptons and quarks though the exact values are unknown. This diagram assumes the normal hierarchy of neutrino masses.

sector ($m_1 << m_2 < m_3$), whereas the inverted scheme requires $m_3 << m_1 < m_2$. Another spectrum which is disfavoured by cosmology is the quasi-degenerate (QD) scheme, in which $m_1 \cong m_2 \cong m_3$.

The discovery of the Higgs boson at the Large Hadron Collider (LHC) in 2012 [29,30] was monumentous: physicists could finally conclude the Higgs boson couples charged fermions to the Higgs field, giving these particles mass. Yet the results do not provide an explanation for the light, neutral particles called neutrinos which also appear to have mass. Studies of nuclear beta decay currently demonstrate the lightest neutrino mass is smaller than 2 eV [52], which is much lighter than the charged leptons and quarks (see Fig. 1.6). An even more sensitive experiment, KATRIN [53], is expected to begin taking data in 2015.

Along with such a small mass, the neutrino's charge neutrality also sets it apart from the other fermions, and with the realization of a non-zero neutrino mass, physicists are returning to Majorana's equation and the study of Majorana particles. The existence of a Majorana neutrino would violate lepton number conservation (a huge discovery on its own), but may also explain its light mass. A Majorana coupling with neutrino mass

would have the form $m_{LL}\bar{\nu}_L\nu_L^c$, where ν_L is the left-handed neutrino field and ν_L^c the CP conjugate (i.e. a right-handed antineutrino field). Meanwhile, the Dirac mass takes the form $m_{LR}\bar{\nu}_L\nu_R$, and if a right-handed neutrino field were introduced with $M_{RR}\bar{\nu}_R\nu_R^c$, where ν_R is the right-handed neutrino field and ν_R^c the CP conjugate (i.e. a left-handed antineutrino field), the mass Lagrangian takes the form:

$$\mathcal{L}_{mass} = \begin{pmatrix} \bar{\nu}_L & \bar{\nu}_R^c \end{pmatrix} \begin{pmatrix} \sim 0 & m_{LR} \\ m_{LR}^T & M_{RR} \end{pmatrix} \begin{pmatrix} \nu_L^c \\ \nu_R \end{pmatrix} \tag{1.16}$$

Assuming that $M_{RR} >> m_{LR}$ (as M_{RR} may be orders of magnitude larger since the right-handed neutrinos are electroweak singlets), the mass matrix may be diagonalized to yield an effective Majorana mass of:

$$m_{LL} \approx -m_{LR}\frac{1}{M_{RR}}m_{LR}^T \tag{1.17}$$

whereas the other is on the order of $m_\nu \sim M_{RR}$. This is the see-saw mechanism, predicting the coupling of the observed light neutrinos (m_{LL}) to those on the scale of $m_\nu \sim M_{RR}$. Estimations of such massive neutrinos place $M_{RR} \sim 0.3 \times 10^{15}$ GeV, close to the grand unified scale $\Lambda_{GUT} \sim 10^{16}$ GeV. Contrary to all observations to date, lepton number is not conserved in many grand unified theories [54]. Furthermore, the CP violation from the decay of these heavy particles could explain the matter-antimatter asymmetry of the universe today, through what is known as "leptogenesis" [55]. As such heavy particles are beyond the reach of accelerators, perhaps the best way to infer their existence is by observing the existence of Majorana neutrinos with neutrinoless double beta decay experiments.

Studies of neutrino masses like KATRIN have their limitations as they rely mainly on kinematics, are independent of the Majorana or Dirac nature of the neutrino, and provide no information on the effective mass parameter, $< m_{\beta\beta} >$, a linear combination of the neutrino mass states. Such a value must be considered during the $0\nu\beta\beta$ decay process in the case of three-neutrino mixing. The experimental data on neutrino masses, phase angles, and mixing parameters - values which are studied to this day - predict a range for $< m_{\beta\beta} >$, which is given as:

$$< m_{\beta\beta} >^2 = \left| \sum_k U_{ek}^2 m_k \right|^2 \tag{1.18}$$

The sum is over light neutrinos and U_{ek} are neutrino mixing matrix elements from the PMNS matrix (which involve both known mixing angles and unknown Majorana phases). Since the Majorana phases remain unknown, the terms in the sum could cancel and the value of $< m_{\beta\beta} >$ could be less than any of m_k. Allowed values of $< m_{\beta\beta} >$ have been calculated as a range and plotted as a function of the lightest neutrino mass, which is dependent on the neutrino mass hierarchy (see Fig. 1.7). The current experimental interest
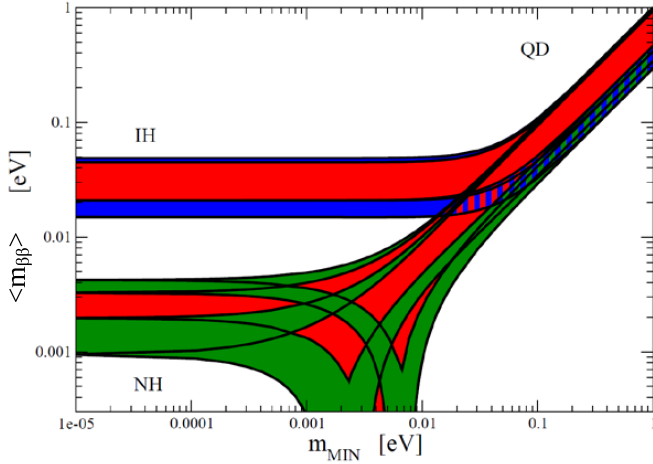
Figure 1.7: Allowed values of the effective neutrino mass $< m_{\beta\beta} >$ as a function of the lightest neutrino mass $(\min(m_j))$, calculated from current experimental data [52]. Areas of the inverted (IH) and normal (NH) hierarchies and quasidegenerate (QD) state are labeled. Red, blue and green bands correspond to different allowed regions for the unknown CP violating phases in $< m_{\beta\beta} >$ and allow for $1\ \sigma$ variation in known parameters.

lies within the inverted hierarchy region, an area which can be probed by $0\nu\beta\beta$ decay experiments with a double beta decay isotope with mass of approximately 1 tonne or more.

Although ruled out in the 1950's due to the belief of lepton conservation and the handedness of massless neutrinos, the prospect of neutrinoless double beta decay provides compelling theoretical arguments. Fig. 1.8 depicts three possible $\beta\beta$ decay processes: $2\nu\beta\beta$ decay, $0\nu\beta\beta$ decay without mixing, and $0\nu\beta\beta$ decay with mixing. New limits of the $0\nu\beta\beta$ process with non-zero neutrino masses demonstrate half-lives above 10^{25} years, of which the decay rate is given by the phase space integral $(G^{0\nu})$, the nuclear matrix element $(M^{0\nu})$, and the effective neutrino mass $(< m_{\beta\beta} >)$ in:

$$(T_{1/2}^{0\nu})^{-1} = G^{0\nu} \cdot |M^{0\nu}|^2 \cdot < m_{\beta\beta} >^2 \tag{1.19}$$

The process of $0\nu\beta\beta$ involves virtual neutrino states, consequently emitted electrons would possess a total kinetic energy equal to the amount of energy released in the reaction (i.e. the Q value of the parent isotope's decay). Most double beta decay experiments are some form of calorimetry work, measuring the total electron energy via scintillation light, ionization, or heat deposition. Candidate decay isotopes are chosen based on compatibility, detector arrangement, and the decay curve. Generally, the higher the Q value, the higher the decay rate [56]. Yet experiments are also concerned with backgrounds which can occur under or near the decay curve. An irreducible background of the $0\nu\beta\beta$ spectrum will come from the $2\nu\beta\beta$ spectrum of the same isotope, requiring excellent resolution or high rates to distinguish the signal from the tail end of $2\nu\beta\beta$.

(a) $2\nu\beta\beta$ decay   (b) $0\nu\beta\beta$ decay without mixing   (c) $0\nu\beta\beta$ decay with three-neutrino mixing
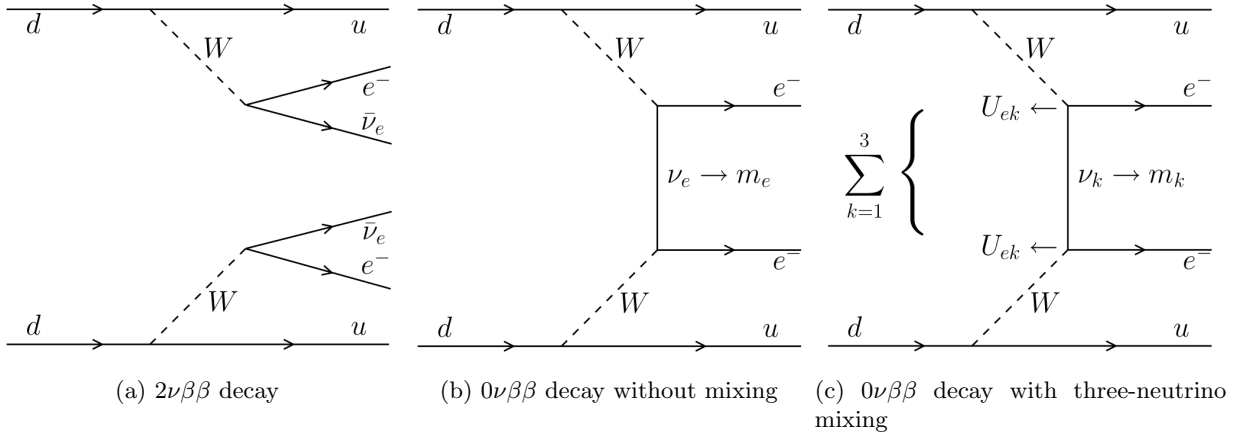
Figure 1.8: Processes of $2\nu\beta\beta$ and $0\nu\beta\beta$ decay [9]. Two "down" quarks within a neutron simultaneously emit a W boson and convert to an "up" quark, changing the neutrons into protons. Both W bosons then decay. (a) $2\nu\beta\beta$ decay. The W bosons decay to two electrons and two Dirac electron- antineutrinos (b) $0\nu\beta\beta$ decay. The W bosons decay to two electrons and two virtual electron-flavoured Majorana neutrinos. (c) $0\nu\beta\beta$ decay. The W boson decays to two electrons and two virtual Majorana neutrinos, with neutrino mixing included through the PMNS matrix.
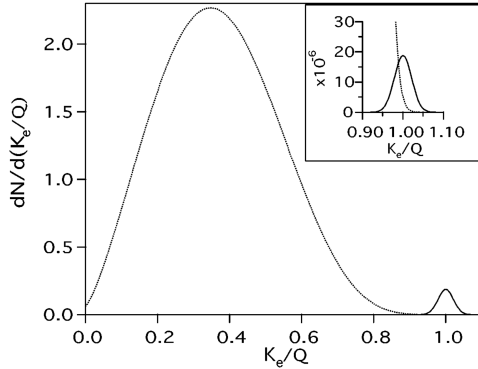
Figure 1.9: Normalized theoretical decay spectrum for any hypothetical $0\nu\beta\beta$ candidate [57]. $0\nu\beta\beta$ events are the small peak about the Q value, while the $2\nu\beta\beta$ spectrum is much broader and taller.

A peak above these backgrounds centered around the Q value would indicate $0\nu\beta\beta$ exists (see Fig. 1.9). Backgrounds are further minimized by placing the detector deep underground, building it with radio-pure materials, utilizing some form of event identification, and placing fiducial volume (FV) and region of interest (ROI) cuts.

A standard approach to publishing $0\nu\beta\beta$ results are in the form of the isotope's half-life for the decay process, drawing conclusions about mass. Thus far, no experiment has demonstrated the sensitivity required to adequately investigate the inverted hierarchy of the neutrino mass scale, so these values are in the form of exclusion limits. Experiments such as EXO-200 [58] and KamLAND-Zen [59] have published exclusion limits for the decay of ^{136}Xe below 1.1×10^{25} and 1.9×10^{25} years respectively, while GERDA reports a limit of $>2.1\times10^{25}$ years for ^{76}Ge [60]. These conflict with the claim of $0\nu\beta\beta$ observations by the Heidelberg-Moscow

13

group [61].

The SNO detector has solved one of the longest-standing questions in neutrino physics, and its accomplishments were recently acknowledged in 2015 when Arthur B. McDonald, the SNO project director, received a Nobel Prize "for the discovery of neutrino oscillations, which shows that neutrinos have mass" [62]. The current location and large size of SNO provide a compelling opportunity for its re-use as SNO+, now in the search for $0\nu\beta\beta$. Once loaded with ^{130}Te, the carefully selected double beta decay isotope, SNO+ has the opportunity to probe the inverted hierarchy of neutrino masses, observe the possibility of lepton number violation, confirm the Majorana nature of light neutrinos, and describe the light neutrino mass through the see-saw mechanism. All of this could lead to a better understanding of the grand unification theories and the knowledge of the leptogenesis of the early universe.

The remaining chapters develop how the SNO+ detector can observe such rare neutrino interactions despite large contributions of backgrounds. Chapter 2 details the main hardware of the SNO+ detector and how neutrino interactions within the scintillation detecting medium are observed. Chapter 3 discusses the large number of backgrounds within SNO+, including the troublesome radioisotope ^{222}Rn, and how backgrounds are reduced. Chapter 4 describes the cryo-trapping assay processes of ^{222}Rn within SNO+, which will verify that the ^{222}Rn levels are acceptable within the scintillation medium, the surrounding cavity water, nitrogen cover gas system, and various selected materials. Chapter 5 studies the expected contribution of α-n backgrounds within the acrylic of SNO+ during the water-filled phase, the reaction of which is fed by ^{210}Po, a daughter of ^{222}Rn. All this work leads to Chapter 6, which summarizes the work, establishes a set of future recommendations, and concludes that SNO+ will be well-prepared to deal with backgrounds introduced by ^{222}Rn, securing its position as a competitive neutrino detector searching for neutrinoless double beta decay.

Chapter 2

The SNO+ Detector

2.1 From SNO to SNO+

After the end of SNO, the detector was drained and refurbished for new neutrino research. The heavy water was returned to Atomic Energy of Canada Limited (AECL), and plans for a new detecting medium composed of a scintillator cocktail formulated. The new scintillator-based experiment [63] reuses the SNO cavity, acrylic vessel (AV), PMT support system (PSUP), most electronics, and the existing ultrapure water (UPW) system, the latter of which has been upgraded. Major alterations include a hold-down rope net for the AV and the exchange of detecting medium (from heavy water to a lighter scintillation cocktail), which in turn requires a new detecting medium purification plant (see Chapter 3) and assay tools for both plants. Small changes include an update of the DAQ, some electronics refurbishment, a new trigger system and analysis tool, an upgrade to the calibration system, and modifications to the nitrogen cover gas system and the universal interface (UI). With all the new additions, the original SNO detector was renamed "SNO+". Refer to Ch. 1.3 Fig. 1.4 for a diagram of the SNO+ detector.

SNO+ is located on the "6800 foot" level of Vale's Creighton mine, 2039 meters underground near Sudbury, Ontario. At this depth, surrounded by mostly norite rock (leading to about 6000 meter water equivalency (m.w.e.) shielding), backgrounds that would render the detector useless on surface are greatly reduced (see Ch. 3 § 3.2). Situated within a "dirty" mine, researchers entering the lab must take showers and change into clean laboratory clothes after the two kilometer ride down and roughly two kilometer walk in from the shaft station. With the success of the SNO experiment, the underground laboratory was expanded into SNOLAB: a class 2000 clean room housing low-background counting experiments and some of the leading detectors in dark matter searches. All entering material must also undergo cleaning within a room at the
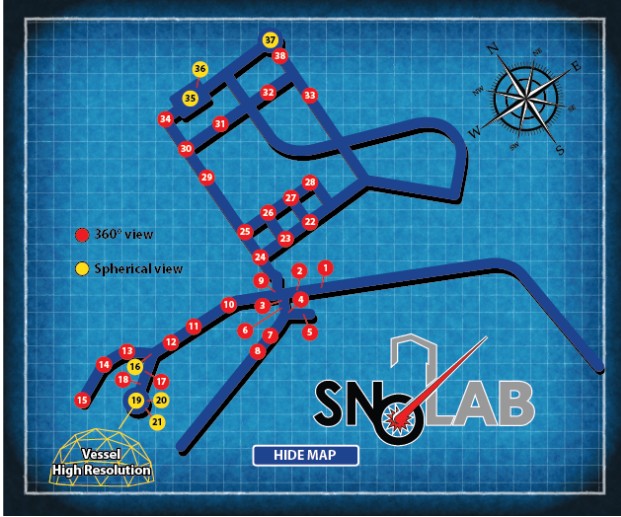
Figure 2.1: SNOLAB's virtual tour map [64]. Markers 19, 20, 21 are the site of the SNO+ detector, 17 indicates the SNO+ control room, while 13, 14, and 15 are locations within the utility room, which house the purification plants for water and scintillator. The entrance to the lab is at position 1.

entry point of the lab, and much of the old SNO area, which is reused by SNO+, remains the same (see Fig. 2.1 for key SNO+ locations).

The large, barrel shaped cavity containing the SNO+ detector is approximately 34 meters tall and 22 meters in diameter. Excavated from the norite rock and sprayed with several coatings of Urylon liner, it is filled with UPW specifically purified by a water plant within the utility room located adjacent to the detector. The detecting medium - 780 tonnes of liquid scintillator - will be contained in the 5 cm thick, 12 meter diameter transparent acrylic spherical vessel situated within the cavity, with excess medium stored within two 60-tonne tanks in the utility room. At the top of the AV exists an acrylic neck, about 1.5 meters in diameter and 6.8 meters tall, which ends inside the DCR, a clean room on deck above the the giant cavity. This clean room and the top of the neck represent the entry point to the innermost place of the detector, and as such must maintain the highest purity levels. Gloves must be worn inside the DCR, and one must change into another set of boots upon entry to preserve cleanliness. The top of the AV neck will be sealed with a new stainless steel universal interface (UI), of which there are two parts: the lower and upper UI. The upper UI contains glove ports, viewing windows, three photomultiplier tubes, and three gate valves (GVs), which allow for the ingress and egress of calibration sources. The calibration sources themselves will be sealed inside a source storage box (SB) when not in use, and transfer from the source box to the detector is performed with specially designed umbilical retrieval mechanisms (URMs). Refer to Appendix A for more information regarding calibration source movement and gate valve position sensing.
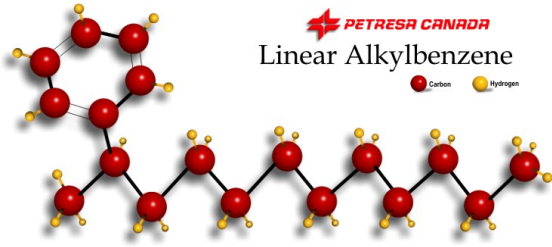
Interactions within the scintillation medium are detected by approximately 9500 inward-looking Hama-

matsu R1408 photomultipliers, housed within a hexagonal black plastic housing made from acrylonitrile-butadiene-styrene (ABS). Reflective light petals (light concentrators) line the inside of the PMT housing, ensuring the number of photons detected is maximized to give ∼56% photocathode coverage, while limiting the angular acceptance of the PMTs to only the central portion of the detector. These PMTs were chosen for their high photon efficiency, low radioactivity, low failure rate, and low sensitivity to external magnetic fields. Regardless of such criteria, measures were taken to increase their efficiencies and decrease their background contribution. Hand-blown glass bulbs were chosen for the PMTs, which will be operated at a reduced temperature of ∼12 °C and a distance of ∼2 meters from the AV walls (the PSUP is 17.8 meters in diameter). To reduce the effect of the Earth's magnetic field on PMTs, 11 functional compensation coils exist in the the cavity walls surrounding the detector. Although the PMTs were chosen for their low failure rate, 8 % (∼800 PMTs) failed during SNO operation. While this loss is not substantial, approximately 500 of those failed PMTs are under repair, and others will be replaced to improve SNO+ operation as appropriate.
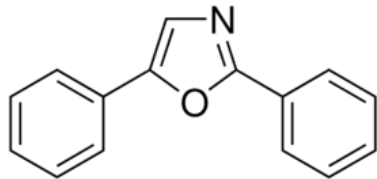
The PMT support structure is a 889 cm radius, three-frequency icosahedron [44], with the top node replaced with a toroidal ring to accommodate the AV neck. Built from stainless steel struts to survive long exposure to water, the structure of the PSUP is critical in that it must provide maximal coverage for the PMTs while acting as a barrier to backgrounds. The PSUP defends against backgrounds via leak-tight plastic seals between each PMT to ensure no waterborne backgrounds leak in, and also supports 91 outward-looking PMTs without reflectors to assist in vetoing backgrounds from muons which reach the detector.

Both the PSUP and the AV are suspended in a large cavity and require support ropes for positioning. 10 synthetic fiber rope loops attached to the equator of the AV sphere ensure it remains suspended when the cavity is empty, while once the AV and cavity are full, a hold-down rope net system looped over the top of the AV anchors it to the cavity floor. The rope net is a SNO+ addition [65] which is necessary because of the differences in scintillator and water density: the scintillator is linear alkylbenzene-based which is only 0.865 as dense as H_2O. The PSUP requires similar tools: fifteen stainless steel wire rope cables suspend the PSUP while the cavity is empty, and anchor points on the cavity floor hold the structure down once the cavity is filled with water (the PSUP is also buoyant in water due to the vacuum within the PMTs). The tensions on the ropes are monitored by a Delta-V$^{\text{TM}}$ system [66], and adjustments to the hold-up ropes are performed by adjusting rope tension rods situated on deck.

Creighton mine is still actively used and owned by Vale, and occasional blasting can be observed by SNO+ monitoring tools (e.g. pressure monitors). Even changes in ventilation can create pressure changes which could cause serious stress and possible damage to the detector. Neither the cavity nor the AV are completely filled with their respective liquids; small spaces exist between these liquid surfaces and the floor of the cavity deck, and are filled with nitrogen gas. These pockets of gas protect the deck, cavity, and AV by

17

(a) Generic linear alkylbenzene molecule [67]. Important for luminescence is the benzene ring.

(b) Chemical structure of PPO wavelength shifter

Figure 2.2: Organic compounds composing the SNO+ scintillator cocktail for neutrino detection

"breathing" during pressure fluctuations within the mine: either by filling with additional gas or by releasing some, ensuring the differences in pressure above and below the deck remain small. Ch. 3 § 3.5 explains the choice of nitrogen gas as opposed to atmospheric air in this "cover gas" system.

2.2 SNO+ Detecting Medium

The detecting medium for SNO+ will be a scintillator mixture of linear alkylbenzene (LAB) and 2,5-diphenyloxazole (PPO) wavelength shifter added at 2 g/L [63] (see Fig. 2.2 for organic structures of LAB, PPO). Commercial linear alkylbenzene is a mixture of alkyl-chain lengths, and as such a number of different chemical compositions will be included (see Table 2.1), but each molecule possesses the benzene ring necessary for luminescence. LAB was chosen for a number of reasons, including its compatibility with acrylic, high scintillation efficiency (light yield of ∼10 000 photons per MeV), good commercial availability, low toxicity, and high flash point [63]. It is produced in large quantities by CEPSA Química, at Bécancour, Quebec [67], which is 850 km from SNOLAB. The plant produces a particularly pure and transparent product due to their DETAL catalyst process, which is critical for SNO+ background and efficiency requirements. This

Chemical Equation	Content (% by mass)
LAB (99.77%)	
$C_{15}H_{24}$	1.2
$C_{16}H_{26}$	20.4
$C_{17}H_{28}$	43.2
$C_{18}H_{30}$	33.4
$C_{19}H_{32}$	1.8
PPO (0.23%)	
$C_{15}H_{11}NO$	2 g/L

Table 2.1: SNO+ scintillator cocktail composition [68]. LAB is a family of organic compounds, and as such several different compounds will compose the scintillator, yet all include the benzene ring required for luminescence.

colourless, odourless liquid has a density of 0.865 g/cm^3, a boiling point spanning 275-316 °C, a melting point less than -50 °C, and a flash point of 130 °C at atmospheric pressure [67].

2.3   Interactions within SNO+

The scintillator cocktail will be sensitive to any charged particles passing through the LAB+PPO mixture, such as electrons and muons. Dominant neutrino signals within the detector will be from the elastic scattering of a neutrino off an electron:

$$\nu_x + e^- \rightarrow \nu_x + e^- \tag{2.1}$$

Eq. 2.1 is sensitive to all active flavours of neutrinos, but the cross-section is largest for electron-type neutrinos. The recoiling electron produces isotropic light as it stops within the scintillator, and the light is detected by the inward-looking PMTs. By summing over the PMT charge and total number of PMTs hit, the electron's kinetic energy is reconstructed, making energy resolution the major discriminate within SNO+.

Meanwhile, antineutrino detection occurs through the inverse beta decay process:

$$\bar{\nu}_e + p \rightarrow e^+ + n \tag{2.2}$$

The positron will possess a kinetic energy that is 1.8 MeV less than the antineutrino's energy (E$_\nu$ > 1.8 MeV) and will quickly annihilate, producing the prompt signal and depositing E$_\nu$ − 0.78 MeV of energy. Meanwhile, the neutron will thermalize and undergo capture on hydrogen, generating the delayed signal: a 2.2 MeV gamma. The coincidence of both prompt and delayed signals will identify this signature reaction.

SNO+ will operate under different phases: a water phase, pure liquid scintillator phase, and a phase when liquid scintillator is loaded with ^{130}Te, a $0\nu\beta\beta$ decay candidate [63]. The first two mentioned phases will allow for proper calibration of the detector and the verification and determination of backgrounds while studying various properties of neutrinos, including geoneutrinos, solar neutrinos, reactor antineutrinos, and neutrinos from a possible galactic supernova. The studies will reinforce any observations to date, and provide a better understanding of neutrinos with more sensitive data. The priority for SNO+ occurs in the third phase, when 0.3 to 0.5 % $^{\text{nat}}$Te will be loaded into the scintillator cocktail via processes within the scintillator plant (see Ch. 3 § 3.7), allowing SNO+ to join the search for Majorana neutrinos (see Table 2.2 summarizing experimental goals and SNO+ phases). SNO+ is also exploring higher Te-loading percentages for more sensitive studies (phase II of Te-loading), and possesses the flexibility to load with a different double beta isotope. Due to the competitive nature of $0\nu\beta\beta$ research, neutrino studies within the pure scintillator phase

19

(e.g. solar neutrinos) will most likely occur after the tellurium loaded phase.

Along with neutrino interactions, SNO+ will also detect a large number of background reactions from undesired particles. Some interactions can mimic various neutrino signals, while others can drive the detector threshold high, or disguise the true signal within background noise. For each phase of SNO+, backgrounds such as ^{238}U and ^{232}Th chain radioisotopes are carefully evaluated and reduced as necessary (Table 2.3 records the ^{238}U limits during each SNO+ phase). Chapter 3 details these and other backgrounds, and how SNO+ will address them throughout the three phases, while Ch. 4 explains how one of the most troublesome radioisotopes, ^{222}Rn, is measured via *ex-situ* methods. This is the core of the thesis work presented here.

Target	Phase			Goals/limits
	H$_2$O	LAB	Te-LAB	
Nucleon Decay	✓			Improve neutron, proton lifetime limits to $>10^{30}$ yrs
Reactor antineutrinos	✓	✓		Constrain neutrino oscillation parameters
Geo- antineutrinos	✓	✓		Constrain radiogenic heat flow of the Earth
Supernova	✓	✓	✓	Study supernova, supernova neutrinos Operate as alert system within SNEWS
Solar ν's	✓	✓		Resolve sun's metallicity Constrain luminosity of sun Confirm MSW effects Study sub-dominant effects of oscillations
$0\nu\beta\beta$			✓	Observe lepton number violation Confirm Majorana property of neutrinos, additional theories Or: set limit on ^{130}Te lifetime

Table 2.2: SNO+ physics goals during each experimental phase. Reactor and geoneutrinos will be visible during the water phase, but most likely analysis will not occur until the pure scintillator phase.

Phase	Internal ^{238}U [g/g]	External ^{238}U [g/g]
Water	3.5×10^{-14}	
LAB-PPO	1.6×10^{-17}	3.5×10^{-13}
Te-loading (phase I)	2.5×10^{-15}	

Table 2.3: SNO+ target levels of ^{238}U in units of g/g, during each detector phase.

2.3.1   Water Phase

The SNO+ detector will first be filled with ultrapure water, which is the first step in safety for LAB loading (refer to Ch. 3 § 3.7). The water phase permits time for the leach-out of impurities, and allows for detector calibration by thoroughly testing the new electronics, DAQ, and analysis tools, and the commissioning of a new fibre-based calibration system. This phase is anticipated to last 6 to 12 months. Background analysis

will be critical, and from this point on the detector is sensitive to core-collapse supernovae (SN) neutrinos and will be part of the SNEWS community known as the SuperNova Early Warning System [69]. Studies of SN neutrinos are possible during water phase, but SNO+ will run with scintillator much longer than water, and more events will occur within scintillator than in water. Refer to the next section for SNO+ SN analysis with scintillator. While running with water, SNO+ also has the potential to study reactor antineutrinos with an energy above 1.8 MeV as described with Eq. 2.2, though extensive studies will also occur during the pure scintillator phase.

During water phase, SNO+ will also collect physics data in the study of invisible nucleon decay. Currently, the best limits have been set by KamLAND as 5.8×10^{29} years for neutron disappearance [70], and by SNO as 2.1×10^{29} years for proton disappearance [71]. SNO+ is expected to perform more efficiently than SNO as it will run with regular "light" water and thus will not be limited by neutral current "backgrounds" as within heavy water. In comparison with KamLAND which uses ^{12}C, an isotope with only a 6% branching ratio to the desired physics, SNO+ plans to study nucleon decay with ^{16}O. If a neutron decays, the resulting isotope will de-excite and emit a 6.18 MeV gamma 44% of the time, while for proton decay, in 41% of the reactions a 6.32 MeV gamma is emitted [63]. Assuming 6 months of data, a 5.5 m fiducial volume, region of interest of 5-9 MeV, and a cut in the solar direction, projected estimates place SNO+ nucleon decay limits of 1.25×10^{30} and 1.38×10^{30} years for neutron and proton modes, respectively [63]. Discussion is underway to increase the projected run time up to nine months of data taking, further improving these values.
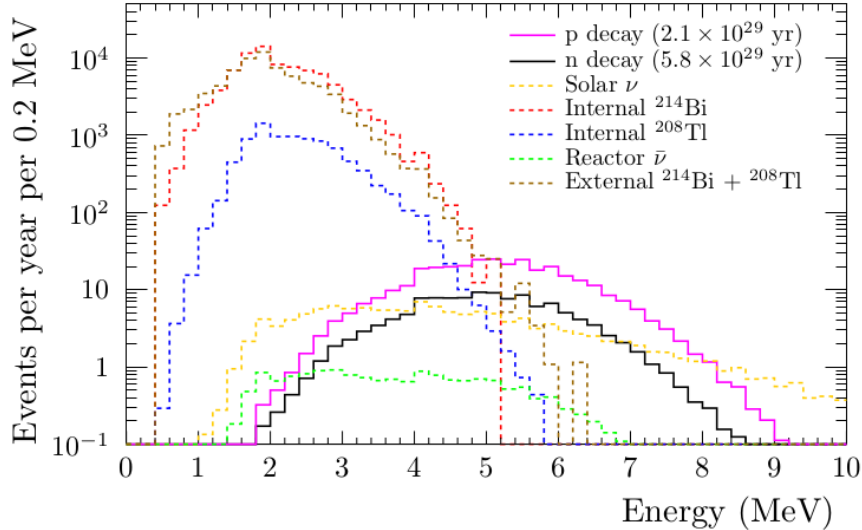
Figure 2.3: Expected energy spectrum for SNO+ water phase depicting nucleon decay signals and expected backgrounds within a 5.5 m fiducial volume cut and using a solar cut of $\theta_{\rm sun} > -0.8$ [63]

During water phase, SNO+ assumes external backgrounds on the same order as SNO observed: 3.5×10^{-13}

g ^{238}U/g H$_2$O and 3.0×10^{-14} g ^{232}Th/g H$_2$O [72], as the same water processing plant is used (see Ch. 3 § 3.6). Meanwhile, internal targets of 3.5×10^{-14} g ^{238}U/g H$_2$O and 3.5×10^{-15} g ^{232}Th/g H$_2$O [63] are estimated for the water inside the AV. *Ex-situ* analysis of the cavity and AV water will be performed with various assay techniques coupled to the water plant to monitor these values, such as the ^{222}Rn assay method described in Ch. 4.

2.3.2   Pure Scintillator/ LAB-PPO Phase

Once the water phase of SNO+ is complete and part of the scintillator cocktail has been successfully delivered and purified underground, the LAB-PPO mixture will be loaded into the AV via simple volume replacement (see Ch. 3 § 3.7). The pure scintillator phase will be broken into two separate studies: the first involving more background analysis in preparation for Te-loading, while the second, occurring after the $0\nu\beta\beta$ phase and the removal of Te from scintillator, will focus on low energy solar neutrinos. Solar neutrinos will provide a diverse study of properties, with a 50% fiducial volume cut and a lifetime of 1 year or more. Neutrinos from a stellar nucleosynthesis process within the sun in which carbon, nitrogen, and oxygen atoms partake (the CNO cycle) will allow physicists to resolve questions of solar metallicity, and direct measurements of proton-proton chain neutrinos allow for a luminosity constraint of the sun. The day/night asymmetry of solar neutrinos can confirm the MSW effects, and precision proton-electron-proton (pep) flux measurements
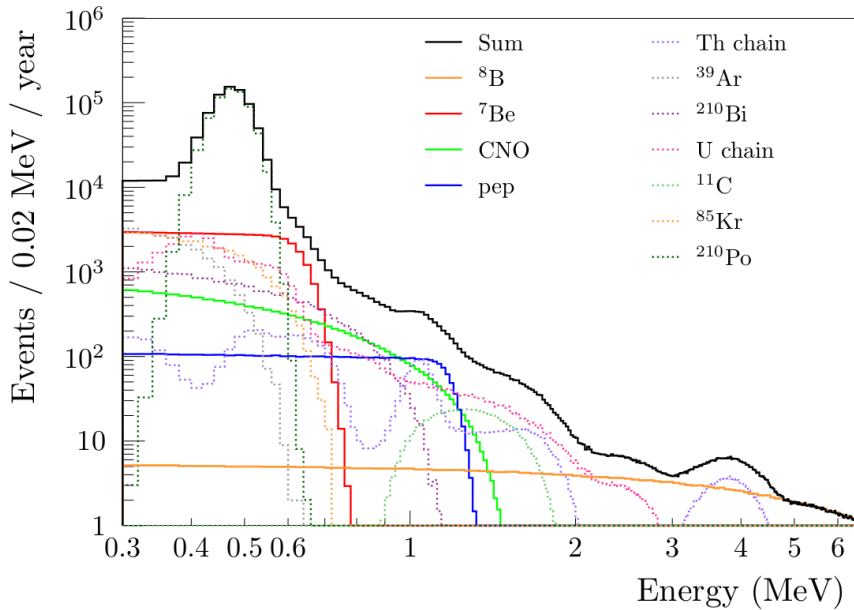
Figure 2.4: Expected ν_{solar} energy spectrum and backgrounds within SNO+ [63]. Background levels are explained in Ch. 3. This assumes a 400 Nhit/MeV light yield PMT efficiency, 5.5 m fiducial volume, and 95% reduction of ^{210}Po, ^{214}Po, and ^{214}Bi-Po via alpha and coincidence tagging.

22

Reaction	No. of Events
NC: $\nu + p \rightarrow \nu + p$	429.1 ± 12.0^a
CC: $\bar{\nu}_e + p \rightarrow n + e^+$	194.7 ± 1.0
CC: $\bar{\nu}_e + ^{12}\text{C} \rightarrow ^{12}\text{B}_{g.s.} + e^+$	7.0 ± 0.7
CC: $\nu_e + ^{12}\text{C} \rightarrow ^{12}\text{N}_{g.s.} + e^-$	2.7 ± 0.3
NC: $\nu + ^{12}\text{C} \rightarrow ^{12}\text{C}^* (15.1 \text{ MeV}) + \nu'$	43.8 ± 8.7
CC/NC: $\nu + ^{12}\text{C} \rightarrow ^{11}\text{C or } ^{11}\text{B} + \text{X}$	2.4 ± 0.5
ν-electron elastic scattering	13.1^b

Table 2.4: Expected supernova neutrino interactions within scintillator [63], assuming a SN at a distance of 10 kpc producing 3×10^{53} erg in the form of neutrinos, equally partitioned. Event rates do not assume flavour-changing mechanisms. Uncertainties only include those for cross-sections. ^{a}118.9 $\pm$ 3.4 above a trigger threshold of 0.2 MeV visible energy. ^{b}The Standard Model cross section uncertainty is $< 1\%$

and studies of the low-energy ^{8}B spectrum allow for a search of new physics, as this sensitive energy region involves research into sub-dominant effects in neutrino oscillations [63]. Figure 2.4 depicts the expected spectrum of solar neutrinos along with backgrounds.

During pure scintillator, SNO+ will continue the search for supernovae neutrinos as well as the study of reactor and geo-antineutrinos. Table 2.4 records the expected supernova (anti)neutrino interactions within SNO+ during the scintillator phase, assuming a supernova at a distance of 10 kpc which produces neutrino energies consistent with SN 1987A [73,74]. SN 1987A is still the only supernova to be detected and analyzed through its neutrino interactions within detectors, with a total of only 24 neutrino events observed [75]. SNO+ will be a promising experiment for the detection of neutrinos from a potential core collapse SN.

Figure 2.5 shows the expected antineutrino spectrum within SNO+. SNO+ is conveniently located
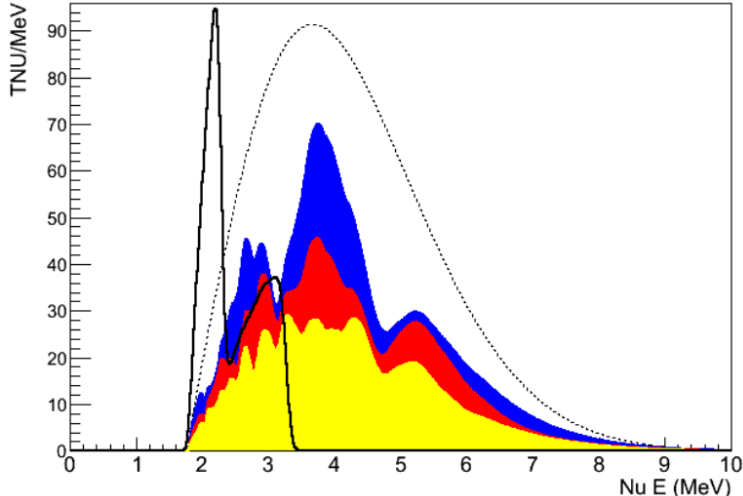
Figure 2.5: Expected visible antineutrino energy spectrum within SNO+ [63]. The geo- antineutrino spectrum (solid black) is arbitrarily normalized, and the non-oscillated reactor spectrum is the dashed line. Three oscillated reactor spectra are given: one 240 km away (blue), two approx. 350 km away (red), and all reactors (yellow).

.

near three reactors (Bruce, Pickering, and Darlington), which leads to a clear oscillation pattern of their antineutrinos and sensitivity in the oscillation parameter Δm_{12}^2 of 0.2×10^{-5} eV^2 in 7 years of data taking with scintillator [63]. Geo- antineutrinos are also of interest to SNO+ and will be detected by the same reaction, yet the reactor energy spectrum is known and extends up to higher energies than their geo- counterparts, and the time evolution of the reactors will help decouple the reactor and geo- antineutrino spectra [63]. Geoneutrino interactions within SNO+ will provide insight into the earth's composition of the mantle and crust, as the production of geoneutrinos depends greatly on the composition of the thick regional crust. Together with data from KamLAND [76] and Borexino [77], SNO+ will contribute in a global analysis of the Earth's processes and composition, which may explain the radiogenic heat flow of the Earth [63].

During the pure scintillator phases, the targeted internal ^{238}U content will be a thousand times less than it was during water phase. As it is necessary to monitor this content via ^{222}Rn assays for all phases of SNO+, an improved ^{222}Rn collection and assay system is currently under construction - see Ch. 4 for its present status.

2.3.3 Te-loaded Phases I, II

Once prepared for the double beta decay study, 0.5 % natural tellurium loading in the form of Te(OH)$_6$ will be added to the liquid scintillator with the use of a surfactant, making a tellurium-liquid scintillator (Te-LS) cocktail. As ^{130}Te is largely naturally occurring (34.08 % natural abundance), no refinement or enrichment is necessary before loading, although purification will occur underground to reduce and remove contaminant backgrounds. With a double beta decay Q value of 2527 keV located above many naturally occurring radioactive backgrounds, ^{130}Te is an excellent choice for underground experiments, for which SNO+ is developing a new scintillator metal-loading technique. If necessary, a second loading (phase II) is possible, increasing content up to 3% Te (8 tonnes of ^{130}Te) or higher, resulting in significant probing of the inverted hierarchy as demonstrated in Fig. 2.6. If a $0\nu\beta\beta$ signal persists after additional loading, the flexibility of SNO+ allows the removal of tellurium to verify the signal was indeed from ^{130}Te decay, and another double beta candidate can also be loaded for $0\nu\beta\beta$ signal observation at a different Q value. The versatility to quickly scale-up, unload, and reload with a different isotope is a strong capability of SNO+ which many other $0\nu\beta\beta$ detectors do not have.

When undergoing decay, ^{130}Te will emit two electrons which deposit their energy within the scintillator, producing photons. These photons will be detected via PMTs, and the charge and number of PMTs hit will be summed to reconstruct the energy of both electrons. The addition of the two electrons' energies will determine if the signal was the result of a $2\nu\beta\beta$ or $0\nu\beta\beta$ decay, the analysis of which occurs from spectrum
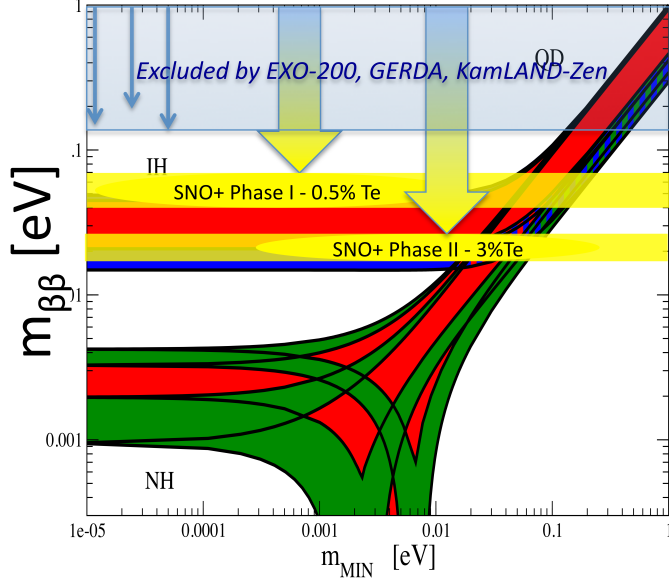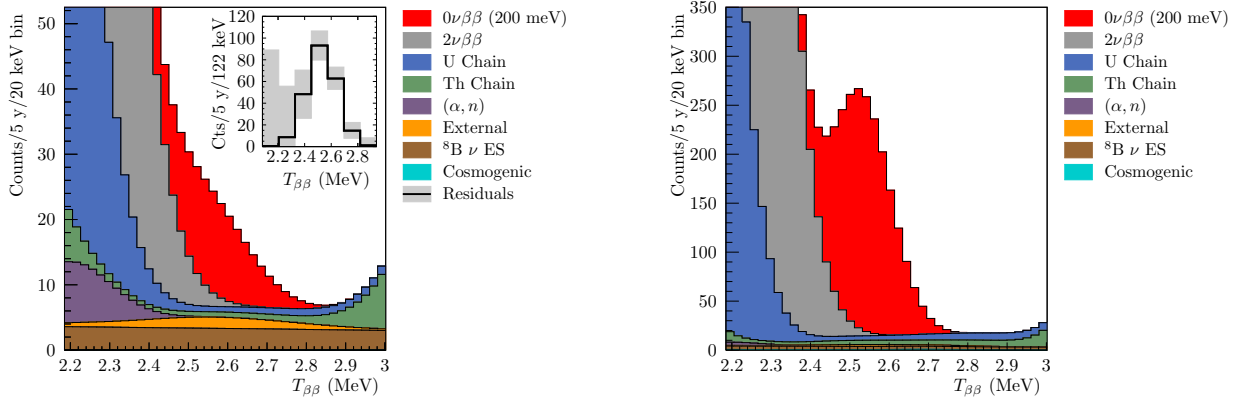
Figure 2.6: Experimental reach of previous $0\nu\beta\beta$ experiments probing the effective neutrino mass parameter (updated Fig. 1.7). Possible 0.5 % and 3 % Te-loading will make SNO+ a competitive experiment.

(a) SNO+ signal assuming 0.3 % Te loading, 200 Nhits/MeV light yield, and 5 years data taking [63].

(b) Preliminary SNO+ signal for 3 % Te loading and 450 Nhits/MeV light yield (assuming a PMT array upgrade) [78].

Figure 2.7: Hypothetical $0\nu\beta\beta$ signal (red) for ^{130}Te decay amongst backgrounds within the SNO+ detector. This assumes $m_{\beta\beta} = 200$ meV, a 3.5 m fiducial volume, and $T_{\beta\beta}$ is reconstructed kinetic energy of the event. If backgrounds are well-defined, the $0\nu\beta\beta$ signal notably improves with increased loading.

fitting (as opposed to an event-by-event basis). Fig. 2.7 indicates the anticipated $0\nu\beta\beta$ signal from ^{130}Te decay amongst backgrounds, of which the irreducible $2\nu\beta\beta$ background and ^{238}U-supported backgrounds are main contributors.

As with the other two phases, ^{238}U chain backgrounds will be monitored via *in-situ* Bi-Po signals (see § 3.3.2) and *ex-situ* ^{222}Rn assays of both the external water and internal scintillator, as described in Ch. 4.

25

If backgrounds from these chains are well defined, and purification techniques ensure the tellurium is significantly radiopure, dominant backgrounds for SNO+ will be from ^{8}B solar neutrinos, a background which allows sensitivity to scale with the amount of tellurium loading.

Chapter 3

Backgrounds in SNO+

3.1 Overview of Backgrounds

The interactions SNO+ is searching for are so rare that any low energy interaction has the potential to mask signals and set the trigger threshold above the detector's trigger. This deep underground, many cosmic ray-induced backgrounds are reduced (see § 3.2), and primary sources of background will be the beta and gamma rays produced from the decay of radioisotopes within the surrounding rock and detector components, namely the ^{238}U and ^{232}Th chains (see § 3.3), as well as ^{40}K (see § 3.4). Clean water surrounding the detector shields from rock contaminants, and all major detector components were chosen for low ^{238}U and ^{232}Th content, yet anything delivered underground to SNOLAB must first be transported on surface, where it is exposed to an increased level of cosmic rays, and then through the mine, where the exposure to mine dust is high if necessary precautions are not taken. Exposure at any time within the transport chain could lead to high levels of both internal and external background sources, in which an internal background is anything which occurs within the detecting medium (i.e. at a radial distance of 600 cm or less), and an external background is produced outside, but propagates into the detector volume.

This chapter introduces some of the abundant backgrounds which must be well-characterized and minimized within SNO+, and the processes undertaken to do so. Reduction of background is performed by a careful selection of materials, and specialized purification plants that are integral in removing impurities within cavity water, linear alkylbenzene, tellurium, PPO, and surfactant (see § 3.6, 3.7). Included within the existing cavity H_2O purification system and the nearly completed scintillator purification plant are assay systems for complete and regular monitoring of ^{238}U and ^{232}Th internal/external content. Determination of ^{238}U content via ^{222}Rn assays is thoroughly addressed in Ch. 4, wherein three similar radon sampling
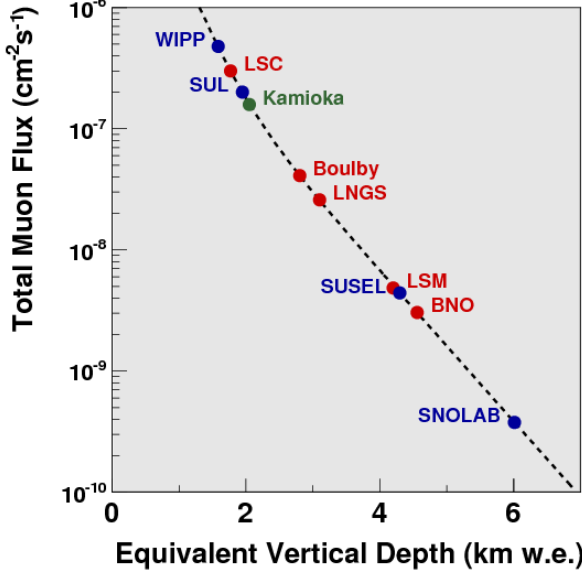
Figure 3.1: Muon flux vs. km water equivalency for underground laboratories [79,80]. The depth of SNOLAB provides a distinct advantage over competing detectors - SNO+ receives only 70 muon interactions per day.

units and the counting system are analyzed in detail. Further contamination of the AV is also due to ^{238}U progeny such as ^{210}Po further down the decay chain, which is fed by the decay of embedded ^{210}Pb just under the AV surface. The long half-life of this embedded ^{210}Pb results in disequilibrium with ^{222}Rn, requiring another technique to address these backgrounds. Monte Carlo simulations of ^{210}Po and other progeny assess expected backgrounds and lead to better decisions for data-taking, such as determining the fiducial volume or region of interest. Chapter 5 undertakes the task of analyzing Monte Carlo data of (α,n) backgrounds introduced by ^{210}Po during the water phase of SNO+.

3.2   Cosmogenics

SNOLAB is located 2 kilometers underground, resulting in high shielding against cosmic rays and a hardening of the resulting spectrum. With approximately 6000 meter-water-equivalency of rock shielding, cosmic rays are greatly reduced, resulting in a muon flux of 3.77×10^{-10} $\mu \cdot$cm^{-2} s^{-1} such that only about 70 muons interact per day within the detector [80]. High energy cosmic rays can interact with stable elements and produce a variety of unstable ones known as cosmogenics. Borexino (at Gran Sasso National Laboratory - LNGS) and KamLAND (Kamioka mine) are two underground detectors operating with liquid scintillator, yet both exist at depths which lead to increased levels of cosmic-induced backgrounds in comparison to SNO+ (see Fig. 3.1). The cosmogenic activation of atoms within the organic scintillators directly leads to internal backgrounds, eg. ^{11}C, which will be orders of magnitude less within the SNO+ detector.

Within the LAB+PPO cocktail specific to SNO+, most cosmic ray interactions will produce unstable isotopes with short half-lives. Vetoing the detector a few seconds after each cosmic muon will remove most events induced by these activated isotopes, including ^{16}N, ^{10}C, and ^{11}Be (half-lives of 7.13 seconds, 19.3 seconds, and 13.8 seconds, respectively), while ^{11}C (half-life of 20.3 minutes) can be reduced with a fiducial volume cut around the muon track. Yet ^{7}Be, with its longer half-life of 53 days, requires a different approach. As all detector materials, including the detecting medium, must be transported first on surface, there remains significant concern for cosmic ray exposure. The LAB in particular will be produced, transported, and stored on surface, before finally making its way underground, allowing for significant ^{7}Be production and accumulation due to its long lifetime. Once underground, the LAB will be circulated through a specifically designed purification plant (see Ch. 3.7) which will remove many cosmogenics, including ^{7}Be and other impurities.

R&D is also underway for tellurium transport, and once delivered underground the $Te(OH)_6$ will be dissolved in water, recrystallized, then rinsed with ethanol. The telluric acid will then be stored underground for at least a 6 month cool-down period before insertion into the detector, providing many cosmogenically activated isotopes the time to decay away [81].

3.3 Underground Backgrounds

The dominant backgrounds within SNO+ will come from the ingress and subsequent decay of radioactive materials from the naturally occurring ^{238}U and ^{232}Th chains present within the surrounding rock and some detector materials. Although possessing extremely long half-lives, ^{238}U and ^{232}Th eventually decay, resulting in the long chain of radioisotopes depicted in Figure 3.2. The levels of these isotopes determine many of the beta and gamma interactions within SNO+, requiring major components of the detector, especially the acrylic vessel, to be low in ^{238}U and ^{232}Th content. The bulk levels of ^{238}U and ^{232}Th within the AV are both < 1.1 picogram per gram of acrylic, and there are also approximately 9500 PMTs in the detector array, each with non-negligible radioactivity: 100 micrograms of ^{238}U and ^{232}Th content [44]. The PMT spacing of ~ 2 m from the AV is strategic and necessary, as well as the cool operational temperature of 12 °C to reduce their thermal noise rate (which drops from ~ 2.3 kHz at 20°C to 500 Hz at ~ 10°C [44]). In addition to selecting radiopure detector materials, via processes such as gamma ray or radon emanation measurements, ^{238}U and ^{232}Th backgrounds within the scintillator and cavity water will be purified and recirculated through dedicated purification plants as often as necessary, combating the emanation of backgrounds from materials and surrounding rock (see § 3.6 for UPW plant, § 3.7 for scintillator plant).

Th 234 · 24.1 d ← 4.270 ← U 238 · 4.47e9 y

0.273

Pa234* · 1.18 min · 4.7 h

2.195

Pb 214 · 26.8 min ← 99.98 % · 6.115 ← Po 218 · 3.10 min ← 5.590 ← Rn 222 · 3.824 d ← 4.870 ← Ra 226 · 1600 y ← 4.770 ← Th 230 · 7.538e4 y ← 4.858 ← U 234 · 2.455 e5 y

1.024 · 0.265 · 0.02 %

Tl 210 · 1.32 min ← 0.02 % · 5.617 ← Bi 214 · 19.8 min ← 99.9% · 6.874 ← At 218 · 1.5 s

5.489 · 3.272 · 99.98%

Hg 206 · 8.15 min ← 1.9E-6 % · 3.792 ← Pb 210 · 22.3 y ← 7.833 ← Po 214 · 162 micro-s

0.0635 · ~100 %

Tl 206 · 4.199 min ← 1.32E-4 % · 5.036 ← Bi 210 · 5.013 d

1.534 · 1.162 · ~100 %

Pb 206 · stable ← 5.407 ← Po 210 · 138.4 d

A=4n+2

BR α · Q α (MeV) — α — Z

Q β (MeV) · BR β — β

Ra 228 · 5.75 y ← 4.083 ← Th 232 · 1.405e10 y

0.0459

Ac 228 · 6.15 h

2.127

Pb 212 · 10.64 h ← 6.906 ← Po 216 · 0.145 s ← 6.405 ← Rn 220 · 55.6 s ← 5.789 ← Ra 224 · 3.66 d ← 5.520 ← Th 228 · 1.912 y

0.574

Tl 208 · 3.053 min ← 35.94% · 6.207 ← Bi 212 · 60.55 min

5.001 · 2.254 · 64.06%

Pb 208 · stable ← 8.954 ← Po 212 · 0.299 micro-s

Figure 3.2: Radioactive decay chains of ^{238}U (top) and ^{232}Th (bottom), with Q values and major branching ratios (if not ~100%). ^{238}U and ^{232}Th are naturally occurring within norite rock surrounding SNOLAB, leading to a long list of potential backgrounds. ^{222}Rn within the ^{238}U chain is particularly mobile and troublesome due to its gaseous form.

3.3.1 ^{232}Th chain

While excessive amounts of ^{232}Th can cause pile-up effects, the main concern comes from the radioactive progeny near the end of the chain, such as ^{208}Tl and ^{212}Bi. ^{208}Tl beta decays with a Q-value of 5.001 MeV, which crosses the ^{130}Te $0\nu\beta\beta$ peak and is a problem for any double beta decay experiment. Studies are underway for *in-situ* analysis which can identify and reject ^{208}Tl events by using an alpha-beta coincidence, as the parent, ^{212}Bi, would have undergone alpha decay to ^{208}Tl whose half-life is around 3 minutes. If instead ^{212}Bi were to beta decay (BR of 64%), a different background arises in the form of the ^{212}Bi beta spectrum, which has a Q value of ~2.2 MeV. This more recognizable event is followed 0.3 microseconds later by ^{212}Po decay, which emits an 8.8 MeV alpha. The combination of ^{212}Bi's beta followed shortly after by ^{212}Po's alpha, known as a Bi-Po event, is key for identifying and rejecting the combined event via coincidence timing.

In addition to *in-situ* measurements, *ex-situ* analysis on parent isotopes higher up in the chain (i.e. ^{224}Ra) will also be performed with the use of assay skids within the water and scintillator plants to sample the radioisotope (such as the process mentioned in § 3.7.5). Once collected, they can be taken to surface and counted within beta-alpha coincidence counters. A concern for SNO+ are also the leaching of backgrounds from the AV, but the solubility of ionic radium in aromatic solvents (i.e. LAB) is vanishingly small, so radium leaching into the scintillator is considered to be a very small background contributor.

The ^{232}Th chain may be in disequilibrium due to the long half-lives of ^{228}Ra and ^{228}Th, as well as the mobility of radium and polonium. Yet for convenience the radioactive content of backgrounds within this chain are stated as g ^{232}Th /g substance by assuming secular equilibrium within the chain. Such an assumption leads to an expected 3 counts per day (cpd) of ^{208}Tl and other ^{232}Th-induced backgrounds within scintillator.

3.3.2 ^{238}U chain

As with ^{232}Th, troublesome isotopes from the ^{238}U chain do not occur until much further down the chain, and the long half-lives of some of isotopes (i.e. ^{234}U, ^{230}Th, ^{226}Ra, and ^{210}Pb) and the mobility of ^{222}Rn can lead to disequilibria within the chain. Regardless, g ^{238}U /g substance levels are still quoted, and the natural presence of ^{238}U (half-life of 4.47×10^9 years) within norite rock can still cause pile-up effects with its decay inside SNO+. A target level of ~10^{-17} g ^{238}U/g LAB leads to about 9 cpd in the radioactive chain of ^{238}U.

^{222}Rn

A universal concern for most underground detectors is the behaviour of ^{222}Rn within the ^{238}U chain. Radon is a heavy, chemically inert gas, but radioactive in nature: all 39 known radon isotopes, only two of which are naturally occurring, are unstable and decay. The gaseous state of radon provides a mobility that is a hazard to experiments, but opposed to ^{220}Rn (half-life of 56 seconds) within the ^{232}Th chain, ^{222}Rn has a longer half-life of 3.8 days, meaning it can traverse further distances and be completely independent of its parent within a local region. The alpha decay of ^{222}Rn is not not a direct background within SNO+, but its ability to travel significant distances before its decay could allow for a large ingress of radioactive daughter isotopes within the ^{238}U chain if substantial precautions are not undertaken. A significant disequilibrium within the ^{238}U chain is anticipated due to its highly unrestricted movement.

Fed by the surrounding rock and mobile due to its gaseous state, radon levels underground are significantly higher than above ground. SNOLAB regularly monitors the ^{222}Rn content in various locations, and a combined concentration level of 3.54 ± 0.18 pCi/L (131.0 ± 6.7 Bq/m^3) [82] is currently reported, which is approximately 10 times higher than levels above ground (typically 0.1 pCi/L on surface). Coupling the high radon concentration with good mobility allows for a high probability of decay inside detector volume, if a number of precautions are not taken. These precautions include the use of nitrogen as a cover gas as described in § 3.5, the water and scintillator purification facilities (§ 3.6 and § 3.7, resp.), and careful selection of detector materials. Several radon collection systems (see Ch. 4) will assay radon from various components of the SNO+ detector, including the liquid scintillator, cavity water, and cover gas system.

^{214}Bi

The first significant background within the ^{238}U chain which could severely limit the sensitivity of $0\nu\beta\beta$ measurements is the beta decay spectrum of short-lived ^{214}Bi, an isotope with half-life of $\sim$20 min. and Q value of 3.27 MeV, resulting in a spectrum which crosses the ^{130}Te endpoint. Yet ^{214}Bi will undergo beta decay with a branching ratio of over 99.9 % to ^{214}Po, which then undergoes alpha decay with a half-life of 164 microseconds, emitting a 7.7 MeV alpha. These Bi-Po coincidence events will be tagged within the detector with high efficiency and used *in-situ* to determine the background levels of these isotopes and thus estimate ^{222}Rn content by assuming equilibrium within the decay chain. With this tagging technique, the ^{214}Bi events can be mostly removed from the data.

^{210}Pb

After SNO was drained in 2008, modifications to the detector for SNO+ began. Yet for about five years the detector sat in open mine air, allowing the ingress and decay of ^{222}Rn atoms to implant many troublesome daughter isotopes within the SNO+ detector components. The majority of these radioisotopes have short half-lives and are of no major concern to SNO+ once the detector is filled and running again, but ^{210}Pb is one particularly long-lived daughter which can act as a new source of internal backgrounds within the AV [83]. There is expected to be a build-up of ^{210}Pb just below the AV surface, and leaching models have been calculated to anticipate levels of ^{210}Pb leaching into the scintillator [83, 84]. During the phases prior to $0\nu\beta\beta$ research, scintillator and water purification will be crucial to extract such leached isotopes. When ^{210}Pb decays its daughters can interact with a variety of molecules, both inside the AV and out, to produce additional backgrounds. As with ^{222}Rn, disequilibrium in the chain is possible due to long half-life and build-up of ^{210}Pb on the AV.

^{210}Bi, ^{210}Po

^{210}Pb will eventually decay by beta emission to ^{210}Bi, which then beta decays into ^{210}Po. These isotopes are direct backgrounds for the SNO+ solar neutrino studies, for example the ^{210}Bi decay spectrum is similar to the CNO neutrino spectrum. Characterizing the timing of these isotope decays may result in rejecting the background: the characteristic signal would be the 5.30 MeV alpha from the ^{210}Po. Yet studies would depend on whether or not Po leaching occurs from the AV, and if ^{210}Po (half-life of 138 days) is even in equilibrium with ^{210}Bi. If the activity of ^{210}Po does not increase over time, the amount of ^{210}Bi can be constrained, and studies demonstrate that if this is possible, then the ^{210}Bi spectrum can be distinguished from the CNO neutrino events. Yet Po could possibly "plate out" into the inner surface of the AV, in which case the radial profile of Po decays and the contribution of Po from the AV would change over time. A second resolution in determining ^{210}Bi and ^{210}Po content within the scintillator may be possible with radium assays within the scintillator plant (see § 3.7.5).

(α,n) Reactions

SNO+ is also concerned with alpha-n (α,n) reactions from ^{210}Po decays:

$$^{210}\text{Po} \rightarrow \,^{206}\text{Pb} + \alpha \,(5.3 \text{ MeV}) \tag{3.1}$$

The alphas from this decay can have enough energy to interact with atoms such as carbon within the AV or scintillator to produce neutrons and gammas. For example:

$$\alpha + {}^{13}\text{C} \rightarrow n + {}^{16}\text{O} + \gamma \, (\sim 6 \text{ MeV}) \tag{3.2}$$

The product of Eq. 3.2 are many more backgrounds: e.x. the neutron can mimic antineutrino signals, the gamma produced from neutron capture, $n + p \rightarrow d + \gamma \, (2.223 \text{ MeV})$, will be another $0\nu\beta\beta$ background, and the 6 MeV gamma may be a background for nucleon decay analysis. Ch. 5 introduces the possible (α,n) interactions within SNO+ and analyzes Monte Carlo simulations of Eq. 3.2 for water phase data taking.

3.4 Miscellaneous Radiation

Radiation from cosmogenics and the ${}^{238}\text{U}$ and ${}^{232}\text{Th}$ chains are by far the largest contributors to backgrounds within SNO+. Nevertheless, all possible backgrounds must be considered, which include the possibility of pile-up events from other radioactive sources. To avoid pile-up, ${}^{39}\text{Ar}$ (half-life of 269 years) and ${}^{85}\text{Kr}$ (half-life 10.8 years) impurities within the detector must each be limited to less than 100 counts per day. The cover gas system (see § 3.5) helps to keep these reduced, and the various processes within the water and scintillator plants (§ 3.6, 3.7) aid in removing any of these contaminants. ${}^{40}\text{K}$ impurity levels, meanwhile, must be at a limit of 1.3×10^{-18} g/g, leading to about 23 counts per day. These impurities have also been considered when designing the scintillator purification plant.

3.5 Nitrogen Cover gas

As mentioned in Ch. 2 § 2.1, nitrogen gas is chosen over typical lab air as the "breathing" mechanism known as the cover gas. Due to the naturally high background levels within lab air, particularly radon gas as mention in § 3.3.2, lab air is not a suitable choice, and thus the cover gas system must also protect the detector by shielding it from the high concentrations of contaminants within mine air. At the top of the AV exist three low-background bags which empty or fill with nitrogen gas depending on the pressure requirements, ensuring the difference in pressure between the AV and on deck remains small. If more gas is needed, the system pulls from the boil-off of liquid nitrogen held within a nearby dewar, and a relief system in the form of a U-trap exists if the pressure within the bags becomes too great. Gas flow in the opposite direction through the U-trap is impossible, as on the other side of it is the cavity cover gas system, which is also protected from the mine air by a buffered volume with slow purge open to mine air. As the AV requires

the purest nitrogen gas, nitrogen may leave through the U-trap to enter the cavity, but flow in the opposite direction cannot occur as it would introduce higher-contamination nitrogen.

Unfortunately, radon is also highly soluble within the linear alkylbenzene, with a Henry coefficient of $k_H \sim 11$ atm/mf [85]. In studying the effectiveness of the cover gas system, one notes that the volume partition fraction of Rn for LAB/N_2 is 7.7; about 87% of the Rn which leaks into the N_2 cover gas is expected to dissolve into the scintillator [85,86]. Rn is more soluble in LAB than in D_2O, yet SNO+ aims for purity levels that are ~ 100 times better than in SNO. This in turn makes designs of the new cover gas system and scintillator purification plant critical, as well as studies for how often the entire LAB volume should be recirculated. Even with nitrogen protecting the scintillator and water, small traces of the surrounding impure gases will enter the cover gas over time and diffuse into scintillator, requiring recirculation of water and scintillator through their respective processing plants (see § 3.6 and § 3.7, resp.). Chapter 4 notes on how to measure radon levels within the cover gas, water, and scintillator.

3.6 Ultrapure Water Purification Plant

The majority of underground backgrounds emanating from the rock within the cavity walls, or from the PSUP, PMTs, or outer AV surface, are stopped or slowed down by filling the cavity with ultrapure water processed within the SNOLAB UPW plant inside the utility room underground. 5300 tonnes of water will exist between the cavity wall and PSUP, and 1500 tonnes between the PSUP and the AV, with regular recirculation through the water treatment plant to remove backgrounds. The water path from Vale's water line through the UPW plant to the SNO+ cavity is described briefly below and also outlined in Fig. 3.3. Water enters from Vale's lines and into a pretreatment area, where it passes through microfiltration units, an activated charcoal filter, zeolite softener, and reverse osmosis (RO). Now clean enough to enter the purification and recirculation system, organics are broken apart by UV lights (at a wavelength of 185 nm), and the organic compound products are removed with ion exchange columns. A large process degasser (PDG) strips the water of all gasses, including Rn, Kr, Ar, and O_2, and removing the latter also reduces biological growth. As the PMTs do not operate well within degassed water, the water is then regassed with N_2 before passing through filters and then another set of UV lights operating at 254 nm to act as another biological sterilizer. The water then enters a heat exchanger which removes process heat and reduces the water temperature to ~ 12 °C before it enters the SNO+ cavity via piping into the area between the PSUP and the AV, where the cleanest water is required. There also exists a chilling loop which only sends the water through filters and is meant to continuously cool the cavity water. The low temperature within the water aids in sufficiently limiting the biological activity within the cavity while keeping PMT noise rates at
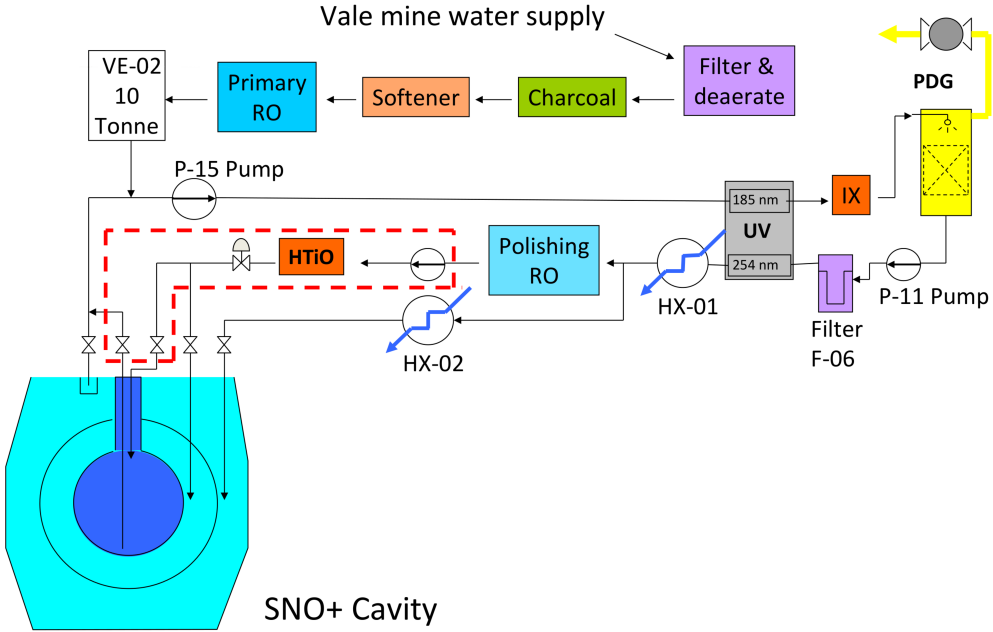
Figure 3.3: UPW processing plant flow diagram [87]. Water enters from Vale lines, undergoes several different treatments, and is finally pure enough for admission into the SNO+ cavity. Recirculation of cavity water will also occur for ^{222}Rn assays via MDG (monitor degasser) system, which is not depicted in the diagram.

an acceptable level.

Through recirculation there exists the possibility to sample water from different cavity locations via assay and extraction systems. HTiO columns assay the water for ionic heavy metals such as Ra, Th, and Pb, while a monitor degasser (MDG) unit from SNO is being recommissioned. The latter system, described in more detail in Chapter 4, extracts ^{222}Rn from the water and sends it through a series of traps to be compressed inside a counting cell for sampling.

For external backgrounds within the ^{238}U and ^{232}Th chains, as well as internal backgrounds during water phase, SNO+ assumes similar levels as achieved in SNO [72], as most major materials (PMTs, PSUP, etc.) and the water purification plant remain the same. However, the D$_2$O plant used for internal purification within SNO has been replaced by the scintillator plant, requiring the use of the H$_2$O plant to purify the internal AV water during water phase. Estimations based on this change result in limits of 3.5×10^{-14} g ^{238}U/g H$_2$O and 3.5×10^{-15} g ^{232}Th/g H$_2$O [63], as opposed to the SNO internal levels of 6.63×10^{-15} g ^{238}U/g H$_2$O and 8.8×10^{-16} g ^{232}Th/g H$_2$O [72]. Assuming the same external levels as SNO's NCD phase, SNO+ expects 3.5×10^{-13} g ^{238}U/g H$_2$O and 3.0×10^{-14} g ^{232}Th/g H$_2$O.

3.7 Scintillator Fluid Handling System and Loading Plan

3.7.1 Scintillator Loading

Scintillator is replacing the D_2O as the detecting medium, and as such a completely new fluid handling and purification system is required. The handling system consists of the surface transfer facility (STF), underground transfer facility (UTF), storage facility (two 60 tonne underground storage tanks), deck valve cabinet (for AV flow control), and the underground purification plant within the SNOLAB utility area. Figure 3.4 outlines the major components of the handling system [85, 86].

The loading plan for scintillator filling has been designed to minimize exposure to contaminants, namely from cosmic rays on surface and mine air while underground, by optimizing transfer times and avoiding contaminant ingress. Linear alkylbenzene will be transported 850 km from Bécancour, QC, to the STF at SNOLAB via 22 tonne road tankers 3 times a week, where it will be unloaded and stored (during the morning) in the 70 m^3 buffer tank on surface until Creighton mine's cage is available for transport down to the 6800 level. A two-way pumping system of the STF allows for receiving the tanker truck load while subsequently filling the 6 stainless steel railcars for transport to SNOLAB underground. Calculations of fill time for AV loading are an estimated 12 weeks, the restriction of which comes from the the transport availability of the railcars from the STF to the UTF. The cage schedule will allow each railcar (each with a volume capacity of 2.2 tonnes) to be transported from surface to underground (and back again) once per day, which corresponds to 13 tonnes/day, or roughly 66 tonnes/week on a five-day schedule (possibly 79 tonnes/week with an extra day). Railcars are expected to take the night cage down (between 6 and 10 pm), and will be transported through the drift to be unloaded between 10 p.m. and 2 a.m. at the UTF, which is located within SNOLAB's "car wash" station (the ingress point for materials entering the underground lab). From the UTF the LAB is transported via piping into the 60 tonne storage tanks within the utility room near the scintillator plant. During scintillator and Te+LS loading, concentrated solutions of PPO+LAB and Te+LS can also be stored within one of the 60 tonne tanks, and blended in when required. LAB will be pulled from the storage tanks and through the underground purification plant, blending in the concentrated solutions and purifying the cocktail at an initial flow rate up to ∼19 LPM, which is due to the limited power and cooling available for the distillation process.

Once purified, scintillator is sent along piping to the AV, which will still be full of water while the first loads of LAB are arriving (data taking in water phase). For better control, the AV will be filled via volume displacement with water; scintillator enters from the purification plant through the AV's top pipes and the denser water is pumped out through the bottom ones. This effort is much safer than immediate scintillator filling as it prevents potential LAB fumes (which could have occurred from air-filling and possibly lead to
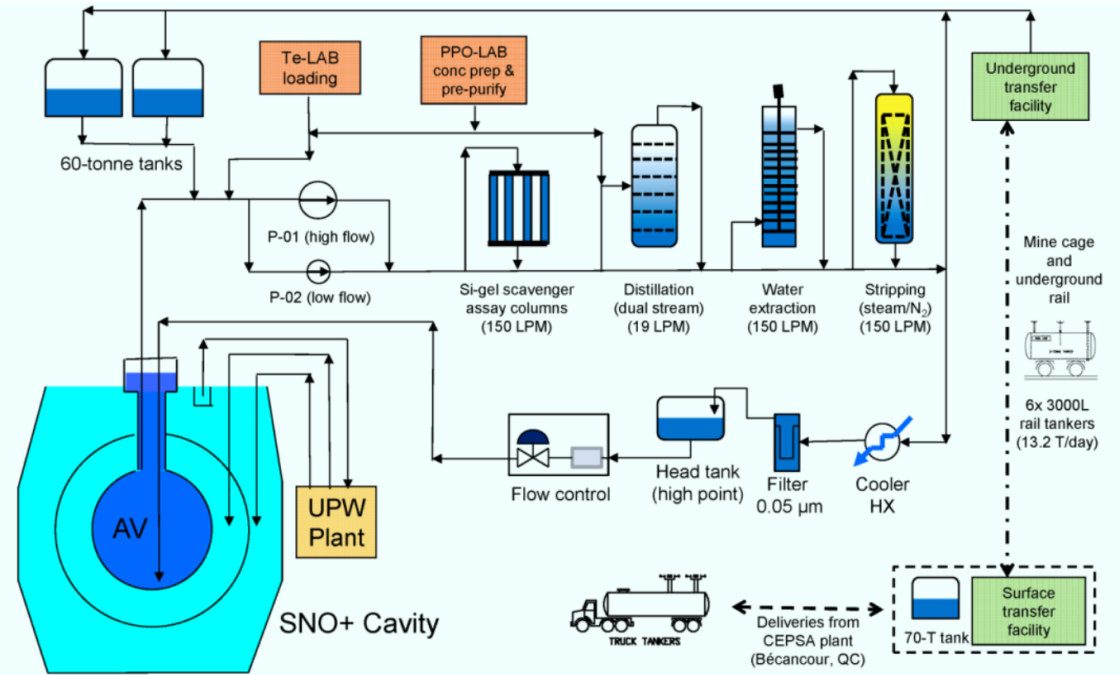
Figure 3.4: Scintillator fluid handling and processing flow diagram [85]. LAB is transported to SNOLAB surface via road tanker, underground via railcar, and enters the processing plant for purification before entering the SNO+ AV. Coupled to the gas output of the steam stripping column is a ^{222}Rn assay skid not portrayed in this diagram.

combustion within the AV), requires considerably less effort from the cover gas system to maintain a proper pressure during the large changes in volume (and thus increased safety against contaminated mine air), allows for better level and AV buoyancy control, and permits data taking while filling.

3.7.2 Underground Scintillator Plant

As with the water purification plant, the purpose of the newly built scintillator plant, represented in Figs. 3.4 and 3.5, is to purify the scintillator both before it enters the detector and during recirculation as necessary. Scintillator is purged of various contaminants with a collection of different purification columns, including distillation (§ 3.7.3), solvent-solvent extraction (§ 3.7.4), metal scavengers (§ 3.7.5), and a steam stripping (§ 3.7.6) column. The steam stripping column will also be coupled to a radon assay skid (currently under construction) for measurements of radon content within scintillator (see Ch. 4). During the distillation process, there is the potential to heat LAB above the flash point (130 °C), and for this reason a firewall surrounds the scintillator purification plant as a necessary precaution against any fire hazard the LAB might present.

In limiting the internal backgrounds during scintillator phases, SNO+ can build on the experience of both Borexino [89] and KamLAND [90]. SNO+ intends on matching the cleanliness and vacuum-leak tightness
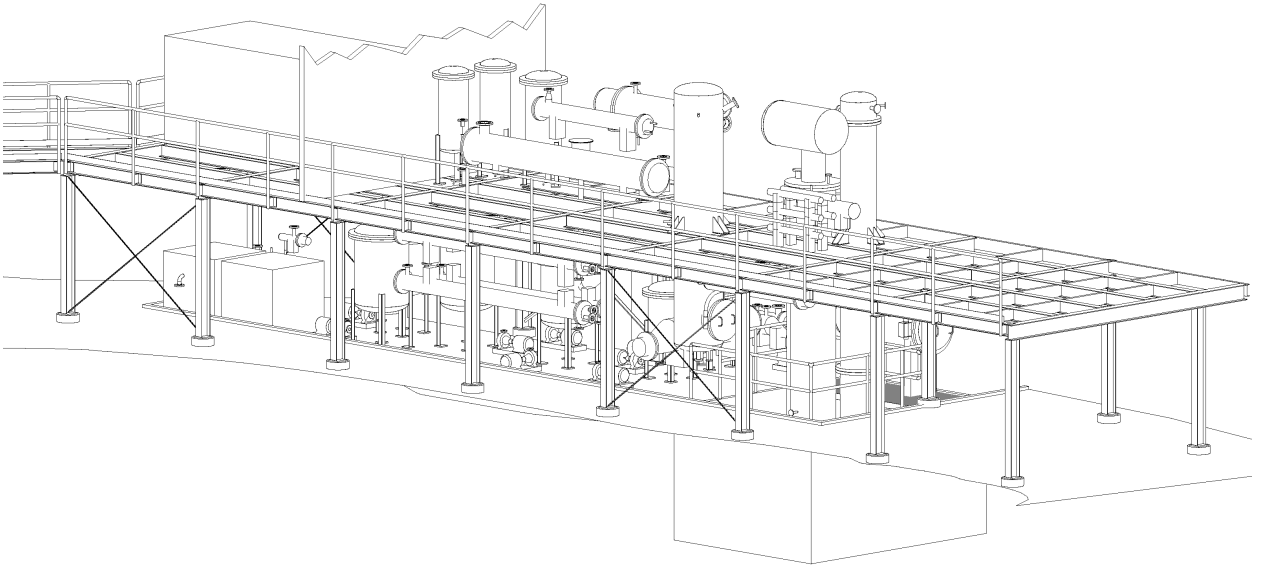
Figure 3.5: Visualization of the SNO+ underground scintillator plant, within the space left when SNO's D_2O purification plant was removed [88]. A pit has been excavated in the floor to fit the tall purification columns.

of Borexino, which is reasonable given the same engineering company was used to design the purification columns. This would result in SNO+ internal background levels of 10^{-17} gU/g LAB and 10^{-18} gTh/g LAB, which was achieved by KamLAND [90]. The introduction of Te, water, and surfactant required to load the scintillator with tellurium adjusts the ^{238}U and ^{232}Th chain limits to 2.5×10^{-15} gU/g LAB and 2.8×10^{-16} gTh/g LAB, respectively, due to the decrease in purity [63].

Initially, the PPO wavelength shifter, a solid at room temperature, will be prepared as a concentrated solution of 120 g/L via nitrogen-purged hopper into LAB within a mix tank under a nitrogen cover gas. PPO tends to have a large ^{40}K contamination, requiring the solution to undergo purification before it enters the AV; this concentrated solution will be distilled within a single-stage kettle parallel to the distillation of arriving LAB. After distillation, the two will be combined and the resulting scintillator cocktail will undergo steam stripping. Once purified, scintillator is reduced to 12 °C to match the cavity UPW temperature necessary for minimizing PMT noise and preventing biological activity, and enters the AV.

While SNO+ is actively running with scintillator (either pure or in Te-LS form), online purification will occur at high flow rates, ensuring the quality of scintillator is meeting required purity levels and dealing with any unanticipated experimental needs or contamination vectors. Recirculation of the scintillator is expected to flow at approximately 150 LPM, which is determined by desiring a full AV volume (910 m^3) turnover within a 100 hour period. A full turnover in roughly 4 days is required for successful assays of ^{224}Ra and ^{222}Rn (half-lives of ∼4 days) within the full AV volume, the desire to minimize mixing of repurified and unpurified

39

scintillator within the AV, as well as the Creighton mine schedule - SNOLAB is cleared once per week for Vale blasting and start-up/shut-down timescales of the plant must be considered. During recirculation, the scintillator can be sent through the distillation, solvent-solvent extraction, metal scavenger process, and steam stripping column as desired. After Te-LS loading during double beta phase, ideally recirculation is never required, but if necessary the cocktail can undergo steam stripping, during which ^{222}Rn assays will be performed. Once SNO+ is finished, the scintillator will be unloaded from the AV via volume replacement with water, and the plant will remove Te and PPO from LAB.

The target level of 10^{-17} g/g within the ^{238}U chain, along with the ingress of ^{222}Rn ($\sim$130 Bq/m^3 within SNOLAB air), sets the leak-tightness requirement of 10^{-6} mbar·L/sec [86], which also meets the Kr and Ar limits. As some purification loops within the plant could have up to 100 of a combination of fittings, valves, etc., general leak-tightness specifications are 10^{-9} mbar·L/sec per piece, such that the overall leak-tightness can be comfortably met. The limit can be relaxed in certain cases, including columns, pumps and control valves, which have limits of 10^{-8} mbar·L/sec. 10^{-9} mbar·L/sec is reasonable, as this is typical for high-vacuum components. Metal diaphragm or metal bellows process side hand valves consistently demonstrate this leak-tightness. A large helium leak checking operation was undertaken to verify leak tightness of the entire plant.

Main recirculation lines are up to a maximum of 2 inch outer diameter 316L stainless steel, which has been electropolished internally and pre-cleaned for high-purity applications. Most materials within the scintillator plant are 316L stainless steel, PTFE, or glass, all of which have shown to be compatible with LAB and can be manufactured to the required cleanliness and smoothness levels required to limit radon and Th, U accumulation due to surface structure and porosity. The plant is constrained to fit inside the existing space left by the D$_2$O plant, which is a two level mezzanine of 3 m high (bottom) and 2-3 m high (top level), the variation in height due to rock cut of the lab. Yet the purification columns required significant overhead, so a 2 m deep pit was cut into the floor of the first level, for the columns. The area of both levels are approximately 15.3 m x 4.6 m.

3.7.3 Distillation

The primary LAB purification column is a 4.4 m high fractional vacuum distillation column with six stages. It can be operated at 1000 kg/hour scintillation feed, 238 °C, and 55 Torr vacuum. The multi-stages and refluxing allow for finer separation of volatility, resulting in an exceedingly pure product. 55 Torr vacuum ensures the column will be safely operated at a temperature less than the atmospheric boiling point of LAB (278-314 °C), which is above the flash point. Due to time-consuming startup/shut-down times, it is best to
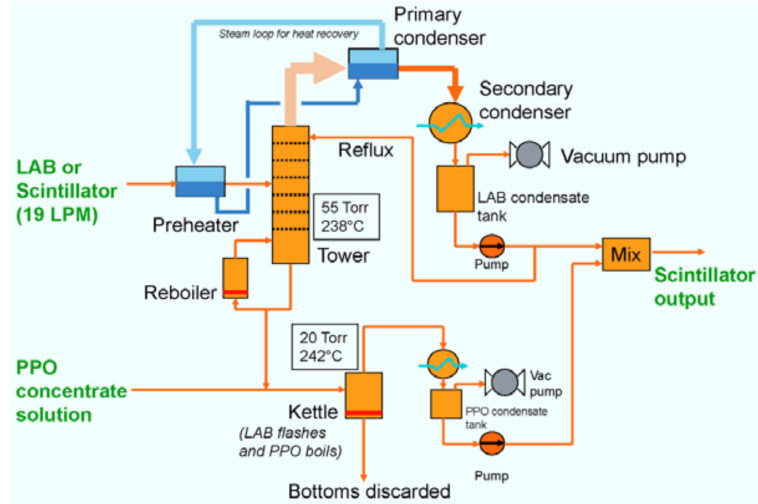
Figure 3.6: Simplified distillation process of SNO+ scintillator [85]. During filling, the column will process pure LAB and the kettle will process concentrated PPO+LAB, then the two are blended together. During recirculation the column will extract PPO into the bottoms, which will be fed into the kettle for PPO recovery.

run 24 hours/day, stopping only during Vale blasting. A simplified flow diagram of the distillation process is given in Fig. 3.6.

Distillation itself is a well known and proven technique in which heat will vapourize a solvent (in this case the LAB) which then condenses into a product at the condenser. Lower volatility (i.e. higher boiling point) materials will remain within the evaporator, and the component of these known as the bottoms will contain contaminants to be discarded. As SNO+ is primarily concerned with many heavy metal radioisotopes which have low volatility, the distillation process is important for removing dust residue, cosmogenic contaminants, and radiochemical components, i.e. ^{7}Be, Pb, Th, U, Ra, Po, Bi, and K. The distillation process is also invaluable for photon detection as it improves the optical transparency of LAB by removing impurities in the form of partially oxidized organic molecules, which also possess lower volatility compared to LAB. The main distillation process was designed for 99% removal of PPO, which will eventually be required at SNO+ decommissioning. Yet the column can be operated online during detector operation, as the tower bottoms is sent to a single-stage kettle operated at 20 Torr and 242 °C. The kettle will initially distill the concentrated PPO+LAB solution in parallel with the LAB, and can be reused during recirculation by processing the column's bottoms. After the dual-stream distillation process of LAB and PPO, the feeds from both column and kettle are combined as scintillator output and sent through the rest of the scintillator plant.
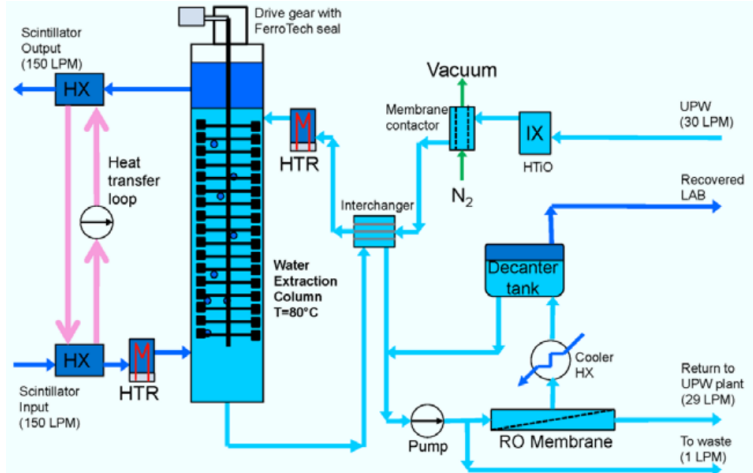
Figure 3.7: Simplified flow diagram of the solvent-solvent extraction process for SNO+ scintillator [85]. Scintillator enters the bottom and water enters the top of the column, the two are mixed with agitating impellers and the exchange of ionic substances from scintillator to water occurs. Scintillator then leaves at the top of the column while water exits at the bottom and is sent through a recovery system.

3.7.4 Solvent-Solvent Extraction with Water

The solvent-solvent extraction with water (commonly referred to as water extraction) is performed within a 5.6 m high SCHIEBEL® column [91] featuring a rotating impeller stack with 30 rotating stages and baffle plates. Operated during recirculation, it is anticipated to run at 80 °C, 150 LPM scintillator feed, and 30 LPM ultrapure water flow rate, the latter of which is limited by the SNOLAB UPW output rate of 130 LPM (the majority of which will be spent purifying water within the SNO+ cavity). The lighter scintillator will enter the bottom of the column and is forced up the column by pump pressure, while the heavier UPW will enter the top and flow downwards due to gravity, countercurrent of LAB. The extraction process of the column is based off the differences in solubility between water and organic scintillator: while LAB is non-polar and immiscible within water, many ionic metal contaminants (K, Ra, Bi, U, Th, some Po) are polar and effectively pulled from the LAB and into water. Po and ^{212}Pb are not completely extracted, as they are believed to form organometallic molecules within the scintillator, yet ^{224}Ra is very effectively removed with this column. The process is intended primarily for removing backgrounds from AV leaching and plate-out. Output water will be pre-cleaned for re-entry into the UPW plant and for the recovery of LAB collected within the water. The process within the column is also effective for removing Te (or Nd, another double beta candidate) from the scintillator at the end of the double beta phase. A simplified flow diagram of the solvent-solvent extraction process is given in Figure 3.7.
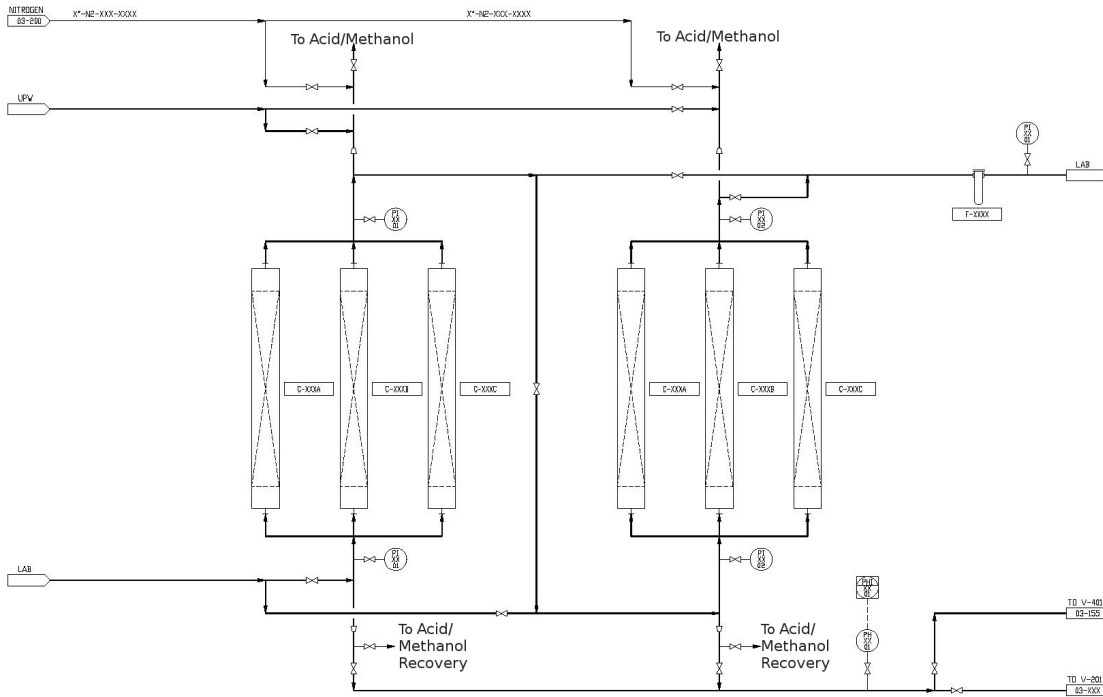
Figure 3.8: Metal scavenger columns flow diagram adapted from [92]. Each column is packed with QuadraSil™ AP beads for the removal of ionic compounds.

3.7.5   Metal Scavengers

There are 6 metal scavenger columns within the scintillator plant, each with a 15.2 cm diameter and 5.1 m height, which together have the capability of processing the scintillator at 150 LPM during recirculation. Figure 3.8 is the flowsheet concerning the arrangement of the columns. These columns will be loaded with QuadraSil™ AP beads [93], a porous, silica-based product with an aminopropyl functional group known to remove a select variety of metals. Highly effective in removing Pb and Ra, these columns will act as a complementary process to the solvent-solvent extraction and remove many metallic contaminants, including the organometallic compounds which the other extraction is ineffective against. Metal scavenger columns have been designed to operate in two banks of three, and even if half-filled, the ^{212}Pb and ^{210}Bi removal efficiency is over 90%. Flushing the columns with HCl removes collected backgrounds from the QuadraSil™ AP beads, and once acid stripped, the columns can be regenerated with UPW and methanol for re-use.

A chemical recovery system can also collect the HCl product, permitting an *ex-situ* background analysis of scintillator through the assaying of ^{224}Ra and ^{226}Ra. Bi-Po events from collected contaminants can be counted within custom beta-alpha coincidence counters, which have sensitivity better than 10^{-16} g/g. The counters can determine ^{238}U content through the collection of ^{226}Ra and counting ^{214}Bi fed β-α events, along with simultaneous ^{232}Th determination via collection of ^{224}Ra and recording ^{212}Bi fed events. The eluate

could also be fully reduced and evaporated for alpha counting: with more than four months of counting time fits could separate ^{210}Po decays from the "grow in" of ^{210}Bi, potentially resolving the CNO spectrum mentioned in section 3.3.2 [86].

3.7.6   Gas Stripping

The column which will always operate as the last major purifier before AV entry is C-300, a packed, 24 inch diameter, 24 foot (7.6 m) tall gas stripping (degasser) column packed with 19 structured packing elements, each of which has a surface area of 500 m^2/m^3. The tower will be operated during initial purification of scintillator and with recirculation of LAB+PPO and/or Te-LS as the process does not remove either PPO or Te from scintillator. The science behind C-300 is a mature industrial process which has been verified to work in a large variety of systems, including Borexino and SNOLAB's water purification plant. Such a column is typically used for removal of O$_2$, but SNO+ also requires the extraction of noble gases Rn, Kr, Ar, all of which have yet to be directly addressed within the processing plant.

Similar to the water extraction process, the gas stripping column also operates by providing several equilibrium phases between the scintillator and a cleansing medium, in this case a purge gas composed of nitrogen and steam. The gas flows upward through the column and exits near the top, while scintillator enters at the top of and disperses over the large surface area of the packing material, eventually exiting at the bottom. The fine spray of scintillator and large surface area leads to a substantial number of equilibrium stages for partitioning between the scintillator and gas, though if operated under vacuum this drops to only a small number. The removal efficiency of gas from the scintillator depends on Henry coefficients; the solubility of a gas within liquid is directly proportional to the partial pressure of that gas while held in equilibrium with the liquid. An extremely low partial pressure of radon and other contaminant gases within the purge gas is obtained by a continuous stream of pure nitrogen and steam. This ensures Rn, Kr, Ar, and O$_2$ within the scintillator are constantly removed from the scintillator and into the purge gas.

Borexino used a similar, smaller column, running with a liquid feed rate of 17 LPM (vs. recirculation within SNO+ of 150 LPM). Their column operated with a chosen nitrogen gas known to be low in krypton and argon which was sent through a radon absorption plant before use within their degasser [94]. SNO+ is limited by the difficulty in shipping large quantities of liquid nitrogen underground, and will resolve this by using a combination of N$_2$ and steam, the latter of which comes purified from the UPW plant underground. If necessary the column can operate with only steam and vacuum, or vacuum only, but the number of effective stages is reduced at low pressure. The gas flows are adjustable, with a steam flow of 0-10 kg/hour and nitrogen flow of up to 3 kg/hour. A temperature of 100 °C and 150 Torr vacuum will ensure scintillator
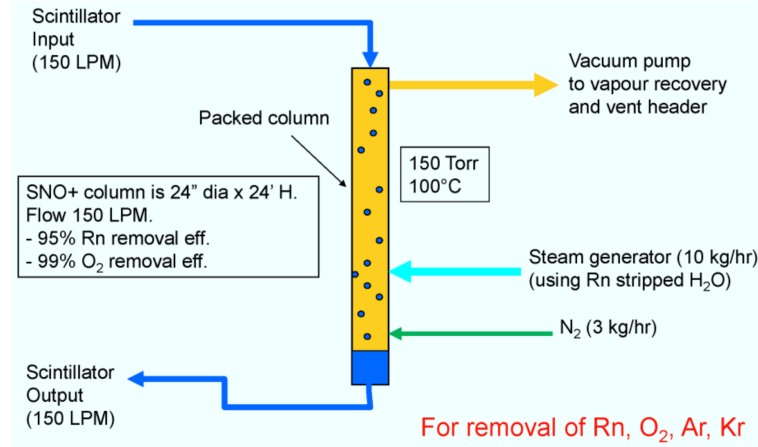
Figure 3.9: Simplified gas stripping process of the SNO+ scintillator plant [85]. Scintillator enters the top and is sprayed as a fine mist over packing material for increased surface area, while UPW steam and N_2 enter the bottom and flow up. Exchange of gas occurs at the boundary between scintillator and stripping gas due to the partial pressures of gases. Gas output of this column is coupled to a radon assay system for sampling internal ^{222}Rn levels.

humidity, effective stripping efficiency, and ensure the steam remains superheated and dry, preventing water saturation within the scintillator. This stripping column has been designed to remove better than 99 % O_2 and better than 95 % Rn from the scintillator, which have been calculated due to partitioning of LAB/N_2 and LAB/H_2O of Rn, Kr, Ar, and O_2 [86]. A simplified process of this column is given in Figure 3.9.

Measurements of ^{222}Rn collected with this tower under pure vacuum mode can provide an *ex-situ* analysis of this section of the ^{238}U chain, and will be invaluable in supporting any conclusions drawn with relevant *in-situ* analysis. An assay skid will be coupled to the stripping column's gas outflow, which will collect radon by a series of cryo-cooled traps similar to a system coupled to the SNOLAB water system. The development, design, and use of this assay system is explained in detail in chapter 4.

Chapter 4

Radon Assays

4.1 Introduction

While the SNO+ detector can effectively monitor internal ^{222}Rn levels with *in-situ* Bi-Po coincidences during detector operation, the gas stripping column within the scintillator plant provides an *ex-situ* assay method which will be crucial in verifying and complimenting the detector's measurements. Moreover, the measurements will be instrumental in clarifying the origin of the *in-situ* measured ^{238}U chain backgrounds as either by ^{222}Rn ingress or via AV leaching or other sources of ^{226}Ra. Also the efficiency of the Bi-Po tagging can be calibrated and monitored. Coupled to the gas output of C-300, a scintillator radon assay system (SRAS) will directly collect radon from the scintillator and pass the gas along for measurement with a different monitoring system than the SNO+ detector. Such an analysis requires no assumptions of leaching or plating models, and no major assumptions of equilibrium within the decay chain. During scintillator and tellurium loading, the SRAS will determine pre- and post- purification levels of ^{222}Rn within LAB+PPO/Te-LS, providing a first look at contamination levels within the delivered product. During scintillator recirculation, these assays will be an effective quality control measure, monitoring ^{222}Rn even if the detector is offline. Such a method will assess the effectiveness of the cover gas and UPW shielding, as well as how often recirculation should occur.

In addition to the SRAS, there are two other radon assay systems for sampling different components of SNO+, both of which were built for the original SNO detector. A mobile system which measures the rate of ^{222}Rn produced from a specific sample can also double to measure Rn levels within the cover gas, and a monitor degasser (MDG) unit similar to C-300 can assay radon within the cavity water. Both of these units are invaluable as there are no other measurements to verify levels within the media they sample. During

SNO another system assayed the ^{222}Rn levels of D$_2$O, but since SNO+ requires lower internal background levels and a different detecting medium, the SRAS is under construction as a replacement piece. All three assay units perform roughly the same function: collect radon with two specific traps from a sample and place it inside a custom Lucas cell (LC) designed to connect to any of the three systems. The Lucas cell is then transported to surface and coupled with a PMT to count the Rn decays. As all three extraction units are located underground with at least an hour of delay time between transport from the lab to surface, this method is only practical for counting the ^{222}Rn (^{238}U supported) contamination within a sample, and alternative methods (e.g. ^{224}Ra assays) must be employed for ^{232}Th supported contaminants, as the half-life of ^{220}Rn is only 56 seconds. However, the short ^{220}Rn half-life means that ^{220}Rn does not cause the same contamination and disequilibrium issue as for ^{222}Rn.

4.2   Lucas Cells

Lucas cells were first universally accepted when Henry Lucas demonstrated the use of a silver-activated zinc sulfide scintillator compound sprayed on the inner walls of a radon containment vessel [95]. A photomultiplier tube coupled to one side of the Lucas cell detects the light emitted when a resulting alpha from radon decay strikes the ZnS(Ag) coating. Lucas also noticed the pulse height of the PMT seemed to correspond to the thickness of scintillator coating, and the use of optically coupling grease led to very little difference in counting efficiency, since the number of photons is large. For SNO+, the freedom to ignore coupling grease is ideal since the custom cells are frequently removed. After Lucas's "invention", Lucas cells were then commercially manufactured, yet significantly few papers were written on them until 1982, when a more extensive study was performed [96]. As with any detector, the design goal behind a Lucas cell is to maximize the difference in signal pulses compared to background pulses, and there are several ways to achieve this. For alpha detection, ZnS(Ag) scintillator produces one photon (at 4500 Å or 2.8 eV [97]) for every 9 eV of radiation energy deposited, whereas a typical PMT photocathode produces one photoelectron for every 7 photons with the correct wavelength [96,97]. As typical alphas for ^{222}Rn detection have about 6 MeV, this corresponds to 10^5 photoelectrons for every alpha. One background of PMT use is dark current - noise from the cathode, yet this is expected to give very few pulses with a number of photoelectrons of 10 or greater [96]. This results in a 10^4 signal to noise ratio sufficient for SNO+ radon studies. Additionally, the cell geometry and reflecting medium must be considered, as cell length increases the volume to increase sensitivity, but will reduce the amount of scintillation light which reaches the PMT.

The custom Lucas cells (see Figure 4.1 below for final product) used within SNO (and now SNO+) were developed at Queen's University after extensive R&D for the SNO experiment [97]. Cells available

commercially produced high background rates: Pylon Electronics Inc. sold units with backgrounds of 700 counts per day (cpd). As SNO+ monitors for sources which emanate on the order of a few radon atoms per day, such a cell would be useless. SNO also required a cell which could measure extremely low radon levels: 10^{-15} gU/g D_2O corresponds to $\sim 6 \times 10^{-3}$ Rn atoms/L, again requiring cells with a background of only a few cpd. Lucas cells developed by Queen's for SNO are directly transferable to the successor experiment: they can still be manufactured consistently and meet SNO+ purity requirements.

As with most scintillators, ZnS emits light via electron excitation, the process of which can be explained with electron energy band theory. Excitation can occur through photoluminescence, thermoluminescence, electroluminescence, as well as radiation (proton, alpha, etc.), and emission will depend on several factors, most notably the composition of ZnS, temperature, and excitation conditions. Activators such as silver within the lattice structure also affect the light output and scintillation decay time, and are typically added to inorganic phosphors to introduce luminescence centers, the transition to ground state via release of a photon. Energy release is also possible via quenching centers, in which the energy is released via radiationless thermal loss, or electron traps, in which the electron returns to ground state through energy transfer to lattice vibrations. The balance of energy release between luminescence centers, quenching centers, and electron traps determines the amount of luminescence the scintillator produces. ZnS activated with silver, ZnS(Ag), has successfully been used in several Lucas cells for the detection of alphas and radon counting [95, 96], and the excellent signal to noise ratio makes it a suitable scintillator choice. Also, ZnS(Ag) is very reflective, and as the thickness of this thin film affects the scintillation light via alpha interaction, different layer thicknesses were researched. Different cell sizes and geometries were also considered, such as the transmission geometry in which the PMT sees through the ZnS(Ag) coating, or a reflective geometry in which the PMT directly sees the light through some kind of window.

Queen's University finally developed a reflection-style Lucas cell in which a hemispherical cavity was milled out of the inside of a clear, ultraviolet transmitting (UVT) acrylic cylinder, a material which is known for its extremely low radioactivity [97]. The hemisphere is coated with 10 mg/cm^2 ZnS(Ag), and once dry a flat acrylic disk (3/16" thick) with the same radius of the cylinder is bonded to the bottom of of the hemisphere (via methylene chloride solvent), providing the viewing window. The hemispherical geometry provides the least variation in pulse sizes due to the uniform distance of each part of the coating from the PMT photocathode, while the thin coating optimizes the amount of scintillation and reflection while reducing the number of backgrounds present in the form of ZnS impurities from cosmic ray interactions, ^{238}U and ^{232}Th chain isotopes (the chosen ZnS scintillator has about 15 background cpd per gram [97]). The uppermost layers of the ZnS provide the scintillation light, while the remaining layers act as a reflecting medium, directing the photons towards the PMT. The pressure within the cell also affects pulse amplitude
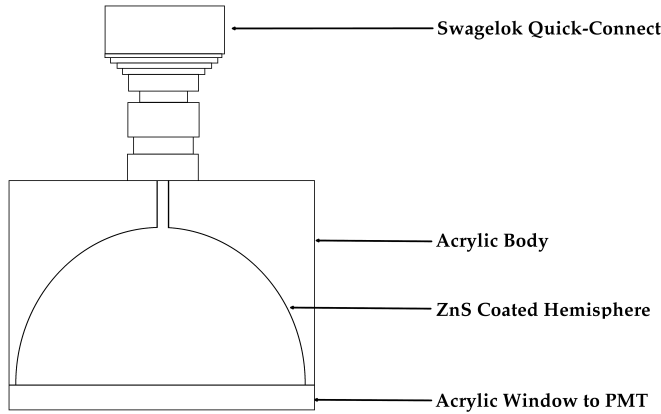
Figure 4.1: SNO+ Lucas cell diagram. Radon enters the cell through the Quick-Connect and decays, producing alpha particles that hit ZnS coated on the hemisphere. The top portion of ZnS scintillates while the lower layer reflects light through the window for PMT observation.

and detection efficiency as the number of gas particles within will affect the range of the alphas. At an internal pressure of 1 atm, a 5 MeV alpha has a range of about 3.8 cm. The radon collection apparatus is fairly good at extracting only radon, and components of the SNO+ detector are chosen to emanate only low levels of radon, meaning the pressure inside the LC is expected to be much less. Regardless, Queen's University designed two different sizes: 2 inch and 1 inch cells. The 2 inch cells have an inner diameter of 3.8 cm, a volume of 15.5 cm^3, and an active area of 20 cm^2. They were designed to fit with the Philips XP2262B PMT used for counting [97, 98], and have very low backgrounds of around 3 cpd. The 1 inch cells possess an inner diameter of 1.9 cm, volume of 2.3 cm^2, and active area of 5 cm^2, leading to a background of only 1 cpd. Although the smaller Lucas cells have lower backgrounds, their filling efficiency (via volume-sharing) is small due to their small size. Techniques to increase filling efficiency via cryo-cooling the LCs and/or the use of a mercury compression pump were considered unnecessary because another solution was so readily available. The 2" LCs meet the necessary detection requirements and, more importantly, their larger size allows for a better transfer efficiency to the cell, 75% vs. 25% for filling with the Queen's device [97]. All analysis work performed for SNO+ will be with the 2" LCs designed at Queen's University. See Fig. 4.1 for a drawing of the 2" LCs.

Radon enters the Lucas cell hemisphere through a small opening drilled and tapped at the top. The threads of a female Swagelok Quick-Connect are wrapped in teflon tape and screwed into the body of the cell at this opening. The other end of the Quick-Connect must match with the correct mating piece, located on radon systems, for the sealing mechanisms within both Quick-Connect pieces to open, allowing for ingress or egress of gas. These connections have demonstrated the required leak-tightness qualities necessary for
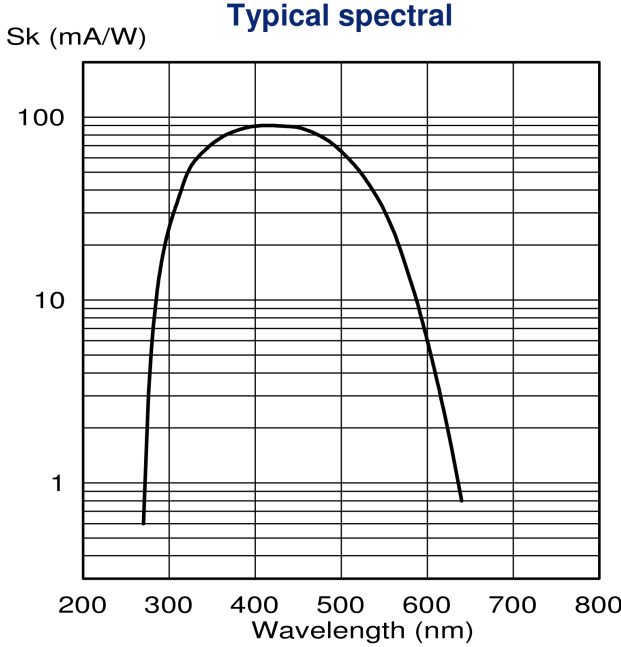
Figure 4.2: PMT XP2262B absorption spectra [99]. Peak sensitivity is at 420 nm, close to the photon emission of 450 nm by the ZnS(Ag) on Lucas cells.

low background collection of radon while within the radon-rich environment of SNOLAB, and were designed for repetitive use. Over time the connections must be maintained, as the O-rings within the Quick-Connect can dry up and crack, or may become covered with dirt. Either would cause an imperfect seal, and for this reason SNO regularly took apart and cleaned the Quick-Connects and replaced broken/dried O-rings. After maintenance the cells were often taken underground to test their leak-tight quality; after counting for one day ∼400 counts within the cell meant it was full of underground lab air (at ∼130 Bq/m^3).

4.3 Counting System

During counting Lucas cells are placed on the top end of a 50 mm diameter Philips XP2262B 12-dynode PMT which has been installed inside a black, cylindrical tubing of the same inner diameter. The XP2252B is an ideal choice for alpha detection as the photocathode has a spectral range from 290 nm to 650 nm and maximum sensitivity at 420 nm [99] (see Fig. 4.2), while the LC ZnS photon production is at 450 nm. A screw-on cap seals the dark box and a black cover is placed over the entire counting arrangement to eliminate outside photons. There are a total of 8 such counters within the low background counting facility in the SNOLAB surface building, 4 of which are operational. The counters are individually named, though currently the scheme poorly represents the configuration.

The manufacturer's recommended high voltage setting of the XP2262B is 1800 V [99], but for alpha

counting they are operated at 1000 V; the lower voltage setting reduces PMT dark noise and false signals by ensuring the dynodes are not stripped of electrons. Typically a trade-off occurs as the lower voltage results in a lower signal, but for radon counting the large number of photons generated from ZnS scintillation by alpha bombardment results in a clear hit regardless of the lower voltage. The signal from each PMT is rather small, even after an alpha decay (100 mV [100]), so it is first sent through a preamp into an amplifier specifically dedicated to the PMT. Signals are then individually fed through a multiplexer into the ORTEC 920-16 Spectrum Master, which labels it with a unique square wave. Now labeled, all signals from every counter are routed into one cable to a multichannel buffer (MCB), where the counts and timing information are stored. The MCB will also keep track of relative signal sizes, such that a maximum pulse is chosen in which all other signals are scaled to. There are a total of 1024 channels in which to record data. Note that the name MCB simply refers to a computer-interfaced MCA (multichannel analyzer), as opposed to a standalone MCA.
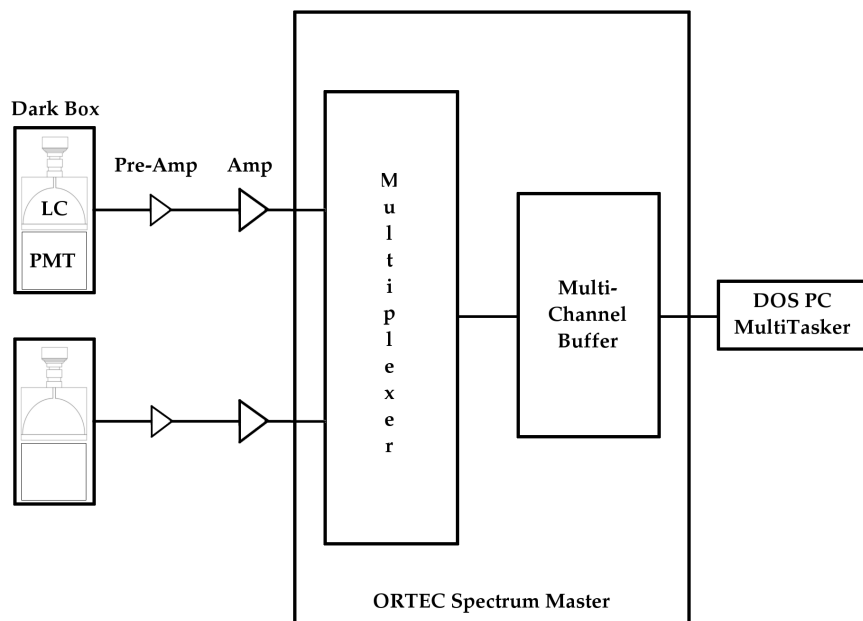
Figure 4.3: LC counting electronics flow diagram. The LC is placed inside a dark box with a PMT to count alpha decay, and signals from the PMT are sent through a preamp and amplifier into an MCA which digitizes the signal and sends it to a computer running MultiTasker.

The MCB is controlled through a dedicated PC with DOS running a program called MultiTasker, which reads the channels, starts, stops, and clears counting. The data from all counters is stored by the MCB and is only read by MultiTasker at certain user-defined times, such as when a procedure is running within MultiTasker. During a typical ^{222}Rn count, cells are placed within a dark box for 8 to 14 days, and a written procedure is started in which MultiTasker is asked to call the data from a specific PMT every 3

51

hours and output a new line in a .log file containing the date, time, PMT live time, and cumulative number of counts. The name of the .log file is eight digits long and of the form YYMMDDCC where YYMMDD is the date the procedure started and CC is the counter number. As low-amplitude noise still occurs, a low-level discriminator within the procedure defines a region of interest to filter the signal from electronic noise, and only about 1 % of the noise gets through. If desired, another file can be created the same time a new line appears in the .log file; this is a spectrum file which can be used as a diagnostic tool to ensure the system is operating as expected, but only the .log file is necessary for ^{222}Rn activity analysis. A flow diagram depicting the signal transfer from an alpha decay within the Lucas cell to the data recalled by the DOS computer is given in Fig. 4.3.

As each Lucas cell is typically counted for over a week, signals from all alpha decays after ^{222}Rn along the ^{238}U chain will also be recorded. In particular, signal-producing isotopes are ^{222}Rn, ^{218}Po, and ^{214}Po, before a long break in the chain occurs due to the lengthy half-life of ^{210}Pb (see Fig. 4.4). If counting is timed correctly (see below), one can expect 3 PMT hits for every radon decay.
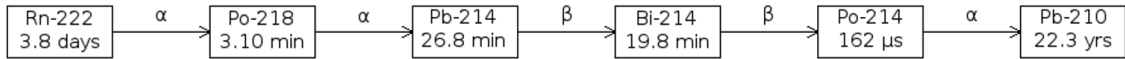
Figure 4.4: Relevant section of ^{222}Rn decay chain which generate signals for Lucas cell counting.

In determining the time, t, when equilibrium along the decay chain is reached inside the Lucas cell, the Bateman equation is used to determine the relative quantities of radioisotopes:

$$N_D(t) = \frac{N_1(0)}{\lambda_D} \sum_{i=1}^{D} \lambda_i c_i e^{-\lambda_i t} \tag{4.1}$$

N_D is the amount of substance D as a function of time, such that $N_1(0)$ represents the original quantity of the parent isotope at $t = 0$. i represents the radioisotope with decay constant λ_i, and the coefficients c_i are given by:

$$c_i = \prod_{j=1, i \neq j}^{D} \frac{\lambda_j}{\lambda_j - \lambda_i} \tag{4.2}$$

Let N_1 represent the quantity of ^{222}Rn atoms, and N_2 represent the number of ^{218}Po atoms. N_3 would represent the quantity of ^{214}Pb, but only its half-life, λ_3, is required in the upcoming calculations. Additionally, N_4 would represent ^{214}Bi, but as the half-life of ^{214}Po is so short, the approximation $N_4 = N_{214Bi} = N_{214Po}$ is accurate, where the half-life $\lambda_4 = \lambda_{214Bi}$ is used. The resulting quantities of radioisotopes which alpha decay are:

$$N_1(t) = N_1(0)e^{-\lambda_1 t} \tag{4.3}$$

$$N_2(t) = \frac{N_1(0)\lambda_1}{\lambda_2 - \lambda_1}\left[e^{-\lambda_1 t} - e^{\lambda_2 t}\right] \tag{4.4}$$

$$N_4(t) = N_1(0)\lambda_1\lambda_2\lambda_3\left[\frac{e^{-\lambda_1 t}}{(\lambda_2 - \lambda_1)(\lambda_3 - \lambda_1)(\lambda_4 - \lambda_1)} + \frac{e^{-\lambda_2 t}}{(\lambda_1 - \lambda_2)(\lambda_3 - \lambda_2)(\lambda_4 - \lambda_2)}\right.$$
$$\left. + \frac{e^{-\lambda_3 t}}{(\lambda_1 - \lambda_3)(\lambda_2 - \lambda_3)(\lambda_4 - \lambda_3)} + \frac{e^{-\lambda_4 t}}{(\lambda_1 - \lambda_4)(\lambda_2 - \lambda_4)(\lambda_3 - \lambda_4)}\right] \tag{4.5}$$

The alpha rate production per ^{222}Rn decay can be characterized as:

$$\alpha \text{ rate per Rn decay} = \frac{N_1\lambda_1 + N_2\lambda_2 + N_4\lambda_4}{N_1\lambda_1} \tag{4.6}$$

Inserting Eqs. 4.3, 4.4 and 4.5 into Eq. 4.6 along with the corresponding decay constants and plotting Eq. 4.6 as a function of time results in a curve where the production rate of 3 alphas per ^{222}Rn decay is reached ∼3 hours after radon has been collected, as is shown in Fig. 4.5.
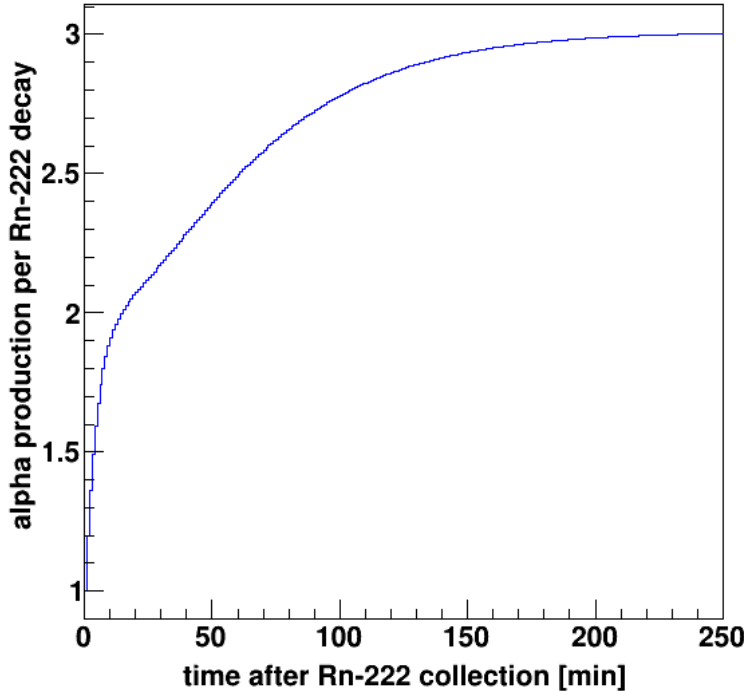
Figure 4.5: Number of alpha particles produced per ^{222}Rn decay as a function of time, as given in Eq. 4.6. Counting of Lucas cells must happen at least 3 hours after radon collection for a dependable alpha rate of 3 alphas per radon decay.

Studies at SNOLAB confirm that equilibrium within the ^{222}Rn decay chain is met as long as counting starts three hours after ^{222}Rn collection [98]. Due to the need to make up for the smaller production before three hours, the alpha production rate is actually 3.01 alphas/Rn. As long as the chain is within secular equilibrium at start of counting (SOC) by waiting 3 hours after the collection of radon, one can thus assume

3 counts occur for every ^{222}Rn decay due to the short half-lives of isotopes between ^{222}Rn's decay and ^{214}Po. Additionally, the three alpha particles will be produced in less than 2 hours from each other, so if coincidence timing was considered, this could further reduce backgrounds such as cosmic rays via timing rejection.

As the Lucas cells were designed for alpha sensitivity (and the dark box effectively eliminates any outside photons), apart from PMT dark noise the only backgrounds within the counting system would come from alphas which are not part of the signal. Impurities within the ZnS(Ag) layer and acrylic were considered an irreducible background during LC development, but can be measured by counting an evacuated cell. Radon extractions occur underground with timelines on the order of several hours, giving any ^{220}Rn captured within the traps plenty of time to decay before reaching the LCs. Very few other alpha-emitting particles should be collected within the Rn system (see § 4.5 for collection procedure), leaving only alpha emitters along the ^{222}Rn decay chain as additional sources of backgrounds. Just like with the SNO+ AV, radon daughters will embed themselves under the acrylic surface the Lucas cells. Next in the decay chain after ^{214}Po is the long-lived radioisotope ^{210}Pb, which is difficult to extract as it will be plated on the acrylic walls. A steady increase in Lucas cell background occurs from ^{210}Po alpha decay, which is fed by the 22 year half-life of ^{210}Pb. A rough calculation demonstrates that after $\sim 10^4$ ^{222}Rn decays, the cell's background will have increased by 1 cpd. For measurements of exceptionally low radon levels, the increase in background will eventually be too high for use in the SNO+ experiment.

4.4   Testing of Lucas Cells

To monitor backgrounds, all existing LCs are flushed with N_2 gas and evacuated three times, before insertion into a dark box for counting (see Appendix C for flushing procedure). Out of all the LCs used during SNO, only a handful now possess backgrounds $\sim$10-20 cpd, which is low enough for use with SNO+ materials. Even fewer meet the required background levels of 1 to 2 cpd for scintillator assays. If the cell's background was reasonable, another test was undertaken to determine if the cell leaked. Many of the cells from SNO also exhibit leaks, probably from the Quick-Connect. LC leak tests can be performed in conjunction with background testing by performing the flushing and evacuation of the cell underground, and then leaving the cell isolated for an entire shift before bringing it up for counting. If the cell leaks, a high count rate is observed after the first day, and a clear ^{222}Rn decay curve is present due to the high radon levels in the underground lab.

During a background test, Lucas cell A exhibited a very high background rate of 642 ± 10 cpd (see Fig. 4.6), which is too high for use with any Rn collection. As it failed the background test, leak-testing this cell was not a priority and has not been performed yet. Cells with high counts like this will be studied in the

future and have the potential to be used as possible calibration pieces.
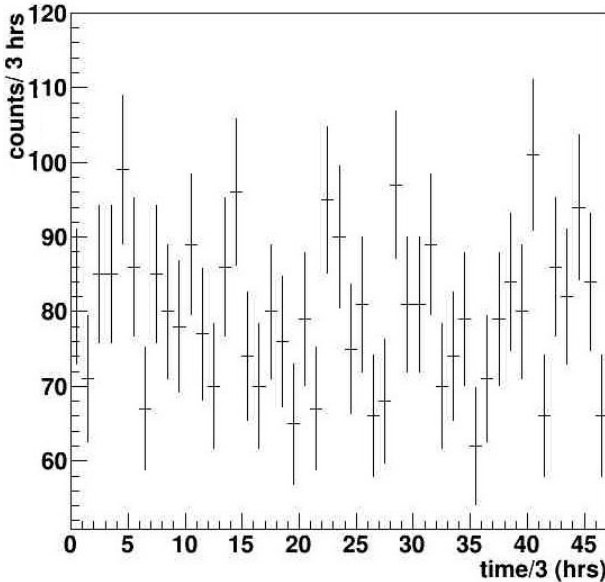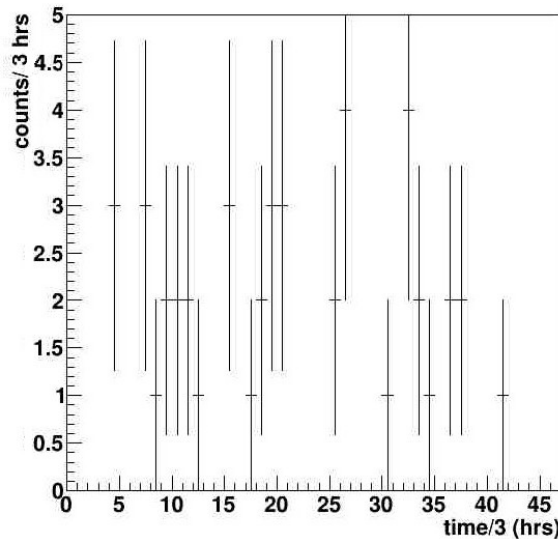
Figure 4.6: Counts observed for Lucas cell ID "A" background run. A high counting average of 642 cpd was reported.
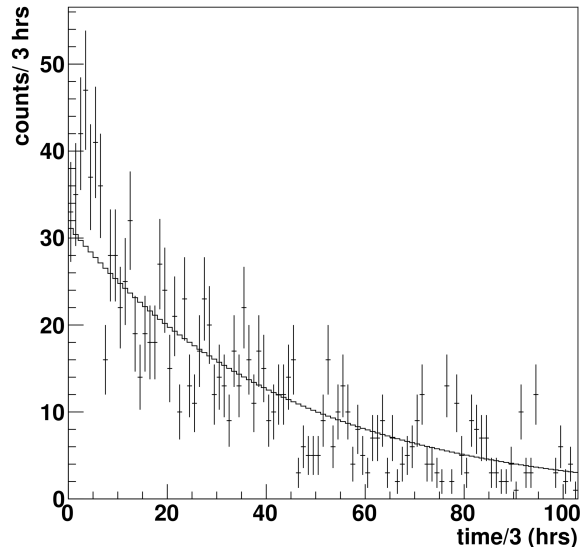
Lucas cell LCT5 possessed the necessary background level for use in some assays (7.7 ± 1.1 cpd), but failed the underground leak-test (see Fig. 4.7). Calculations estimate that 600 Rn atoms entered the cell over the ∼6 hour period the cell spend underground. Leak rates of this amount would cripple analysis of SNO+ materials.

A Lucas cell which exhibited a low background rate and passed the leak test is LCT6. Performed parallel to LCT5's tests, the leak-test of LCT6 contains no sign of ^{222}Rn ingress, and the low number of counts recorded means LCT6 is an ideal choice for emanation runs and cavity water assays. Incidentally, the leak-tests tend to have a more thorough evacuation than the background run evacuations, resulting in a lower count rate (2.88 ± 0.47 cpd) for the leak-test run, while a count rate of 9.8 ± 1.3 cpd is recorded for the background run (see Fig. 4.8). As the current set-up for assays allows for long evacuations of LCs with the same system leak-testing was performed on (and consistency in coupling LCT6 with the same PMT for counting), the former value is chosen as LCT6's background rate.

Since very few SNO LCs exhibit qualities required for sensitive SNO+ measurements, a new shipment of LCs was manufactured, tested, counted, and sent over from Queen's University. As the calibration between counting systems is expected to be different, these LCs are currently undergoing background and leak tests at SNOLAB before their use in the SNO+ experiment. In the meantime, LCT6 is commonly used for most radon extractions reported in this document. Tests will be periodically carried out during the SNO+ experiment for all LCs to ensure the backgrounds of each cell remain well-understood.
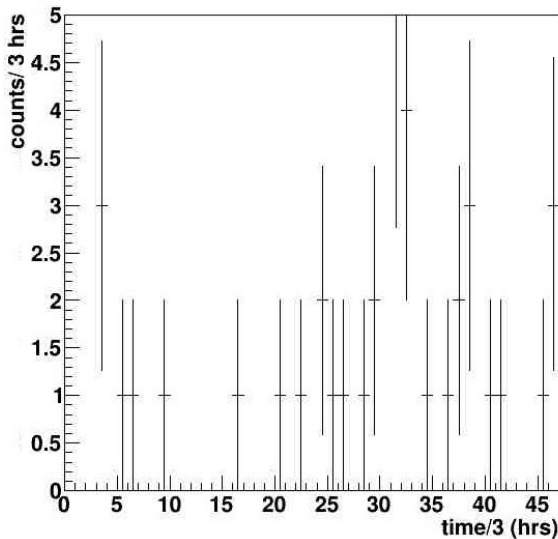
(a) Background test of LCT5
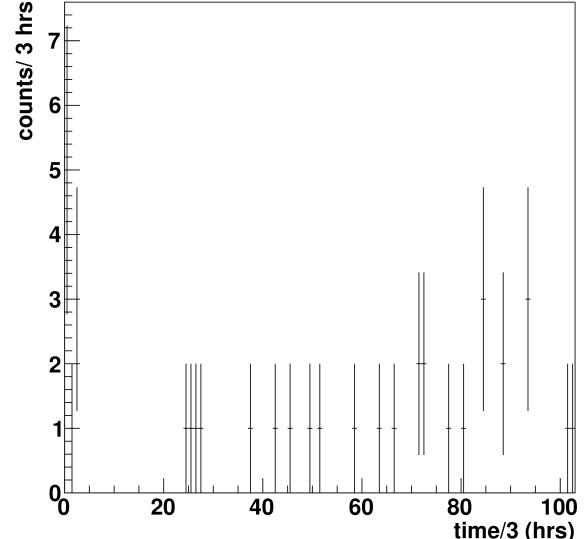
(b) Leak test of LCT5

Figure 4.7: Counts observed in 3 hour bins for tests of Lucas cell LCT5. Points are data, curved line indicates the expected curve if ^{222}Rn were collected within the cell. (a) The cell exhibits a satisfactory background of 7.7 cpd of ^{210}Po. (b) Counting after the leak test exhibited a high-leak rate of 100 Rn atoms entering the cell per hour.

(a) Background test of LCT6

(b) Leak test of LCT6

Figure 4.8: Counts observed in 3 hour bins for tests of Lucas cell LCT6. (a) The cell exhibits a satisfactory background rate of 9.8 cpd. (b) The leak-test evacuation result of 2.9 cpd is due to a more thorough evacuation of the cell, and is used in analysis. No radon decay curve is present, consistent with no leak present in the cell.

^{222}Rn detection efficiency of the custom LC counting system was measured by sending two SNO LCs to

Pylon Electronics Inc. in 2000 [101]. There, SNO LCs were filled alongside Pylon's cells with high levels of Rn

from the parent ^{226}Ra, and immediately sent back to SNOLAB for counting. Pylon counted their own cells and reported the concentration such that SNO could compare the value to their own recorded concentration and thus properly determine counting efficiency. As the two SNO cells had high counts, counting was stored in 10 minute bins instead of the typical 3-hour bins. The results led to an efficiency of $3 \times (0.74 \pm 7 \%)$ [102] for the detection of ^{222}Rn with the current arrangement of Lucas cells.

Yet the counting facility for Lucas cells is decades old, and while the system remains functional, the hardware demonstrates an upgrade to the counting facility is necessary for reliable counting of cells. Temporary replacements and quick fixes occur regularly, and another PMT failed in August 2015. The gains to the PMT/amplifiers was just reset the year before, in August 2014, by calibration with a hot cell of known activity of 20 counts per second, but consistency in LC and PMT coupling is still highly recommended and priority in well-behaved (i.e. less noisy) counters is given to more sensitive measurements. LCT6 has been coupled to PMT 16 for most analysis runs as this is the PMT the leak-test was counted with. Cross-talk between PMTs is negligible as adjacent stations to an active counter do not exceed 0.5 cpd above background [102]. Long-term gain drift measurements varied by no more than 3.5 ± 2.0 % over the course of SNO measurements. These will be carried out during SNO+ operations as well to ensure the deviations remain small, but, significant upgrades to the system are planned for the near future for reliable measurements while SNO+ is online. Once upgraded, re-calibration will occur with the hot cell, and the counter response due to varying pressures within the LC will be recorded for each PMT (by filling the LCs with known amounts of radon from the underground SNOLAB air).

4.5   Scintillator Radon Assay System

Measuring impurity levels on the order of 10^{-17} g ^{238}U /g LAB within the SNO+ scintillator requires exceptionally pure, efficient devices, such as the scintillator radon assay system (SRAS). Driven by a scroll vacuum pump and composed of a series of key cooling and heating positions known as traps, the SRAS is a stainless steel vacuum tubing system which is currently under construction and will be installed downstream the gas output of C-300. See Fig. 4.9 for SRAS parts and instrumentation diagram (P&ID) and Table 4.1 for item descriptions. Throughout the design and manufacturing of the SRAS, SNO+ is again fortunate in utilizing the experience and, sometimes, materials, gained during the development of SNO's radon assay systems [103].

Coupled to components within the scintillator plant, the SRAS is subject to the same restrictions and specifications as all pieces within the plant, including materials (stainless steel, acrylic), leak-tightness (10^{-9} mbar·L/sec), and valve requirements (cleanliness, low emanation and good leak tightness). To comply with
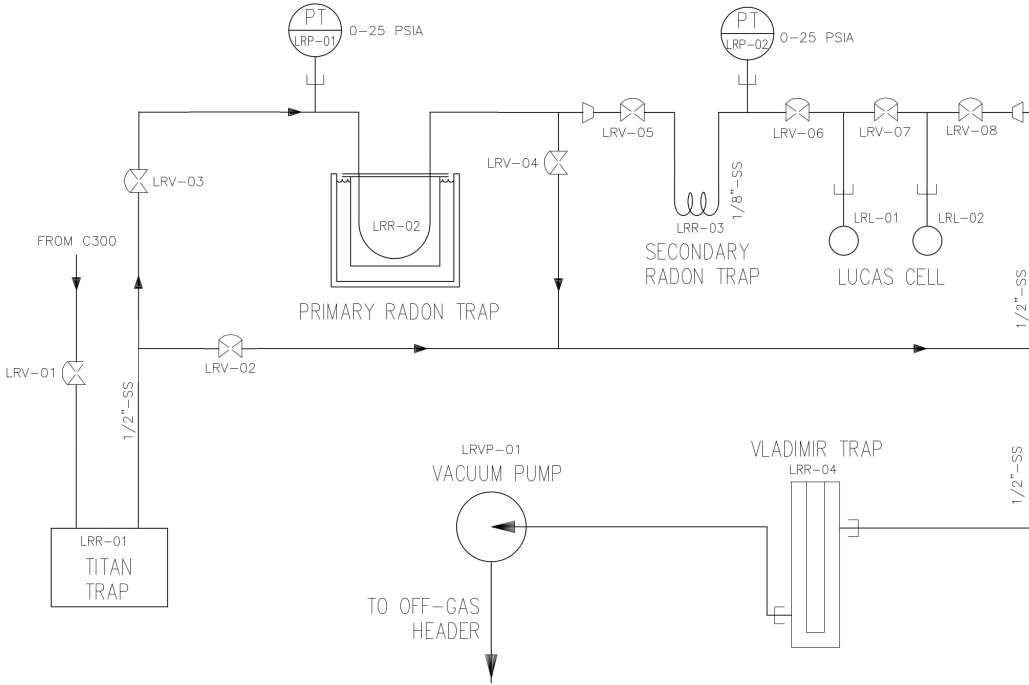
Figure 4.9: SRAS P&ID for the cryotrapping of ^{222}Rn within scintillator. The vacuum pump pulls gas from C-300 and along the assay system to be collected in Lucas cells connected downstream the secondary radon trap. Descriptions of each component are summarized in Table 4.1.

Label	Description
LRV-01	Entry to FTS trap
LRV-02	Rn traps bypass to vacuum
LRV-03	Entry to Rn Trap A
LRV-04	Rn trap B bypass to vacuum
LRV-05	Entry to Rn Trap B
LRV-06	Exit of Rn Trap B to first LC
LRV-07	Valve between two LCs
LRV-08	Exit of Rn traps to vacuum
LRP-01	Rn Trap A pressure transducer
LRP-02	Rn Trap B pressure transducer
LRP-03	Vacuum pump pressure transducer
LRR-01	Modified FTS Titan Trap
LRR-02	Rn Trap A
LRR-03	Rn Trap B
LRR-04	Vladimir Trap
LRL-01	Lucas cell 1 port
LRL-02	Lucas cell 2 port
LRVP-01	Vacuum pump for system
C-300	Gas Stripping Column

Table 4.1: SRAS equipment list for Fig. 4.9. LR represents LAB-Radon, V (valve), P (pressure transducer), R (trap), L (Lucas cell), P (pump), C (column).

scintillator plant standards, all process piping within the SRAS will be 316 stainless steel and electropolished, as this surface finish has the lowest radon emanation due to low surface porosity. Joints are orbital welded for best leak tightness and low emanation. The lid of the modified FTS trap is clear acrylic, with two tapped holes for NTP fittings, which are glued to the lid with a two-part clear epoxy for a maximum seal. The other end of the fittings are male VCR ports, which connect to the remainder of the system. Both the FTS and the pressure transducers are coupled to the SRAS via VCR connections as opposed to a direct weld. The Vladimir trap, reused from the SNO D_2O system, and the vacuum pump are both to be connected via KF vacuum flanges. Although these connections have weaker seals, leaks are unlikely to contaminate anything upstream the Vladimir trap due to the cryotrapping effect while held at LN_2 temperature. With the exception of the Quick-Connect ports for the Lucas cells, all other parts of the system will be welded together, the majority using an orbital welder located at SNOLAB. Welding on the system has begun while awaiting the arrival of a custom piece (see below), the FTS trap has been reassembled, and all required fittings are in SNO+ possession.

The large quantity of steam required during scintillator process purification (10 kg/hour) will most likely be too much for the compact size of the SRAS to handle, so during assays C-300 may operate under only nitrogen gas or most likely with vacuum alone. Regardless of the change in stripping medium, C-300 can still operate at 100 °C and 150 Torr vacuum (can be lower with no stripping gas), such that only gaseous particles at these settings are extracted, verifying that assays of pure scintillator and Te-LS are achievable. The new degassing efficiency during assays will have to be calculated, as it is expected to shift from > 95%. This efficiency can be determined by injecting a known amount of Rn into scintillator, running it through the degassing column under the new settings, and collecting Rn within the assay system for counting with a Lucas cell. The pressure range induced on the SRAS by the vacuum pump is expected to be on the order of a few millitorr, as the pressure of <10 mTorr is consistently obtained by the still-operational H_2O assay system, which uses a less-effective oil pump and is composed of the less leak-free polypropylene and stainless steel Swagelok® connections (see § 4.8).

The first trap within the SRAS is a vapour recovery container (LRR-01) which operates at -100°C to freeze out any residual scintillator (LAB freezing temperature is -91 °C) that has evaporated inside C-300 and was carried along the vapour line. During recirculation C-300 may be operated after the water-extraction column to pull any residual water from that process out of the LAB, and as such water may also be carried along and collected within LRR-01. Water and LAB are separated from the remaining gasses at this stage for two reasons:

- Scintillator (or H_2O) presence is unnecessary for the trapping and collection of ^{222}Rn. If left, the

relatively large quantity of this fluid would only serve to impede Rn trapping by increasing system pressure and forming ice-plugs within the radon traps.

- Scintillator processing is to be as efficient as possible, requiring any collected scintillator to be sent through the drain line of the freeze trap to a recovery system.

The freeze trap is a commercially purchased FTS Titan-Trap from SP Industries, Inc. [104] [105] which is normally operated in freeze drying applications. The commercial trap contained a helically wound titanium coil filled with a coolant called R290/R1150 (a blend of propane and ethylene) and placed centrally inside a 4 liter Teflon-coated stainless steel condenser chamber with a safety-coated glass dome top. Ingress and egress of gas occurs at the top of the chamber, through ports in the glass dome, and a drain port at the bottom of the chamber allow condensed fluids to be removed (see Fig. 4.10 for FTS general appearance). Yet background tests of the condensing chamber of a similar system demonstrated significant Rn emanation and leaks (9.74×10^3 Rn atoms/day [103]), the solution of which was to replace the chamber and lid with a new stainless steel bucket coupled to a clear acrylic lid by bolts and sealed by two concentric O-rings. The same process was completed here, though size and functionality (entry and exit points) remain the same as the original trap. This trap is responsible for limiting the use of steam as a cleansing medium within C-300: the new bucket also possesses a volume of 4 L which would fill up too quickly. Once reassembled, the modified freeze trap will be leak-tested and background tested.

The minimum temperature of the freeze trap is constrained by the refrigerant used and the effectiveness of the seals and insulation. In this case R290/R1150 allowed the chamber temperature to drop to -95 °C without vacuum, and is expected to reach -100 °C while under vacuum. The cold temperature is required to ensure LAB freezes out while under vacuum pressure. A study of radon gas at this low pressure confirms it will remain in a gaseous state and will not freeze out along with LAB and water (see Fig. 4.11) [106].

During an assay radon will pass through LRR-01, traverse along 1/2" stainless steel tubing and through LRV-03 (LRV-02 is closed) towards a U-bend in the system known as the primary radon trap (LRR-02). The experience of SNO was used in determining the size and composition of the trap, resulting in a trap volume that is approximately 50 cm^3 when empty and packed with the brass and stainless steel mesh which was used within the D_2O assay system. Experience with the D_2O trap and traps from the other existing systems suggests that such a geometry will result in a 100% radon trapping efficiency [102]. The trap will be submerged within a dewar of LN_2, causing radon and other gas particles inside to cool down to the boiling temperature of LN_2, approximately -196 °C. The composition of gases extracted from scintillator will be mainly Rn, N_2, O_2, Kr, Ar, and CO_2, and a review of the phase diagrams for these gases suggests that at conditions of $\sim$ 10 mTorr (10^{-3} kPa) and -196 °C (77 K) within the trap, only carbon dioxide will
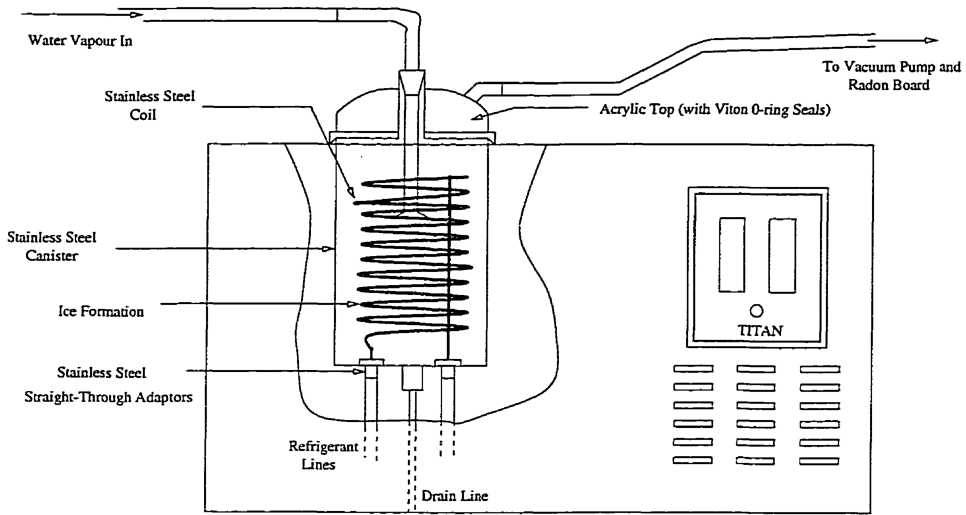
Figure 4.10: FTS Titan Trap general appearance [103]. Gas enters the top of the chamber, and vapours such as LAB or H_2O are frozen within the bucket due to the -100 °C temperature inside, while other gases such as radon pass unimpeded and exit through the other top line. Once thawed, liquid is removed from the bucket through the drain line.
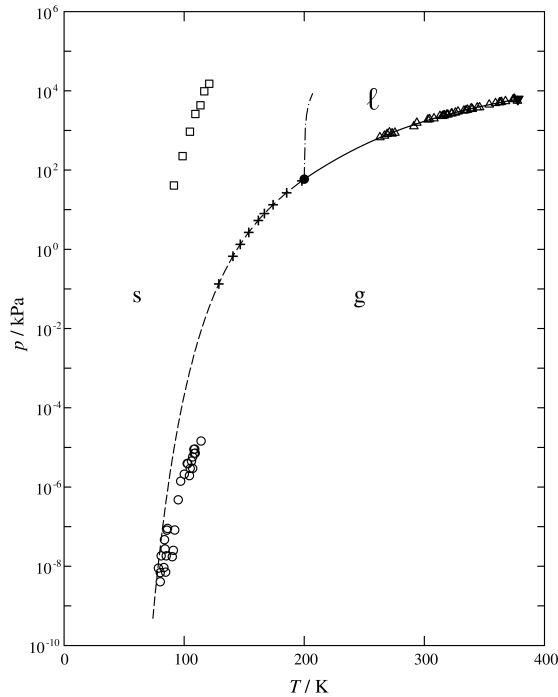
Figure 4.11: Phase diagram of radon. Points are experimental whereas curves are calculated [106]. s, l, g correspond to solid, liquid, and gas phases respectively, and the solid black dot represents the triple point. With the system operating at $\sim$ 10 mTorr (10^{-3} kPa), at -100 °C (173 K) radon remains comfortably within the gas phase, yet at -196 °C (77 K) radon will freeze.

freeze alongside radon within the trap, while the rest will pass to vacuum exhaust [102] (LRV-04 is open, while LRV-05 is closed). The quantity of frozen gases should be exceptionally small given scintillator purity, resulting in a pressure which does not exceed atmospheric pressure within the LC, and among these gases, radon is the only unstable alpha emitter. The extraction procedure will also include measures taken in the event that the pressure within the trap does exceed a safe pressure for the transfer to the LC, and timescales for the collection of gas in Trap A will be depend on the efficiency of C-300 while under vacuum mode, as well as scintillator feed rate.

Once collection of radon into trap A is complete, valves connecting C-300 to the SRAS will be closed (including LRV-01), and Trap A isolated by closing the valves immediately up- and down-stream of it (LRV-03 and LRV-04). Trap A will be heated, restoring radon to its gaseous state, and the pressure recorded (using LRP-01). Now that radon has been collected, the task is to transfer it to the relatively small, 15.5 cm^3 volume Lucas cell. An efficient practice utilized here is to collect the radon into a second, much smaller trap called trap B (LRR-03), then transfer radon into the LC from this trap via simple volume sharing. In comparison to trap A, the volume of trap B is just over 1 cm^3 while empty, but it will also contain an insert to reduce the volume even more. This compressing trap will also be submerged in LN_2, and LRV-05 opened such that Traps A and B are coupled, but isolated to the rest of the system (LRV-06 remains closed). Throughout the transfer, trap A will be heated to $\sim$80 °C, and the large temperature gradient between the traps induces a cryopumping of gas from the primary trap to the secondary trap. Experience suggests the transfer efficiency from trap A to trap B will also be 100%. Meanwhile, the LC is attached to the quick-connect port closest to trap B (LRL-01), and allowed to evacuate (open LRV-08, LRV-07 to couple the LC to vacuum), before it too is isolated (close LRV-07, LRV-08). Note that for every assay the LC is to be prepared ahead of the assay through the same equipment and procedure as the LC background preparation, and this is a final purification before Rn enters the cell. Once sufficient time passes ($\sim$15 min.), trap B is then isolated (close LRV-05), and brought to room temperature. The pressure of trap B will be recorded (LRP-02) to ensure pressure inside the LC is below 1 atm and thus the range of alpha particles are acceptable. If so, the valve separating trap B and the Lucas cell (LRV-06) will be opened, and the transfer of radon into the LC depends only on the volume ratios of the LC compared to the total system within the coupling (i.e. volume between LRV-05 up to and including LC volume). If the pressure within trap B is too high, the sample may still be collected by attaching a second LC to the other quick connect port, and the valve between both LCs (LRV-08) opened such that the collection of Rn will be evenly distributed into both LCs. These cells would be counted simultaneously to ensure they are consistent with each other. To anticipate any of these transfers, the additional volume in the system between LCs must also be minimized for maximum fill ratios.

A second cryopump to the LC is not recommended as the cold temperature stresses the acrylic and causes it to crack, and volume sharing provides the safest, non-invasive gas transfer. For this reason, the volume of the LC must be significantly larger than that of trap B and the connecting units, and the 2" LCs developed by SNO work best for this. Trap B dimensions were optimized by choosing a balance between collection and transfer efficiencies, resulting in ~30 cm of 1/8" OD stainless steel tubing bent in a loop with a 1/16" SS rod inserted. The inner volume of Trap B will be about 1 cm^3 while empty, but the entire path between trap B and the LC must also be minimized, requiring short and small fittings between LRV-05 and LRV-08. The design of the volume-sharing components of the system (essentially everything between trap B and the end of the LC ports) was planned by the author and carefully designed by coordination between the author and Swagelok personnel (see Fig. 4.12 and Table 4.2 for current arrangement). The piece is currently undergoing assembly within a Swagelok facility [107] under the author's supervision.

Due to the complexity between LRV-05 and LRV-08, assembly on-site is not possible; a micro welding unit is required for 1/8" tubing welds, and Swagelok does not provide many 1/8" pieces with weld connections (e.g. valves). Swagelok fittings are prone to unacceptable leak-rates for SNO+, requiring valves, Quick-Connects, etc. to undergo modifications within the Swagelok facility for weld-application. With the exception of the pressure transducer (LRP-02), all fittings between LRV-05 and LRV-08 will be 1/8" connections welded together. The chosen PT requires a 1/4" VCR connection, which is the smallest VCR fitting available. VCR connections are allowed within the scintillator plant as they meet leak-rate restrictions, and in this case VCR is chosen over the weld option as the PT must be easily replaceable in the event of a PT failure. Note that for this reason, LRP-02 will also be connected via 1/4" VCR fitting. Volume within the assembly piece will be further reduced with the insertion of 1/16" stainless steel rod pieces within the connecting tee-intersections, and within the VCR gland for the pressure transducer. A quick calculation based off of the estimation of internal volumes (before the 1/16" rod inserts) leads to roughly 85% as the transfer efficiency from trap B to the LC, although the efficiency should be much better once the 1/16" rods are inserted. This is a significant improvement over the existing assay systems, or even the preceding D_2O system, which had a transfer efficiency of 63.8% [102]. For a quick weld insertion into the remaining pieces of the SRAS, the compressors which adjust the tubing size from 1/2" down to 1/8" and back up again are included on this piece. The assembly piece and all of its components are to be cleaned to Swagelok's SC-11 specifications, which comply with ASTM G93 Level C standard. The exception to the cleaning is the 1/8" outer dia. tubing, which was cleaned to SC-11 standard except for the inner surface finish of 32 microinch roughness average.
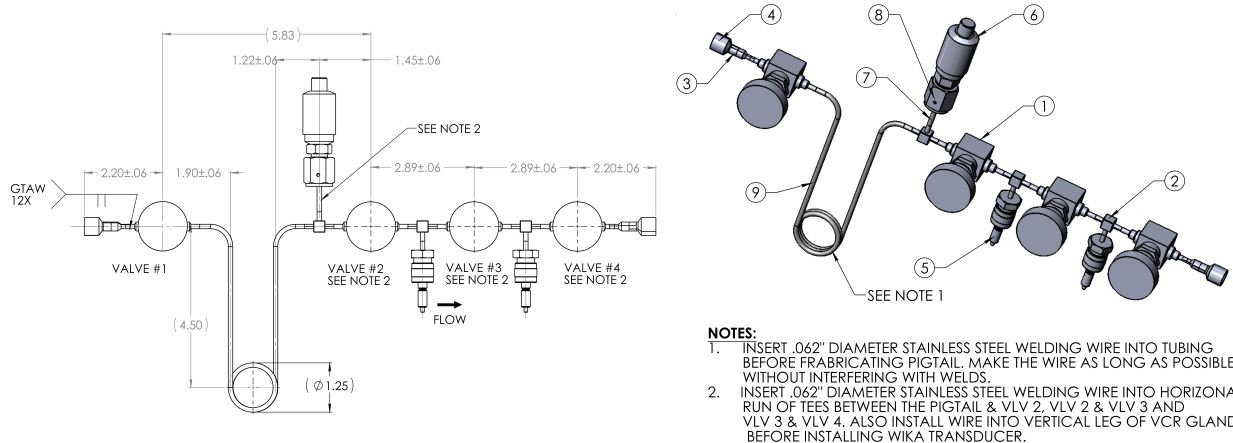
Figure 4.12: Design of the SRAS assembly piece undergoing custom manufacturing at Swagelok due to complex manufacturing conditions and lack of resources at SNOLAB [108]. It consists of everything between LRV-05 and LRV-08 as well as the compressors from 1/2" to 1/8" tubing. See Table 4.2 for bill of material.

Item no.	Part Number	Description	Qty
1	SS-2H-44055-SC11	1/8" H Series Bellows Valve	4
2	6LV-2MW-3-SC11	1/8" welded micro fit tee	3
3	6LV-4MW-6-2-SC11	Micro-fit(R) Reducing union, 1/4" x 1/8" OD	2
4	6LV-8MW-6-4-SC11	Micro-fit(R) Reducing union, 1/2" x 1/4// OD	2
5	SS-QC4-D-2PM-SC11	1/8" Quick Connect	2
6	WU-20-AZ-PK321-71ZZ-M4ZC-ZZ	Wika Transducer	1
7	6LV-4-VCR-3S-2TB7	1/4" VCR Butt-weld gland, short	1
8	SS-4-VCR-1	1/4" VCR female nut	1
9	SS-T2-S-028-20	1/8" x 0.028" tubing	1

Table 4.2: SRAS custom assembly piece bill of material corresponding to Fig. 4.12.

Once the collection of radon into the LC is complete, valves will be closed to isolate the LC (i.e. LRV-06) and the cell will be disconnected from the system. The radon traps are then baked to remove any excess radon and gases which have yet to exit the traps. At the end of the SRAS, right before the vacuum pump, exists a final trap (LRR-04) known as the Vladimir trap. This equipment consists of an inner and outer container, and the only ingress and egress of the inner container is through a loosely capped lid at the top. Before an assay is started, this inner container is filled through this lid with LN_2, and is regularly checked and topped off as the assay proceeds. The outer container will be connected only to the assay system, with a lower port connecting to the vacuum pump of the SRAS, while the higher port is downstream all traps of the SRAS. Any residual vapour which has passed through the traps can be caught here, but even more importantly, this Vladimir trap acts to restrict the back-flow of radon and gas particles from the pump into the SRAS.

4.6 Calculating Radon Concentrations within a Liquid

Once radon has been collected into a LC and counted for 8 to 12 days within the dark boxes on surface, the data can be analyzed. From the .log file created by Multitasker, the most important values are the total number of counts, S, obtained during the live time, t_{count}. Values are determined through the radioactive decay law:

$$dN/dt = -\lambda N \tag{4.7}$$

where dN/dt is the rate of decay, λ is the decay constant (for ^{222}Rn, $\lambda \approx 0.182$ days^{-1}), and N is the current amount of radon. It is possible to determine N_{SOC}, the number of radon atoms within a Lucas cell at the start of counting, given $N(t_{\text{count}})$, the number of Rn atoms that remain after time t_{count}, by integrating the radioactive decay rate:

$$N(t_{\text{count}}) = N_{\text{SOC}}e^{-\lambda t_{\text{count}}} \tag{4.8}$$

Yet this does not incorporate counting efficiency, ϵ_{count}, which is a function of the cell geometry and the coupling between the cell and PMT. ϵ_{count} also includes the 3 alphas expected for one ^{222}Rn decay, as long as the delay time between the end of the assay and the start of counting is 3 hours or more. Recalling this and the fact that the cells also have their own background rate, B, one must examine the rate of signals produced. Differentiating Eq. (4.8) and including counting efficiency and background rate, one can obtain the rate of counts detected by the PMT:

$$\frac{dN}{dt} = \lambda \epsilon_{\text{count}} N_{\text{SOC}}e^{-\lambda t} + B \tag{4.9}$$

Integrating (4.9) (and recognizing that there are no signals the moment counting starts, i.e. when $t_{\text{count}} = 0$) provides S, the total number of counts detected within the cell after a time t_{count}:

$$S = \epsilon_{\text{count}} N_{\text{SOC}}(1 - e^{-\lambda t_{\text{count}}}) + Bt_{\text{count}} \tag{4.10}$$

Rearranging this solves for N_{SOC}, the number of ^{222}Rn atoms within the cell at the start of counting. Working backwards, one can calculate the number of Rn atoms which have been collected at the end of an assay extraction, N_{EOA}. Radon collection occurs up until trap A is isolated, from then on the finite amount of Rn trapped will only decay. Recognizing t_{delay} as the delay time spent between the end of this collection and the beginning of counting, one may rewrite the decay law as:

$$N_{\text{SOC}} = N_{\text{EOA}}e^{-\lambda t_{\text{delay}}} \tag{4.11}$$

Yet there exist backgrounds from the assay system which will also be collected in trap A. This means $N_{\text{EOA}} = N_{\text{sample}} + N_{\text{back}}$, where N_{sample} are the number of Rn from the sample and N_{back} are the background Rn atoms produced from the assay system. The transfer process from trap A to the LCs has a transfer efficiency value, $\epsilon_{\text{transfer}}$, that must be included. Transfer efficiency from trap A to B is typically 100%, meaning $\epsilon_{\text{transfer}}$ is essentially the transfer efficiency from trap B to the LC which is governed by a ratio of volumes. Incorporating all of this results in:

$$N_{\text{SOC}} = \epsilon_{\text{transfer}}(N_{\text{sample}} + N_{\text{back}})e^{-\lambda t_{\text{delay}}} \tag{4.12}$$

A somewhat naïve approach is taken where it is assumed N_{back} is produced early in the assay system, approximately at the same time and location that N_{sample} is collected. Subsequently, this requires no background atoms to be produced after the collection into trap A. This is not inaccurate as one expects the largest background contributions to be areas which are large and used for a long time, such as the massive volume of C-300, or even the FTS system. The rest of the system is small, and with the exception of trap A, the remaining system is also used for a much shorter period of time during an extraction. Both N_{sample} and N_{back} must be calculated by again integrating their respective decay rates. For N_{sample}, one expects:

$$\frac{dN_{\text{sample}}}{dt} = R - \lambda N_{\text{sample}} \tag{4.13}$$

R is the rate of the ^{222}Rn atoms produced from the sample, either due to emanation of a sample or by extracting it from a flowing sample. Integrating Eq. 4.13, a first order linear ODE with integrating factor $e^{\int \lambda dt}$ and solving for the constant of integration with the initial condition $N_{\text{sample}}(t = 0) = 0$ (i.e. nothing inside the traps at the beginning of the assay) provides:

$$N_{\text{sample}} = \frac{R(1 + Ce^{-\lambda t_{\text{assay}}})}{\lambda} \tag{4.14}$$

Where the collection of radon into trap A occurs for a time of t_{assay}. Although assumed to be 100%, the trapping efficiency of the primary trap, ϵ_{trap}, is included for completeness, such that the number of radon atoms collected within the primary trap is:

$$N_{\text{sample}}(t_{\text{assay}}) = \frac{\epsilon_{\text{trap}}R(1 - e^{-\lambda t_{\text{assay}}})}{\lambda} \tag{4.15}$$

Similarly, for background atoms collected:

$$N_{\text{back}}(t_{\text{assay}}) = \frac{\epsilon_{\text{trap}} R_{\text{back}}(1 - e^{-\lambda t_{\text{assay}}})}{\lambda} \tag{4.16}$$

where R_{back} is the rate of background Rn atoms produced during Rn collection. Substituting both Eq. 4.15 and Eq. 4.16 into Eq. 4.12, then substituting Eq. 4.12 into Eq. 4.10 and rearranging for R as a function of S results in:

$$R = \frac{(S - Bt_{\text{count}})\lambda}{\epsilon_{\text{count}}\epsilon_{\text{transfer}}\epsilon_{\text{trap}}(e^{-\lambda t_{\text{delay}}})(1 - e^{-\lambda t_{\text{assay}}})(1 - e^{-\lambda t_{\text{count}}})} - R_{\text{back}} \tag{4.17}$$

Eq. 4.17 defines the rate at which ^{222}Rn atoms are being extracted from a sample. Analyses of liquid samples require one more step, as instead of a production rate, radon is extracted from a degasser while the liquid is flowing at a specific rate, F. This is demonstrated as:

$$C = \frac{1}{F\epsilon_{\text{degasser}}} \left[\frac{(S - Bt_{\text{count}})\lambda}{\epsilon_{\text{count}}\epsilon_{\text{transfer}}\epsilon_{\text{trap}}(1 - e^{-\lambda t_{\text{count}}})(e^{-\lambda t_{\text{delay}}})(1 - e^{-\lambda t_{\text{assay}}})} - R_{\text{back}} \right] \tag{4.18}$$

where $\epsilon_{\text{degasser}}$ represents the Rn removal efficiency of the degasser and C is the concentration of Rn atoms within the liquid. Times are recorded in units of days, production rates in cpd, flow is converted from L/min to L/day, resulting in a concentration of atoms/L. This value is typically converted into a more universal unit of g ^{238}U/g substance by assuming ^{222}Rn is in secular equilibrium with ^{238}U. If so, then the following relationship is true:

$$\frac{N_{\text{U}}}{N_{\text{Rn}}} = \frac{T_{\text{U}_{1/2}}}{T_{\text{Rn}_{1/2}}} \tag{4.19}$$

where N_{U} and N_{Rn} are the quantities of ^{238}U and ^{222}Rn, respectively, with half-lives $T_{\text{U}_{1/2}}$ and $T_{\text{Rn}_{1/2}}$, respectively. The number of ^{238}U atoms is calculated and converted to grams, while the volume of solvent (LAB, H_2O, etc.) is converted to the amount of grams it would be depending on its density. Altogether, this leads to a conversion of:

$$C[\text{g }^{238}\text{U}/\text{g}] = C[^{222}\text{Rn/L}] \times \frac{1.69 \times 10^{-13}}{\rho} \tag{4.20}$$

where ρ is the density of the solvent in g/cm^3; $\rho_{H_2O} = 1.0$ g/cm^3 and $\rho_{LAB} \approx 0.865$ g/cm^3. For internal target levels of 1.6×10^{-17} g U/g LAB during the pure scintillator phase, this corresponds to $\sim 8.2 \times 10^{-5}$ Rn atoms/L, while the internal level of 2.5×10^{-15} g/g during Te-LS phase leads to 1.3×10^{-2} Rn atoms/L. During water phase, internal levels of 3.5×10^{-14} g U/g H_2O correspond to 0.2 Rn atoms/L, and external cavity levels of 3.5×10^{-13} gU/g for every phase corresponds to about 2 radon atoms/L.

A macro written in ROOT takes in the two values from the .log file and calculates the expected ^{222}Rn production rates and/or concentrations. It also reads in every line in the data file and outputs a decay spectrum with the number of observed counts plotted in 3 hour bins. After the calculation of N_{SOC}, a second decay curve (using Eq. 4.9) is plotted over top to ensure the data matches that of an expected ^{222}Rn decay with N_{SOC} number of Rn atoms at the start of counting.

4.7 Calculations for SRAS

The efficiencies and background of the SRAS will be determined experimentally once the system is fully assembled. The background procedure is determined as though an actual assay were taking place, except that the system is not actually sampling any material, other than itself. Trapping and transfer efficiencies of the system will be calculated by injecting a known concentration of radon gas into the system. Radon levels underground are high, so Lucas cells can be filled with the lab air, then coupled to the system via their Quick-Connects. Two cells should be filled during testing: one to act as the control cell for accurate knowledge of radon levels, and the other for injection into the system. Three tests will determine three efficiencies:

1. $\epsilon_{\text{transfer}}$: The LC is coupled to the Quick-Connect on the SRAS, and the valve between the LC port and trap B opened and left for 15 minutes to allow the gas to disperse evenly throughout the whole volume. Both cells are then taken to surface and counted; the reduced concentration within the injection cell determines the transfer efficiency between trap B and the LC.

2. Transfer efficiency from trap A to B, assumed to be 100%, but should be calculated. Trap A is submerged within LN$_2$ while valves between the LC port and between traps B and A opened. After 15 minutes trap A is isolated and the remaining tubing and Lucas cell is evacuated, then the procedure is similar to an actual assay in which trap A is heated, trap B cooled with LN$_2$, etc. to pass the collected radon back into the Lucas cell.

3. ϵ_{trap}: Same procedure as item 2, except that during radon collection into trap A the valve on the opposite side of trap A is also open, such that the flow is from the LC through trap B to trap A to vacuum. The remaining procedure is the same as an actual assay.

While these tests can be performed as soon as the SRAS is built, the remaining efficiency and background tests require LAB and the commissioning of the scintillator plant (specifically C-300). A background run of C-300 is essential, as it will determine the range of use for the SRAS. For example, if the same background rate is assumed from SNO's D$_2$O monitor degasser (430 Rn atoms/day [102]), use of the SRAS may be

Variable	Value	Description
λ	0.182 days^{-1}	^{222}Rn decay constant
ϵ_{count}	3×0.74	Typical counting efficiency
$\epsilon_{\text{transfer}}$	0.85	Minimum SRAS transfer efficiency
ϵ_{trap}	1.00	Expect perfect trapping efficiency
ϵ_{degas}	< 1.00	Unknown degassing efficiency
B	2 cpd	Lowest achievable LC background
t_{count}	12 days	Typical LC counting time
t_{delay}	3 hours	Typical delay time
t_{assay}	0 to 100 hours	Possible range of time for assays
R_{back}	0 Rn/day	No system background, for simplicity
F	150 LPM	Standard flow through C-300
C [LAB+PPO]	8.1×10^{-5} Rn atoms/L	Rn concentration in LAB+PPO
C [Te+LS]	1.3×10^{-2} Rn atoms/L	Rn concentration in Te+LS

Table 4.3: Hypothetical parameters for theoretical calculations with the SRAS

restricted to quality control checks of C-300 during the pure scintillator phase, as the sensitivity of the assay system would only reach 4×10^{-16} gU/g LAB with this high background rate. As the scintillator plant has been designed with a higher purity in mind, background levels are expected to be much lower, and assays throughout scintillator running are intended. The scintillator plant is not yet commissioned so studies of C-300 background rates and the SRAS range of scope will come after this thesis. However, several theoretical calculations can still be made under several assumptions (see below).

If the desire is to achieve a signal from the ^{222}Rn extracted from scintillator during LC counting, a signal excess of 50 % should be adequate (based on approximate 2σ for 12 counts). Then, from Equation 4.10, one requires $S > 1.5Bt_{\text{count}}$, or:
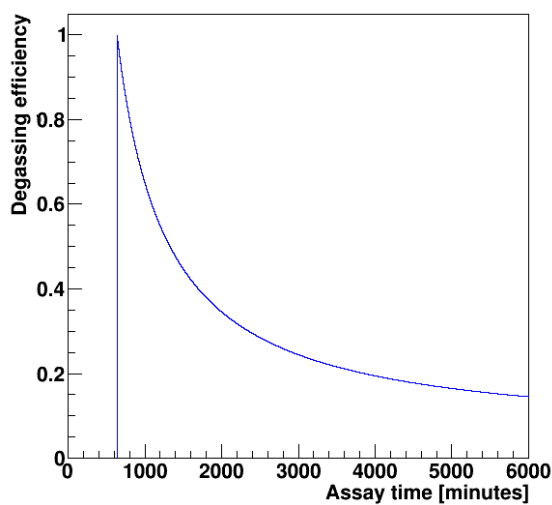
$$S - Bt_{\text{count}} > 0.5Bt_{\text{count}} \tag{4.21}$$

which, for the case of a LC with a background of 2 cpd, results in a total of 12 counts. Carrying through this inequality and rearranging Eq. 4.18 to make ϵ_{degas} a function of t_{assay} results in:
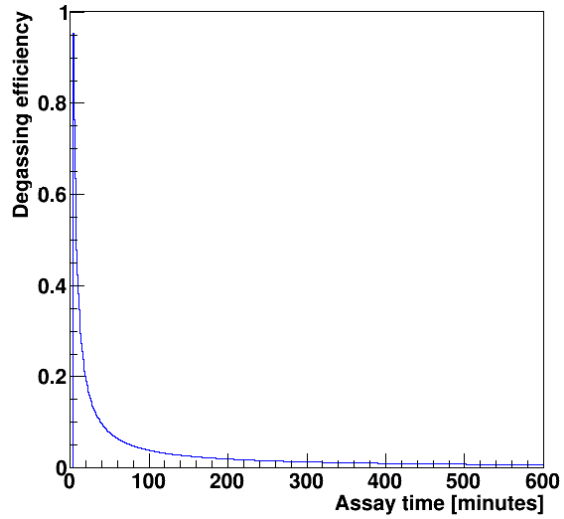
$$\epsilon_{\text{degas}} > \frac{0.5}{CF}\left[\frac{Bt_{\text{count}}\lambda}{\epsilon_{\text{count}}\epsilon_{\text{transfer}}\epsilon_{\text{trap}}(1 - e^{-\lambda t_{\text{count}}})(e^{-\lambda t_{\text{delay}}})(1 - e^{-\lambda t_{\text{assay}}})} - R_{\text{back}}\right] \tag{4.22}$$

The values of Eq. 4.22 are tabulated in Table 4.3 for a hypothetical case of running the SRAS during the scintillator phases with no background in C-300, a LC background of only 2 cpd, and the remaining typical assay values. Using these conditions, the relationship in Eq. 4.22 is then plotted for $\epsilon_{\text{degas}} < 1$ and the possible range of $0 < t_{\text{assay}} < 100$ hours. Figure 4.13 depicts the relation, in which physical values for ϵ_{degas} and t_{assay} must be above the curve.

Figure 4.13a shows that even if C-300 operates with perfect degassing efficiency and has no background, an assay of LAB+PPO will still require at least 11 hours of assay time to achieve a signal with LC counting.

(a) Limit curve for pure LAB+PPO phase ^{222}Rn assays.

(b) Limit curve for Te-LS phase ^{222}Rn assays.

Figure 4.13: Curves depicting the lowest possible limits of ϵ_{degas} and t_{assay} while operating a ^{222}Rn assay with C-300 and the SRAS. Values must be above the curve for a signal during LC counting. The curve is plotted using Eq. 4.22 and values from Table 4.3 (a) Pure LAB+PPO phase (b) Te+LS phase

Full recirculation of the scintillator within the scintillator plant will take 100 hours, and if the entire time is used to conduct the assay, the degassing efficiency can be relaxed significantly to 15 %. Note that due to radon's high affinity for LAB, at equilibrium conditions the Henry coefficient for Rn in LAB is ∼11 atm/mf, resulting in a Rn partitioning of 87 % in LAB and 13 % at liquid-gas equilibrium [85]. If assumed that ϵ_{degas} is no better than 13 % for single stage equilibrium, such a partition within C-300 may result in too low a signal to noise ratio: only ∼11 counts from radon decays within the LC may be counted if the full 100 hours is used for an assay time. If this is indeed C-300's efficiency with vacuum, the LC background rate, B, must be less than 1.8 cpd for the signal to be visible, and the background rate of the SRAS and C-300 will have to be less than $R_{\text{back}} = 2.3$ Rn/day for a visible signal. Note that even a small N_2 gas flow in the column (e.g. < 5 LPM) will not reduce the SRAS trapping efficiency, ϵ_{trap}, but will increase the C-300 degassing efficiency for radon significantly above the vacuum case. The best N_2 flow within C-300 will need to be configured during commissioning of the system.

In comparison, if one considers the relaxed concentration of $1.3{\times}10^{-2}$ Rn atoms/L scintillator during the Te-LS phase, a signal within the LC is achieved after only 4 minutes of assay time, as Figure 4.13b depicts. Additionally with this concentration, if the degassing efficiency is only 13 %, a signal is still achieved after a relatively short assay time of 30 minutes. If again the degassing efficiency of C-300 is reduced to 13 % while operating with only vacuum (the anticipated worst case scenario), the background radon from the system can be relaxed to R_{back} ∼360 Rn/day while operating with Te+LS, and LCs with backgrounds of a few cpd

70
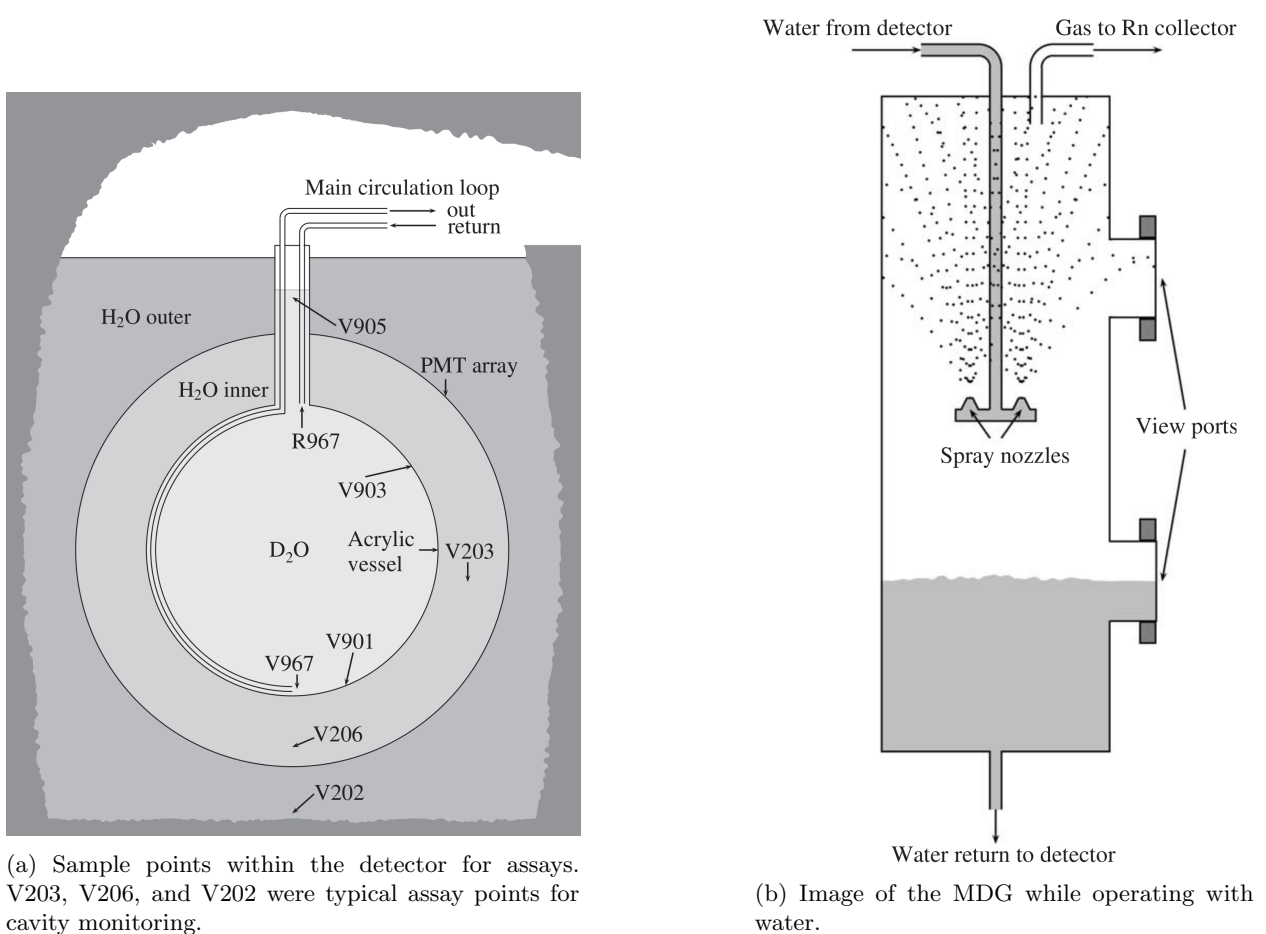
can be used.

4.8   Cavity Water MDG Unit

In addition to monitoring internal radon levels, a monitor degassing (MDG) column and assay system was installed during SNO for regular monitoring of ^{222}Rn within the cavity water surrounding the detector. Connected to a variety of sampling points, this H_2O assay system was capable of sampling the cavity water at a total of six cavity locations: two at the bottom of the cavity, one at the bottom of the PSUP, and three at the equator of the acrylic vessel [102]. The most commonly sampled points were V203 at the equator, V206 at the bottom of the PSUP, and V202 at the bottom of the cavity, as depicted in Fig. 4.14a. Various loops of the H_2O process system could also be sampled for additional monitoring as required. The diversity of sampling points allowed for a strong monitoring system which can identify key locations with high Rn rates, ensuring the leak-tight seal of the PSUP keeps less pure H_2O from the inner PSUP region, and for monitoring external and process areas which the SNO detector could not.

Opposed to C-300, which is a 24' high stripping tower, or even the H_2O process degasser, the MDG for water assays is only a 4' high degassing column, with two clear view ports and a nozzle which sprays H_2O upwards to fall and disperse on the walls of the column (see Fig. 4.14b). A nitrogen sweep gas is not typically used in the MDG radon removal process as it generates significant exhaust for the vacuum pump to process, instead the MDG is placed under vacuum for water assays. The reduction in size and in equilibrium stages leads to $\epsilon_{\mathrm{degasser}} = 0.58 \pm 0.10$ while operating at typical settings of 13 °C and $F = 19$ L/min [102]. This degassing efficiency is sufficient for monitoring Rn levels in H_2O but would be extremely ineffective for process degassing the H_2O, or for assaying the exceptionally low Rn levels within the scintillator since the Henry coefficient for radon in LAB is low. A pressure transducer near the vacuum pump illustrates that the system typically maintains vacuum pressures of ~ 10 mTorr or better.

Just like with the SRAS, extracted radon gas first encounters a modified freeze-trap, this time operated near -66 °C to freeze out residual water vapour. Radon is then collected into traps A and B, which function very similarly to the SRAS, as well as the Lucas cell ports and the Vladimir trap right before the vacuum pump. Various components of this system are either stainless steel Swagelok® fittings, NTP connections, or polypropylene tubing, resulting in higher leaks and emanation rates and a less effective vacuum pressure than the SRAS. Additionally, vacuum is generated by a rotary vane pump, which possesses less of a vapour tolerance than scroll pumps, possibly reducing the vacuum efficiency of the system. Due to increase in backgrounds and decrease in vacuum efficiency, this system is inadequate for measuring the low levels of radon within scintillator, but is readily available for accurate measurements of the ^{222}Rn levels within the

(a) Sample points within the detector for assays. V203, V206, and V202 were typical assay points for cavity monitoring.

(b) Image of the MDG while operating with water.

Figure 4.14: Former operation of the H$_2$O MDG while hooked up to the SNO detector [102]. Operations will be similar once recommissioned for use in SNO+. (a) Typical valve sampling points for radon assay during SNO. (b) The MDG operating with water inside.

cavity water and UPW plant.

As this system had not been run since SNO times, many of components had been locked and tagged out, and some necessary lines were even disconnected from the water processing system. Furthermore, the SNO assay procedure and UPW flowsheets have been modified over the years since this decoupling, yet changes within the water system were not always reflected in the most recent procedure for running the MDG. Up-to-date flowsheets have now been cross-checked with the existing system components, and the most recent procedure was cross-checked against these flowsheets. Nitrogen gas lines were re-routed, and some status tags were removed. Effort is still required to reconnect the MDG to the UPW water lines, but the system itself is now functional and has been operated for internal tests of its components.

A modified procedure has been written such that a user may perform background runs of the assay system (see Appendix B for procedure and MDG P&ID). This is executed by pulling vacuum on the MDG, which is open only to the assay traps and vacuum pump. Once a steady vacuum with flow through the FTS

trap is established, a LN$_2$ dewar is placed under Rn trap A and valves turned such that the flow starts with the MDG, flows through the functioning FTS and primary Rn traps, then through the Vladimir trap to the vacuum pump. Any Rn which would be produced from the MDG, FTS trap, Trap A, or any of the process tubing in between would be collected into Trap A. This background radon is assumed to come either by emanation or through diffusion from these larger and more often used pieces of the assay system. Transfer from trap A through trap B to the LC is considered quick relative to the use of these pieces, and thus possesses negligible background contributions. The background rate of the system can be determined with Eq. 4.17 where $R = 0$ and one solves for R_{back} by assuming the efficiencies are the same as those quoted during SNO (see [102] in Table 4.4).

The first background run was performed on April 21, 2015 (run 15042116), while the MDG was $\sim 1/3$ full of H$_2$O, undoubtedly this is remainder UPW from the last SNO assay. As valves still isolated the MDG from the remaining water plant, there was no way to remove the water, but this is not problematic as during a typical water assay the water level inside the MDG is held near this level. Flow from the MDG through the FTS trap into LN$_2$ cooled Rn trap A was established late in the shift (2:09 p.m.) due to the large volume of gas contained within the MDG and the slow removal of this gas with the vacuum pump, resulting in much shorter timescales than recommended for extraction and transfer. Extraction to trap A ended at 2:30 p.m. (t_{assay}=21 min), and throughout extraction the MDG's temperature remained a steady 19 °C (lab temperature). Transfer from trap A to B started and finished at 2:36 p.m. and 2:46 p.m. respectively, while transfer to LC started and finished at 2:50 p.m. and 3:00 p.m., respectively. Due to the rushed collection near the end of the shift, trapping and transfer efficiencies may be less than quoted, and undoubtedly not enough time proceeded during the assay to gather sufficient ^{222}Rn ingress. The LC was then disconnected from the system and transported to surface for counting with PMT 16, which began at 4:25 p.m. Unfortunately shortly after the beginning of counting, the LC counting system experienced power failures, and counting efficiencies may not even be accurate. Regardless, the data was analyzed assuming typical collection and counting efficiencies (see Table 4.4), which at least provides a minimum background rate of the MDG of 11.41 cpd. As it is impossible to characterize the change in efficiencies, there is no uncertainty accompanying this value.

A complete MDG background run was performed on July 23, 2015 (run 15072316). In comparison to run 15042116, the pressure within the system dropped quickly, indicating that the MDG still held a good vacuum from the run three months ago, and suggesting that the system was full of air previous to the first run, the reason of which is unknown. After establishing a steady vacuum of 6 mTorr within the assay traps and MDG vessel, the background assay began and ran for 1 hour, 18 minutes. 2.75 hours after the assay, the Lucas cell was taken to surface and began counting with PMT 16 within the designated counting apparatus.

After 12.82 days of counting, the data was extracted and analyzed, the values of which are also tabulated in Table 4.4.

Sample	Typical SNO data [102]	MDG (cut short)	Complete MDG Background
File	-	15042116	15072316
λ	0.182 days^{-1}		
ϵ_{count}	$3\times(0.74 \pm 0.07)$		
$\epsilon_{\text{transfer}}$	$64\pm2\%$		
ϵ_{trap}	$100.5\pm2.3\%$		
ϵ_{degas}	$58\pm10\%$		
LC ID	-	LCT6	LCT6
B	20 cpd	2.88 ± 0.47 cpd	2.88 ± 0.47 cpd
S	740 counts	115	67
t_{count}	8 days	12.98 days	12.82 days
t_{delay}	2 hours	0.21 days	5.75 hours
t_{assay}	30 min.	21 min (0.014 days)	1.31 hours
R_{back}	460 Rn/day	>11.41 Rn/day	446.6 ± 157.8 Rn/day
F	19 LPM	-	-
C	$\mathcal{O}(10^{-13}gU/g)$	-	-

Table 4.4: Summary of H_2O MDG runs. The first column is data from SNO [102], of which the efficiencies are still used in current-day analysis. The second column is an incomplete MDG background which establishes a lower bound on the MDG background rate. The third column is a complete MDG background run which establishes the background rate as 446.6 ± 157.8 cpd.

The analysis of run 15072316 also uses the efficiencies from SNO, and uncertainties of times were not considered. Additionally, the first entry (i.e. the first three hours of counting) was cut from the analysis, as it recorded a high number of counts. This is not the first time this counter (PMT 16) has exhibited this behaviour, and it is understood to be dark noise of the PMT, which is characteristic in some PMTs when they are first turned on. Until the counting system has been upgraded, the first entry with PMT 16 should always be cut from the analysis. Cutting the first three hours changes $t_{delay} \to 5.25$ hours and $S \to 67$ total counts, resulting in an MDG background rate of $R_{\text{back}} = 446.6 \pm 157.8$ Rn atoms/day. This value is consistent with SNO data which reports an MDG background rate of 460 Rn atoms/day [102], and concludes the MDG exhibits very little change from SNO operation, verifying the quoted efficiencies. In establishing the sensitivity of the MDG system, the background rate of 446.6 Rn atoms/day permits assays to observe concentrations of 4.75×10^{-15} gU/gH_2O or higher. This background value will be used during upcoming water assay analysis with this system, measuring anticipated levels of 10^{-14} g/g at the inner PSUP and 10^{-13} g/g outside the PSUP. If the proper connections to the AV are possible, the H_2O within the AV during water phase, at an estimated ^{238}U content of 10^{-14} g/g, can also be monitored *ex-situ* with this system.

4.9 Mobile Radon Emanation System

The most versatile radon assay system is a small apparatus, similar to the other two but built completely on a movable cart. Designed to be lightweight, this mobile system does not require an FTS trap as no assays are performed on liquids, nor does it have a Vladimir trap for the backflow of radon gas. Inputs on this mobile system allow for connections to a vacuum-sealed stainless steel emanation chamber, in which a sample can be placed to emanate radon gas, or to tubing on the cover gas system, allowing for radon assays of the N_2 cover gas. If for N_2 assays, a steady flow rate of less than 1 LPM must be established to ensure trapping of Rn within trap A is unity, and Eq. 4.18 solves for the radon concentration within the cover gas. The emanation chamber, meanwhile, has been instrumental in maintaining the SNO+ radon budget with the selection of SNO+ detector materials, but requires a slightly different analysis approach.

For emanation runs, a small sample is placed inside the chamber, which is then flushed with nitrogen gas three times, and pumped down to a suitable vacuum pressure after each flush. A valve located at the entry point of the chamber is then closed, isolating the sample for typically 1 - 2 weeks before the assay occurs (see Appendix C for assay procedure). As the samples are typically quite small and are expected to posses low backgrounds, this longer sampling time, denoted t_{eman}, is required to obtain enough statistics for the sample, and often several of the same sample are emanated together for higher radon output. Ideally, equilibrium is approach between the emanation and decay rates of ^{222}Rn, so emanation time is a few times the ^{222}Rn half-life. Simply pulling vacuum on a sample within the chamber for an hour or so will not collect enough radon for an accurate analysis.

The addition of t_{eman} requires an adaptation to the radon production rate, since radon production occurs for a time $t_{eman} + t_{assay}$, and not simply t_{assay}. Yet $t_{assay} \sim 1$ hour whereas $t_{eman} > 1$ week, so the approximation $t_{eman} + t_{assay} \approx t_{eman}$ is made. Returning to Eq. 4.15 and replacing t_{assay} with t_{eman} results in a modified production rate of:

$$R = \frac{N_{sample}\lambda}{\epsilon_{trap}(1 - e^{-\lambda t_{eman}})} \tag{4.23}$$

Which, along with a similar formula for background rates, is carried through to find the ^{222}Rn production rate of a sample left inside an emanation chamber, changing Eq. 4.17 to:

$$R = \frac{(S - Bt_{count})\lambda}{\epsilon_{count}\epsilon_{transfer}\epsilon_{trap}(e^{-\lambda t_{delay}})(1 - e^{-\lambda t_{eman}})(1 - e^{-\lambda t_{count}})} - R_{back} \tag{4.24}$$

Once the radon production rate of a particular substance has been calculated, the value determines if a sample will break the allowed radon budget, depending on how large the entire piece is, how many there will

Run	15021916	14121709	15020615	15050616
Sample	System bkg.	W 6001	W 6001-2Z	W 6001-2Z (ultrasonically cleaned)
λ (days^{-1})	0.182			
ϵ_{count}	$3\times(0.74 \pm 0.07)$			
$\epsilon_{\text{transfer}}$	0.618 ± 0.01			
ϵ_{trap}	1.0 ± 0.023			
LC ID	LCT6	N8	LCT5	LCT6
B	2.9 cpd	17.55 cpd	7.70548 cpd	2.9 cpd
S	224 counts	1003 counts	367 counts	484 counts
t_{count} (days)	13.8033	28.7157	6.85968	6.72772
t_{delay}	3.40 hours	4.33 hours	4.20 hours	6.15 hours
t_{assay}	1.2 hours	1.0 hours	1.0 hours	1.0 hours
t_{eman}	13 days	20 days	51 days	21 days
R_{back} (Rn/day)	30.11	30.11	30.11	30.11
R_{sample} (Rn/day)	N/A	40.67	30.30	63.46

Table 4.5: Mobile emanation runs. Run 15021916 is a background test of the system, while the remaining runs are emanations of metal bearings performed with the new background value. Even after the re-run, values are high and inconsistent. Transfer and trapping efficiencies are from [109].

be, and the object's location.

As with the other assay systems, a background run is performed by mimicking a sample extraction when no sample is present. For this system, the chamber was emptied, flushed with N_2 gas and evacuated, then sealed and left for 13 days. On day 13, the background assay was performed. A background run of this system had been performed much earlier, yet surprisingly high results of samples (in particular two sets of two bearings, each only $\sim$ 1" dia.) led to the belief that fittings in the system had become loose.

The background test (15021916 in Table 4.5) demonstrates that the emanation system possess a somewhat acceptable background of 30.11 Rn atoms/day, and for clarity the data from the bearings was then re-run with this background level (runs 14121709 and 15020615). Yet the emanation rate remained high for such small samples, so the bearings were ultrasonically cleaned before undergoing emanation runs again. Run 15050616 shows that after ultrasonic cleaning, sample W 6001-2Z apparently possessed an even higher production of ^{222}Rn atoms, while the run of the other ultrasonically cleaned sample (sample W 6001) was aborted due to the high chamber pressure. The runs after ultrasonic cleaning are clear indicators that leaks occurred during the emanation/assay.

After some experience with this system, it becomes clear that the tubing connecting the emanation chamber to the traps is rather leaky, obtaining only a vacuum pressure of 60 mTorr instead of <30 mTorr which the traps and remaining system hold, and if not connected correctly may introduce large quantities of radon atoms. Additionally, the emanation chamber must be properly secured after each sample is swapped, otherwise when placed under vacuum a fitting which may seem secure at atmospheric pressure will become loose. Unfortunately, the emanation chamber must be disassembled and reassembled for the insertion of

each sample, which leads to a high uncertainty in background levels for each individual sample. Finally, if a LC is improperly disconnected from the board, a large number of ^{222}Rn atoms can enter the cell. Any one of these complications generates useless data, and a number of changes to this system should be made before data is again reliable. In comparison, the SNO H$_2$O Rn assay system consists of much larger volumes (MDG, FTS, Vladimir trap, large 1" polypropylene tubing) compared to the mobile system (all tubing is under 1/2" diameter), but achieves a vacuum pressure which is three times better. The mobile board is currently undergoing modifications to improve vacuum and background levels.

Chapter 5

The alpha-n Problem from Radon

5.1 The Problem with ^{210}Pb

As demonstrated in the previous chapters, radon is a troublesome parent of radioisotopes which are direct backgrounds in SNO+. Previous chapters have established the means of preventing ^{222}Rn ingress into the detector through barriers such as the Urylon-lined and UPW-filled cavity, leak-tight PSUP barrier, N$_2$ cover gas, and materials low in radon. Means of ^{222}Rn extraction from the detector via scintillator and UPW degassing columns have been described, and user-defined parameters such as a fiducial volume and ROI cuts will reduce the number of backgrounds in the interested region, while *in-situ* and *ex-situ* monitoring of the detector will be ongoing. These and other processes will ensure the SNO+ detector remains as pure as possible while running, but careful consideration must be taken to account for backgrounds that leached in before SNO+ was turned on.

The AV is the final barrier between external backgrounds and the SNO+ detecting medium, and as such must be exceptionally pure. Yet exceedingly small traces of impurities can always be found in any material, and the AV can possess two forms of radioactivity: bulk radioactivity, which is intrinsic to the acrylic and impossible to remove, and surface radioactivity, which can accumulate over time. During the acrylic bonding of the AV, electrostatic attraction of ^{222}Rn lead to an increase in surface radioactivity. With short lifetimes, ^{222}Rn and its daughters within the acrylic would have decayed before or shortly after the detector was turned on, until the long-lived radioisotope ^{210}Pb, with its 22 year half-life, was reached. Embedded about ~0.2 microns below the AV surface, these particles are expected to be decaying throughout the course of SNO+ [83]. In addition to initial construction, ^{210}Pb was also allowed to embed itself below the AV's surface during reconstruction of the detector, much the same as how the Lucas cells gain in background over time.

At the end of SNO, the AV and cavity were drained, and renovations went underway for the SNO+ detector. In that time, major construction was performed in the cavity: the new hold-down rope net was placed over the AV, then anchored to the floor, which had been re-lined. Many broken PMTs were removed, repaired, and replaced, and a new optical-fiber based calibration system was installed on all nodes of the PSUP. In the 5 years it took to renovate the detector, radon-rich lab air (approx. 3.54 ± 0.18 pCi/L) circulated around the detector and decayed, eventually leaving behind the long-lived ^{210}Pb. The recoil energy of the ^{210}Pb daughter is large enough to embed itself a few microns below the AV surface. To combat this the AV was cleaned [110,111]. As the the AV could no longer be sealed during this process, a tent was built over the top of the neck through which compressed air was blown, preventing further radon ingress during cleaning [112]. After cleaning the top of the neck was sealed, yet one still expects ^{210}Pb to have embedded itself on both inner and outer layers of the AV. A severe break in the ^{238}U chain is expected within the SNO+ detector due to this ^{210}Pb contamination.

Careful consideration was made on whether or not to sand the AV to remove embedded impurities, the decision driven by the complexity of the task and concern for accurately undertaking such an effort within a reasonable schedule with the available resources [111,113]. Sanding such a large area could lead to a increase in opacity from a possibly rough surface, an increase in radioactivity by introducing other contaminants in the process, and accidental hotspots as a result of removing too much or too little of the acrylic in localized places. For these reasons the AV was not sanded, but instead SNO+ will take advantage of the water and initial pure scintillator phases to soak the Rn daughters from the AV, an act of pre-purifying for the $0\nu\beta\beta$ and solar neutrino studies. Considerable effort is also undertaken with Monte Carlo simulations to characterize the embedded contaminants on the SNO+ AV surface during each phase, such as in § 5.3.2. Such simulations are performed with the SNO+ RAT (Reactor Analysis Tool) simulation and analysis software [114]. This custom simulation package integrates several other software packages, including CLHEP [115] (a library containing classes useful to physics software), Geant4 [116] (GEometry ANd Tracking toolkit typically used for simulations, here used for its command interpreter), ROOT [117] (a modular scientific software toolkit developed at CERN, used in RAT to load and save objects to/from disk and over the network), and GLG4sim [118] (a Generic Liquid-scintillator Anti-Neutrino Detector Geant4 simulation, the classes of which are used to create a Monte Carlo event producer in RAT).

It is important to note that ^{210}Pb would have also embedded itself in other detector materials, such as the PSUP. With the large quantity of UPW and 5 cm of acrylic separating the PSUP and other materials from the detecting medium, backgrounds from ^{210}Pb on these materials will be much less likely to enter the SNO+ fiducial volume. Yet diverse backgrounds come from ^{210}Pb decay, requiring a large number of collaborators to investigate all possible reactions, including the effects of ^{210}Pb embedded within other materials. This

chapter explores one particular problem while the detector is running with H_2O for an estimated 9 months: what will occur when ^{210}Po, the daughter of ^{210}Pb decays within or near the AV surface. The decay will lead to an energetic alpha which can undergo $^{13}C(\alpha, n)^{16}O$ reactions which are potentially dangerous for the invisible nucleon decay search.

5.2   Alphas from ^{210}Po

The long half-life of ^{210}Pb embedded within the AV leads to a steady source of ^{210}Po (half-life 138.4 days), which will be the most abundant alpha source in SNO+. From SNO experience, a total of 1.2×10^9 ^{210}Po events are expected within 9 months of running during the SNO+ water phase (see Table 5.1).
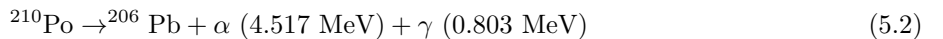
Material	Th (Bq)	U (Bq)	^{210}Po (Bq)
AV (Internal)	0.12 (bulk)	0.37 (bulk)	1150
AV (External)	0.12 (bulk)	0.37 (bulk)	1180
H_2O	0.011	0.39	*$L_0 = (1.2\times10^9)$

Table 5.1: Expected radioactivity levels of alpha emitters within the SNO+ AV (internal and external boundaries) and in the H_2O detecting medium [83]. *During water phase $L_0 = 1.2\times10^9$ ^{210}Po events are expected within 9 months of running.

^{210}Po atoms decay via:

$$^{210}\text{Po} \rightarrow^{206} \text{Pb} + \alpha \text{ (5.3 MeV)} \tag{5.1}$$

or, at a branching ratio of only 1.2×10^{-5}:

$$^{210}\text{Po} \rightarrow^{206} \text{Pb} + \alpha \text{ (4.517 MeV)} + \gamma \text{ (0.803 MeV)} \tag{5.2}$$

The alphas from ^{210}Po decay are often energetic enough to interact with atoms in reactions known as (α, n) interactions. Specifically, $^{13}C(\alpha, n)^{16}O$ reactions, in which the α strikes a ^{13}C nucleus and produces a neutron and ^{16}O atom, will be the most prominent (α, n) reaction within SNO+ due to the large quantity of both reactants and the favourable reaction threshold. Relevant abundances of target atoms and their thresholds for the H_2O phase are listen in Table 5.2.

Element	Natural Abundance [%]	Density in H_2O [cm^{-3}]	Density in PMMA [cm^{-3}]	(α, n) thres. [MeV]
^{13}C	1.1	N/A	3.94×10^{20}	0
^{17}O	0.038	1.27×10^{19}	5.44×10^{18}	0
^{18}O	0.2	6.69×10^{19}	2.86×10^{19}	0.85

Table 5.2: Target atoms of ^{210}Po alpha bombardment within SNO+ during the H_2O phase and their thresholds [83]. ^{13}C is the most common target.

During water phase, ^{13}C, ^{17}O, and ^{18}O are the only possible isotopes to interact with ^{210}Po's 5.3 MeV alpha. ^{17}O and ^{18}O will be present in both H_2O and the PMMA acrylic, but these interactions will occur less often and only result in 2.7 MeV gammas. During H_2O running the detector threshold will be 5 MeV for the search of nucleon decay (region of interest is from 5 MeV to 9 MeV), so the signals from these interactions will be of no interest. They are, however, under investigation for the Te+LS phase as they can be a $0\nu\beta\beta$ background.
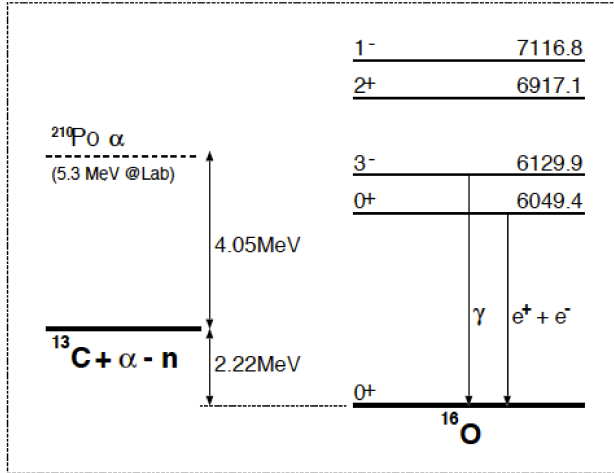
Figure 5.1: Energy levels of the ^{13}C$(\alpha, n)^{16}$O reaction with α from ^{210}Po decay [83]. De-excitation of oxygen leads to backgrounds during the nucleon decay search.

In comparison to oxygen, interactions with the more common ^{13}C within the AV will produce gammas which are a direct concern for the nucleon decay search. Products from this ^{13}C$(\alpha, n)^{16}$O reaction depend on which intermediate ^{17}O* state is generated, which in turn depends on how the reaction branches. Branching ratios to the first and second excited states of ^{17}O are both 10 %, and both states will generate signals within the detector (see Fig. 5.1 for energy level diagram). All other excited states of ^{17}O return to ground state ^{16}O without the emission of gammas. The first excited state transitions to ground state ^{16}O by electron-positron emission with creation energy of 6.05 MeV, while for the second excited state, a problematic 6.13
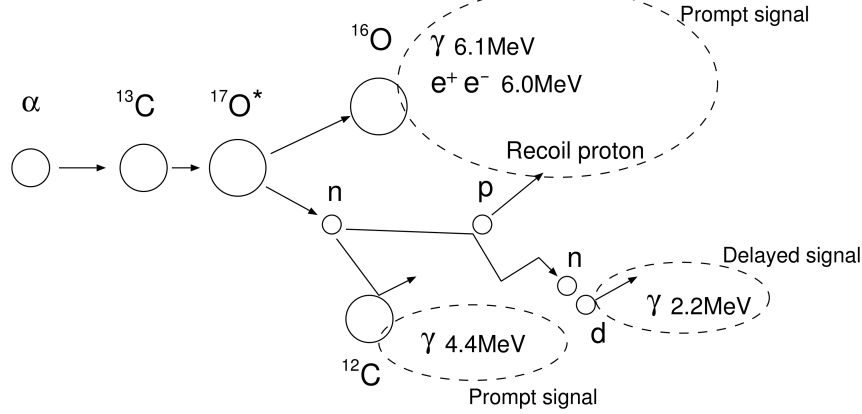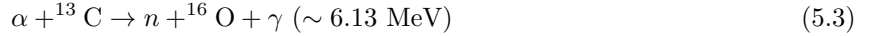
Figure 5.2: Prompt and delay signals in SNO+ for the ^{13}C$(\alpha, n)^{16}$O reaction [119]. Concerning for the nucleon decay search are the prompt signals from oxygen de-excitation.

MeV gamma is emitted upon transition to ground state:

$$\alpha + ^{13}\text{C} \rightarrow n + ^{16}\text{O} + \gamma \; (\sim 6.13 \text{ MeV}) \tag{5.3}$$

Apart from the $\sim$6 MeV photon, a wide variety of background signals can be induced within SNO+, depending on how the remaining reaction(s) proceed (see Fig. 5.2). In total, prompt signals from ^{13}C$(\alpha, n)^{16}$O reactions can come from:

- De-excitation of oxygen's second excited state, emitting a 6.13 MeV photon

- De-excitation of oxygen's first excited state, creating an e$^+$e$^-$ pair with creation energy of 6.05 MeV

- ^{12}C(n,nγ)^{12}C scattering, emitting a 4.4 MeV gamma

- Neutron scattering off a proton, in which the recoil proton produces scintillation light

- Quenched scintillation light of 0.2 MeV from the alpha

Meanwhile, the delayed signal from the α, n reaction will be the 2.2 MeV photon emitted during neutron capture: $n + p \rightarrow d + \gamma$ (2.223MeV).

The ^{13}C$(\alpha, n)^{16}$O reaction induces backgrounds during every phase of SNO+. The neutron mimics antineutrino interactions ($\bar{\nu}_e + p \rightarrow e^+ + n$), potentially hindering any reactor or geoneutrino analysis. For the $0\nu\beta\beta$ phase, the 2.2 MeV photon emitted from neutron capture is dangerously close to the ^{130}Te spectrum endpoint, and can potentially occur anywhere throughout the internal detector volume. For the nucleon decay search, any interaction with energy between 5 and 9 MeV is a potential background, such as the 6.13 MeV photon or the e$^+$e$^-$ pair. Fig. 5.3 is a spectrum plot of ^{13}C$(\alpha, n)^{16}$O signals within the
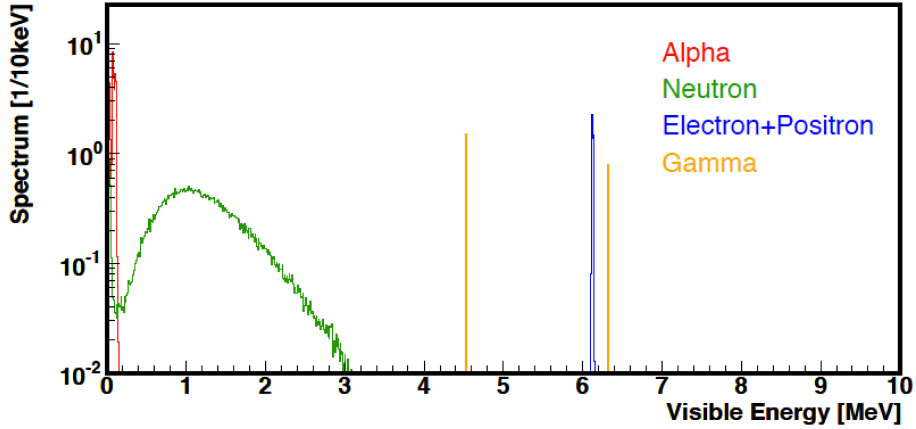
Figure 5.3: Visible energy spectrum of ^{13}C(α, n)^{16}O reactions in KamLAND [120]. During SNO+ water phase the only visible signals should be the 6 MeV gamma and the electron+positron pair, which may be backgrounds for the nucleon decay search.

KamLAND detector, and although the majority of these particles won't likely be seen within SNO+ during water phase, they may aid in coincidence tagging techniques to remove backgrounds that do fall in the ROI. The next section described the detailed simulations of ^{13}C(α, n)^{16}O which have been carried out for the SNO+ water phase, to ensure the appropriate region of interest and fiducial volumes have been chosen to reduce such backgrounds.

5.3 ^{13}C(α,n)^{16}O Reactions in Water Phase

5.3.1   Criteria for Monte Carlo Simulations

During water phase, the ^{13}C(α, n)^{16}O reactions will be induced by ^{210}Po alphas hitting a ^{13}C atom within the AV. As ^{210}Po will be embedded within the surface of the AV, the first step in evaluating the frequency of ^{13}C(α, n)^{16}O reactions is to determine how many of the ^{210}Po alphas deposit full energy within the acrylic. Using the SNO+ RAT simulation and analysis software, embedded ^{210}Po decay was mimicked by simulating alpha particles with energies of 5.3 MeV up to two different depths on both the inner and outer surfaces of the AV. First, a total of 500 000 alphas were simulated at a depth up to 0.1 μm on both sides of the AV, resulting in only 50.17 % of the alphas depositing all their energy within the AV. A second simulation for 500 000 alphas at a depth up to 1.0 μm show that the fraction changes by very little: 50.81 % remain within the acrylic. Tracking was implemented during the simulations such that the location of the alphas could be easily determined by demanding to know what medium the alpha existed within at the end of its track.

In addition to determining the profile of alpha particles while ^{210}Po resides within the acrylic, leaching

of either ^{210}Pb and/or ^{210}Po into the water must also be considered. This added complication changes the radial profile of the (α, n) reactions over time, resulting in a decrease in reactions as time proceeds. A study of the AV suggests leaching rates into water are 2×10^{-3} parts/day at 25 °C, and a factor of 6 smaller when at a temperature of 12 °C [83]. Summarizing all known characteristics of ^{210}Po and ^{13}C$(\alpha, n)^{16}$O reactions during water phase leads to the established set of criteria:

- 9 months of UPW as the SNO+ detecting medium

- 12 °C UPW temperature

- Leaching rates at 12 °C, estimated to be a factor of 6 lower than the leaching rate at 25 °C (which is 2×10^{-3} parts/day) [83]

- Initial internal AV activity of 1.15 kBq and external AV activity of 1.18 kBq (from Table 5.1)

- 50 % of ^{210}Po alphas depositing full energy in water (internal and external)

- A neutron yield of 4.70×10^{-8} assuming 5.3 MeV alphas from ^{210}Po decay interact with ^{13}C within PMMA acrylic [83]

From the above criteria, the expected number of events for the 9 month running period of water phase are tabulated in Table 5.3.

Material	Decay Isotope	No. Decays	^{13}C	^{18}O	^{17}O
AV internal	^{210}Po	2.56×10^{10}	604	696	59
AV external	^{210}Po	2.63×10^{10}	618	714	61

Table 5.3: Expected (α, n) events from ^{210}Po decay for 9 months of H$_2$O running [83]

Where AV internal are (α,n) events which occur on the internal surface of the AV, and AV external occur on the outer surface.

To analyze the ^{13}C$(\alpha, n)^{16}$O process, 1.9 GB of data was generated with the SNO+ RAT, and exists on WestGrid. The data is stored as 82 Ntuple files, which contain Monte Carlo information of ^{13}C$(\alpha, n)^{16}$O reactions within the SNO+ detector during H$_2$O phase.

5.3.2 Batch Data of Monte Carlo Simulations

Once all the simulations were run, the data was copied from WestGrid and analyzed offline. Counting experiments were first performed to check the quantity and fractions of various interactions, which were then normalized to the expected values in Table 5.3. A total of 9.9 million ^{13}C$(\alpha, n)^{16}$O events were simulated on

the outer AV surface, and 9.99 million events on the inner AV, values which were determined by summing all the first trigger and non-triggered events of the detector. Two counts of the first triggered events were then performed: one simply demanding the event be a first trigger, the other requiring that the event also have a valid fitter. Such a fitter is a reconstruction tool composed of a series of fits and functions to verify that the event fits the expected detector response. For each of the two cases, fitter and no fitter, the criteria was then broken down again, to search for the number of these events which fall within the FV, the ROI, and the two together. Once all these values were established, the numbers were normalized to realistic values expected over a 9 month running period. This was performed by taking the fraction of desired events over the total number of (α,n) events simulated, and multiplying it by the expected number of events as tabulated in Table 5.3. The same was then performed for all of the retriggered events recorded, and the results of both counting experiments are given in Table 5.4.

		No fitter considered			Valid fitter	
Criteria	# Events	Fraction of total events	Expected in SNO+	# Events	Fraction of total events	Expected in SNO+
External AV analysis: 9 900 000 (α,n) events simulated, expect 618 events in 9 months						
First Triggered Events						
Total	905727	0.091	56.5	905338	0.0914	56.5
Within FV	36054	0.0036	2.25	35665	0.0036	2.23
Within ROI	150182	0.015	9.38	150182	0.015	9.38
Within FV+ROI	3201	0.00032	0.200	3201	0.00032	0.200
Re-triggered Events						
Total	23839	0.0024	1.49	23711	0.0024	1.48
Within FV	2108	0.00021	0.132	1980	0.00020	0.124
Within ROI	552	0.000055	0.0344	552	0.000056	0.0344
Within FV+ROI	9	9.1e-7	0.000562	9	9.1e-7	0.000560
Internal AV analysis: 9 990 000 (α,n) events simulated, expect 604 events in 9 months						
First Triggered Events						
Total	746218	0.075	45.1	745863	0.075	45.1
Within FV	40386	0.0040	2.44	40031	0.0040	2.42
Within ROI	66148	0.0066	4.00	66148	0.0066	4.00
Within FV+ROI	3128	0.00031	0.189	3128	0.00031	0.189
Re-triggered Events						
Total	18867	0.0019	1.14	17482	0.0017	1.06
Within FV	3083	0.00031	0.186	1698	0.00017	0.103
Within ROI	481	0.000048	0.0291	481	0.000048	0.0291
Within FV+ROI	13	0.0000013	0.000786	13	0.0000013	0.000786

Table 5.4: Breakdown of ^{13}C$(\alpha, n)^{16}$O events occurring on the surface of the AV as the detector will observe them during water phase. The expected events in SNO+ have been normalized by the fraction of relevant Monte Carlo events and the total number of expected (α,n) events in the region.

Combining the expected number of events for both the inner and outer AV surfaces results in Table 5.5.

Condition	No fitter considered	Valid fitter
First Triggered Events		
Total	102	102
Within FV	4.69	4.65
Within ROI	13.4	13.4
Within FV+ROI	0.389	0.389
Re-triggered Events		
Total	2.63	2.54
Within FV	0.318	0.226
Within ROI	0.0635	0.0635
Within FV+ROI	0.00135	0.00135
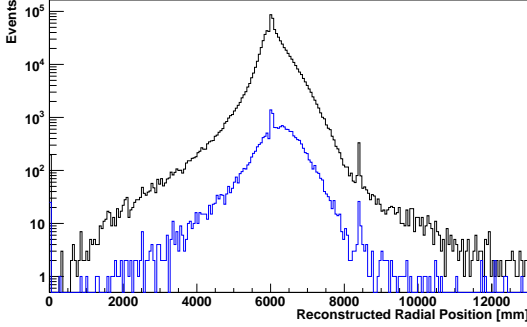
Table 5.5: Summary of expected $^{13}C(\alpha, n)^{16}O$ events during water phase over a 9 month period.

In comparing the number of first triggered events which have a valid fitter to all first triggered events regardless of whether the fitter is valid or not, there is very little change in numbers: 99.96 % of all first triggered events also have a valid fitter. This value changes only very slightly for retriggered events (99.5 % and 92.7 % for outer and inner AV, resp.), but in all cases the fitter is valid for every event which reconstructs within the defined region of interest. For this purpose the remaining analysis performed is on the events which possess a valid fitter.
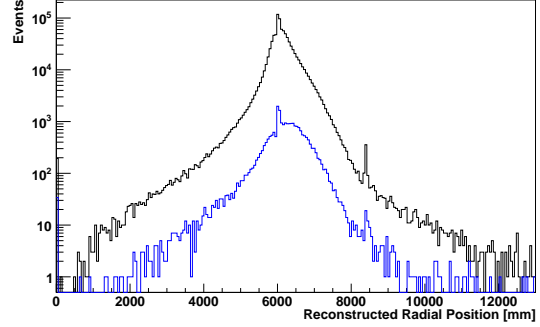
Even with 9 months of running with the AV filled with water, not even one first triggered event will reconstruct within the defined region of interest and fiducial volume. The chance of a retriggered event within the defined cuts is much less, as expected since the majority of retriggered events should be from neutron capture which produce energy of 2.2 MeV outside the ROI. Although SNO+ can expect 102 first trigger events during running, the majority of these reconstruct on or near the AV surface, so that only about 5 reconstruct within a radius of 5.5 m from the center of the detector, and < 0.4 events within the FV and ROI. Fig. 5.4 exhibits the radial distribution of all simulated events for both the inner and outer AV surface.

Interestingly, there is a spike in the number of events which occur at a radial distance of 8.5 m, which would roughly correspond to the placement of the PMTs (PSUP radius is 8.75 m). The PMTs and their housings are also composed of traces of plastic, which are undoubtedly recorded within the geometry of the Monte Carlo tool, meaning the simulations would have specified only the material in which to simulate the initial reactions within, and not the position. Exclusion of these PMT positions would be difficult as the AV is not only just the 12 m diameter sphere, but is also composed of the 6.8 meter tall neck, resulting in possible productions up to a radial distances of 12.8 m. Yet the existence of these simulations are negligible,
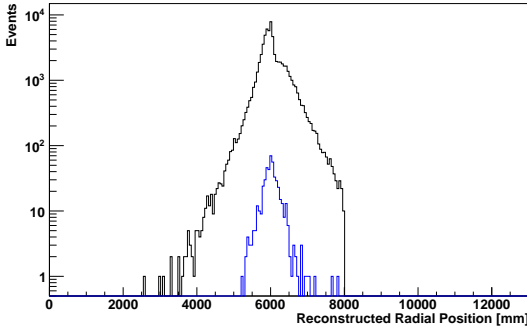
since an examination of events within the 5 - 9 MeV ROI shows that events at a radial distribution greater than 8 m sharply drop out, as Figs. 5.4c and 5.4d depict.
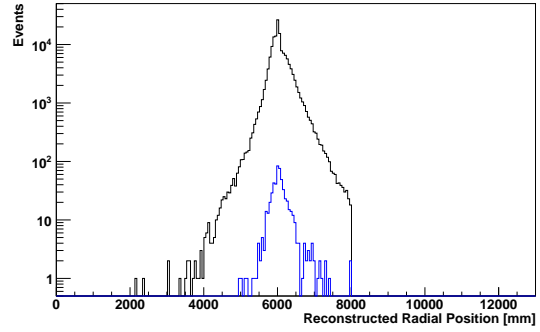
(a) Inner AV event distribution for all events with a valid fitter.
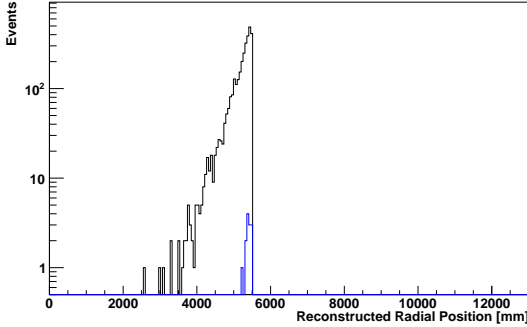
(b) Outer AV event distribution for all events with a valid fitter.
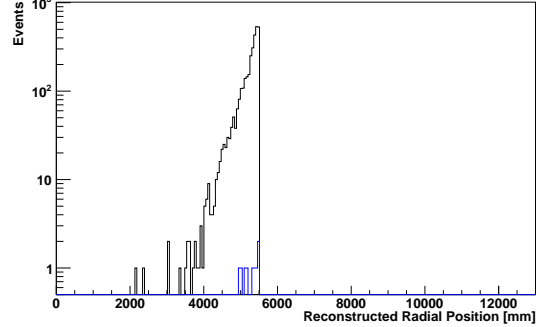
(c) Inner AV event distribution for all events with a valid fitter and reconstructed energy within the ROI.

(d) Outer AV event distribution for all events with a valid fitter and reconstructed energy within the RIO.

(e) Inner AV event distribution for all events with a valid fitter within the ROI and FV.

(f) Outer AV event distribution for all events with a valid fitter within the ROI and FV.

Figure 5.4: Reconstructed radial distribution of all detected ^{13}C$(\alpha, n)^{16}$O events within the SNO+ detector using Monte Carlo methods. Black represents first triggered events, while blue are retriggered events.

In examining the energy spectrum of triggered events within the detector (see Fig. 5.5), a large spread of energy is recorded in both the first triggered and retriggered events. However, clear peaks occur at $\sim$2 MeV, which is especially noticeable for the retriggered events, corresponding to neutron capture on hydrogen.

When examining the energies of particles reconstructed within the fiducial volume, the retriggered peak of ~ 2 MeV is even more clear, and higher energy retriggered events drop out, such that exceptionally few retriggered events ($\mathcal{O}10^{-3}$ events/9 months) will occur within the SNO+ VF and ROI cuts.

(a) Inner AV energy distribution for all events with a valid fitter.

(b) Outer AV energy distribution for all events with a valid fitter.

(c) Inner AV energy distribution for all events with a valid fitter and reconstructed energy within the FV.

(d) Outer AV energy distribution for all events with a valid fitter and reconstructed energy within the FV.

(e) Inner AV energy distribution for all events with a valid fitter within the ROI and FV.

(f) Outer AV energy distribution for all events with a valid fitter within the ROI and FV.

Figure 5.5: Reconstructed energy distribution of all detected ^{13}C$(\alpha, n)^{16}$O events within the SNO+ detector using Monte Carlo methods. Red represents first triggered events, while blue are retriggered events.

A number of tasks are still required for a complete analysis of the expected ^{13}C$(\alpha, n)^{16}$O events during water phase, however, the counting experiments clearly show that no events are expected within the SNO+

FV and ROI for nucleon decay studies spanning 9 months of detector running. Additional steps for completing the study of these reactions involve examining the timing and energies between first and retriggered events to identify a signature for the reaction, and to compare the spectrum of first triggered events within the FV to that of ^{208}Tl, which are expected to be somewhat similar. ^{208}Tl simulations within SNO+ have been simulated for the water phase, while the comparison of first triggered and retriggered events has begun.

Chapter 6

Conclusions

6.1   Radon in SNO+

Radon is a serious source of background for any underground detector searching for rare events and small signals, and the SNO+ experiment has a firmly established protocol to reduce, eliminate, and monitor the radon levels both by *in-situ* and *ex-situ* methods. A cover gas system, UPW-filled cavity, water-tight PSUP seals, and FV and ROI cuts will prevent Rn ingress from outside the detector. Purification plants for both the cavity water and scintillator will remove radon, along with its parents and daughters, from either of those mediums. Three assay systems, discussed in Chapter 4, will be in place to monitor the UPW, scintillator, and N_2 cover gas to ensure the mediums are meeting the required purification levels, while coincidences such as Bi-Po can monitor directly the activity of daughter radioisotopes. Leaching rates for the radon daughter ^{210}Pb have been calculated and are used, along with Monte Carlo simulations, to better anticipate how detector operations will unfold during data taking. Monte Carlo simulations of backgrounds from ^{13}C$(\alpha, n)^{16}$O events were discussed in Chapter 5.

6.2   Radon Assays

The Lucas cells SNO established for radon assays are directly transferable to assays performed for the SNO+ experiment. Radon enters the cell and decays within, causing ZnS(Ag) to scintillate and a PMT to record the signal. Accumulation of ^{210}Pb within the cell occurs over continual use, and tests are ongoing to establish the new background rates of the cells. Some cells exhibit high background rates, for example LC A has a background rate of 642 ± 10 cpd. Few cells possess low backgrounds of a few cpd, and others such as LCT 5 leak. Leak and background tests of the cells are ongoing for the SNO LCs, as well as the recently

manufactured cells which have yet to be used. LCT 6 has passed both the leak and background test, with a background of only 2.88 ± 0.47 cpd, and is currently used for most assays reported in this thesis. The newly manufactured cells should possess backgrounds which are equal to or lower than LCT6's.

Assays of scintillator will be performed through the coupling of C-300 and the SRAS. C-300 exists within the scintillator plant, which will soon be commissioned, while the SRAS is still under construction. The key hardware for the SRAS and a general procedure to run it have been established. All components of the SRAS are ready for assembly and are awaiting a custom piece: the connection of all 1/8" pieces currently undergoing custom assembly in a Swagelok facility. The sensitivity of the assay system will depend on the background rate of C-300. Calculations show that even with only $\epsilon_{\text{degas}} = 13$ %, relaxed backgrounds of $R_{\text{back}} \sim 360$ Rn/day and B of a few cpd are allowed for Te+LS assays. This assumes the quoted ^{238}U content of 2.5×10^{-15} g ^{238}U/g LAB. If operating at $\epsilon_{\text{degas}} = 13$ % for LAB+PPO assays, the reduced ^{238}U content of 1.6×10^{-17} g ^{238}U/g LAB requires background levels of $R_{\text{back}} = 2.3$ Rn/day and $B < 1.8$ cpd. These are considered worst case scenarios, i.e. if the degassing efficiency is only determined by one equilibrium stage with a Henry coefficient of Rn in LAB of ~ 11 atm/mf. True values will be established once C-300 and the SRAS are commissioned. The assays of scintillator within the AV will provide a first look at contamination levels within the arriving LAB, will be an effective quality control measure while the detector is running with scintillator, and assess the effectiveness of the cover gas and UPW shielding. Furthermore, the assays will determine if internal contaminants within the ^{238}U chain are from radon ingress or from AV leaching.

Assays of the cavity H_2O during every phase will be performed by the existing MDG unit SNO built. Recently, the development to operate the MDG with the AV water during water phase has been explored, and appears feasible. The system has not been used since SNO last drained the cavity, and many changes have occurred since then which required adjustments to the MDG apparatus and procedure. Recommissioning is ongoing for use with water produced from the UWP plant, or for assays with cavity water. Commissioning with vacuum has been achieved, and background levels performed under vacuum establish the background rate of $R_{\text{back}} = 446.6 \pm 157.8$ Rn/day, leading to a sensitivity of 4.75×10^{-15} g ^{238}U/g H_2O. This is low enough for assays with both cavity water (3.5×10^{-13} g ^{238}U/g H_2O) and AV water (3.5×10^{-14} g ^{238}U/g H_2O).

6.3 Radon Daughters: The ^{13}C$(\alpha,$n$)^{16}$O Reaction in Water

Internal radon daughters such as ^{210}Po are expected to be out of equilibrium with ^{222}Rn, due to the build-up of its parent ^{210}Pb just below the AV surface. Consideration of these radioisotopes require an alternative approach than the radon assay method. Monte Carlo studies allow the SNO+ collaboration to best char-

acterize expected reactions within the detector, including the $^{13}C(\alpha, n)^{16}O$ reactions expected from ^{210}Po decay. Chapter 5 studied the reaction for the anticipated 9 months of detector running with water for the nucleon decay study. Of concern during the water phase are the products of this reaction when the intermediate oxygen state decays, emitting a 6.13 MeV gamma or a e^+e^- pair with creation energy 6.05 MeV. Both products are within the energy region of interest of 5 - 9 MeV specified for the nucleon decay search. However, the Monte Carlo studies of this reaction conclude that after nine months, only about 5 events from these reactions will have reconstructed within the SNO+ fiducial volume of 5.5 m, and of these, less than 0.4 events will possess an energy within the 5 - 9 MeV region of interest. Next steps, for completeness, include the comparison of first triggered events and their associated retriggered event for the interest in identifying a signature to the reaction.

Bibliography

[1] W. Pauli. Dear radioactive ladies and gentlemen. Gauverein meeting in Tübingen. Dec. 1930. Original letter available at http://microboone-docdb.fnal.gov/ (2014).

[2] M. Lucibella. Looking at physics history. *Capitol Hill Quarterly*, 6(2), Oct. 1933.

[3] J. Chadwick. Possible existence of a neutron. *Nature*, 129:312, 1932.

[4] E. Fermi. *Ricerca Scientifica*, 2:12, 1933.

[5] F. Perrin. *Comptes Rendues*, 197:1625, 1933.

[6] E. Fermi. *Z. Phys.*, 88:161–177, 1934. Translation: F. Wilson, *Am. J. Phys.* 36:1150–1160, 1968.

[7] E. Fermi. Tentativo di una teoria dei raggi β. *Nuovo Cim.*, 11:1–19, 1934.

[8] M. Goeppert-Mayer. Double beta-disintegration. *Phys. Rev.*, 48:512–516, Sep 1935.

[9] C. Giunti and C. W. Kim. *Fundamentals of Neutrino Physics and Astrophysics*. Oxford University Press Inc., 2010.

[10] R. Saakyan. Two-neutrino double-beta decay. *Annu. Rev. Nucl. Part. Sci.*, 63:503–529, Oct 2013.

[11] G. Racah. Sulla simmetria tra particelle e antiparticelle. *Il Nuovo Cimento*, 14:322–328, 1937.

[12] E. Majorana. *Nuovo Cimento*, 14:171, 1937.

[13] W. H. Furry. On transition probabilities in double beta-disintegration. *Phys. Rev.*, 56:1184–1193, Dec 1939.

[14] M. Inghram and J. Reynolds. Double beta-decay of Te^{130}. *Phys. Rev.*, 78:822–823, Jun 1950.

[15] E. L. Fireman. A measurement of the half-life of double beta-decay from $_{50}$Sn^{124}. *Phys. Rev.*, 75:323–324, Jan 1949.

[16] M. I. Kalkstein and W. F. Libby. An investigation of the double beta-decay of $_{50}$Sn^{124}. *Phys. Rev.*, 85:368–369, Jan 1952.

[17] C. A. Levine, A. Ghiorso, and G. T. Seaborg. Half-life for double beta-decay. *Phys. Rev.*, 77:296–296, Jan 1950.

[18] E. J. Konopinski and H. M. Mahmoud. The universal fermi interaction. *Phys. Rev.*, 92:1045–1049, Nov 1953.

[19] F. Reines and C.L. Cowan Jr. The neutrino. *Nature*, 178:446–449, Sept 1956.

[20] C.L. Cowan Jr., F. Reines, F.B. Harrison, H.W. Kruse, and A.D. McGuire. Detection of the free neutrino: A confirmation. *Science*, 124(3212):103–104, July 1956.

[21] F. Reines. *Nobel Lectures in Physics, 1991–1995*. World Scientific Publishing Company, 1997.

[22] C. S. Wu, E. Ambler, R. W. Hayward, D. D. Hoppes, and R. P. Hudson. Experimental test of parity conservation in beta decay. *Phys. Rev.*, 105:1413–1415, Feb 1957.

[23] G. Danby et al. Observation of high-energy neutrino reactions and the existence of two kinds of neutrinos. *Phys. Rev. Lett.*, 9:36–44, Jul 1962.

[24] B. Pontecorvo. Neutrino experiments and the problem of conservation of leptonic charge. *Soviet Physics-JETP*, 26(5):984–988, 1968.

[25] S.M. Bilenky and B. Pontecorvo. Again on neutrino oscillations. *Lettere Al Nuovo Cimento Series 2*, 17(17):569–574, 1976.

[26] St. Weinberg. A model of leptons. *Phys. Rev. Lett.*, 19:1264–1266, Nov 1967.

[27] Standard model of elementary particles. Own work by uploader, PBS NOVA, Fermilab, Office of Science, United States Department of Energy, Particle Data Group. Image on Wikimedia Commons `https://commons.wikimedia.org/wiki/File:Standard_Model_of_Elementary_Particles.svg` Accessed 2015-06-06.

[28] F.J. Hasert et al. Observation of neutrino-like interactions without muon or electron in the gargamelle neutrino experiment. *Physics Letters B*, 46(1):138 – 140, 1973.

[29] G. Aad et al. Observation of a new particle in the search for the standard model higgs boson with the ATLAS detector at the LHC. *Physics Letters B*, 716(1):1 – 29, 2012.

[30] S. Chatrchyan et al. Observation of a new boson at a mass of 125 GeV with the CMS experiment at the LHC. *Physics Letters B*, 716(1):30 – 61, 2012.

[31] M. L. Perl and others. Rev. Lett. Evidence for anomalous lepton production in $e^+ - e^-$ annihilation. 35:1489–1492, Dec 1975.

[32] K. Kodama et al. Observation of tau neutrino interactions. *Physics Letters B*, 504(3):218 – 224, 2001.

[33] Q. R. Ahmad et al. Measurement of the rate of $\nu_e + d \rightarrow p + p + e^-$ interactions produced by ^{8}B solar neutrinos at the Sudbury Neutrino Observatory. *Phys. Rev. Lett.*, 87:071301, Jul 2001.

[34] J. N. Bahcall and R. Davis Jr. Solar neutrinos: A scientific puzzle. *American Association for the Advancement of Science*, 1976.

[35] B.T. Cleveland et al. Measurement of the solar electron neutrino flux with the Homestake chlorine detector. *Astrophys.J.*, 496:505–526, 1998.

[36] K. S. Hirata et al. Observation of ^{8}B solar neutrinos in the kamiokande-II detector. *Phys. Rev. Lett.*, 63:16–19, Jul 1989.

[37] K. S. Hirata et al. Results from one thousand days of real-time, directional solar-neutrino data. *Phys. Rev. Lett.*, 65:1297–1300, Sep 1990.

[38] J. Hosaka et al. Solar neutrino measurements in Super-Kamiokande-I. *Phys. Rev. D*, 73:112001, Jun 2006.

[39] J.N. Abdurashitov et al. Results from SAGE (the Russian-American gallium solar neutrino experiment). *Physics Letters B*, 328(1):234 – 248, 1994.

[40] W. Hampel et al. GALLEX solar neutrino observations: results for GALLEX IV. *Physics Letters B*, 447(1–2):127 – 133, 1999.

[41] M. Altmann et al. Complete results for five years of GNO solar neutrino observations. *Physics Letters B*, 616(3–4):174 – 190, 2005.

[42] J N Bahcall. Solar Models and Solar Neutrinos. *Physica Scripta*, 2005(T121):46, 2005. Updated colour plot from `http://www.sns.ias.edu/~jnb/` Accessed 2015/08/27.

[43] H. H. Chen. Direct approach to resolve the solar-neutrino problem. *Phys. Rev. Lett.*, 55(14):1534–1536, 1985.

[44] J. Boger. et al. The Sudbury Neutrino Observatory. *Nuclear Instruments and Methods in Physics Research A*, 449:172–207, 2000.

[45] Z. Petriw. An Underwater Six-Camera Array for Monitoring and Position Measurements in SNO+. Master's thesis, University of Alberta, 2012.

[46] B. Aharmim et al. Independent measurement of the total active ^{8}B solar neutrino flux using an array of ^{3}He proportional counters at the Sudbury Neutrino Observatory. *Phys. Rev. Lett.*, 101:111301, Sep 2008.

[47] A. Yu. Smirnov. The MSW effect and solar neutrinos. pages 23–43, 2003. 11th workshop on Neutrino Telescopes, Venice, March 11- 14, 2003.

[48] S. Hatakeyama et al. Measurement of the flux and zenith-angle distribution of upward through-going muons in Kamiokande II+III. *Phys. Rev. Lett.*, 81:2016–2019, Sep 1998.

[49] R. Wendell et al. Atmospheric neutrino oscillation analysis with subleading effects in Super-Kamiokande I, II, and III. *Phys. Rev. D*, 81:092004, May 2010.

[50] T. Araki et al. Measurement of neutrino oscillation with KamLAND: Evidence of spectral distortion. *Phys. Rev. Lett.*, 94:081801, Mar 2005.

[51] A. de Gouvea et al. Working Group Report: Neutrinos. *Workshop on Fundamental Physics at the Intensity Frontier Proceedings*, 2012.

[52] K.A. Olive et al. (Particle Data Group), Chin. Phys. C, 38, 090001 (2014).

[53] Katrin: Karlsruhe Tritium Neutrino Experiment. `https://www.katrin.kit.edu/` Accessed 2015-05-27.

[54] H.V. Klapdor-Kleingrothaus. *Seventy Years of Double Beta Decay: From Nuclear Physics to Beyond-standard-model Particle Physics.* World Scientific Publishing Co. Pte, Ltd., 2010.

[55] P. Di Bari. An introduction to leptogenesis and neutrino properties. *Contemporary Physics*, 53:315–338, Aug 2012.

[56] J. Kotila and F. Iachello. Phase-space factors for double-β decay. *Phys. Rev. C*, 85:034316, Mar 2012.

[57] S. Elliott and P. Vogel. Double beta decay. *Annu. Rev. Nucl. Part. Sci.*, 52:115–151, Dec 2002.

[58] J.B. Albert et al. Search for majorana neutrinos with the first two years of EXO-200 data. *Nature*, 500:229–234, 2015.

[59] A. Gando et al. Limit on neutrinoless $\beta\beta$ decay of ^{136}Xe from the first phase of KamLAND-Zen and comparison with the positive claim in ^{76}Ge. *Phys. Rev. Lett.*, 110:062502, Feb 2013.

[60] M. Agostini et al. Results on neutrinoless double-β decay of ^{76}Ge from phase I of the GERDA experiment. *Phys. Rev. Lett.*, 111:122503, Sep 2013.

[61] H. V. Klapdor-Kleingrothaus and I. V. Krivosheina. The evidence for the observation of $0\nu\beta\beta$ decay: The identification of $0\nu\beta\beta$ events from the full spectra. *Modern Physics Letters A*, 21(20):1547–1566, 2006.

[62] "The Nobel Prize in Physics 2015". Nobelprize.org. Nobel Media AB 2014. Web. 6 Nov 2015. <`http://www.nobelprize.org/nobel_prizes/physics/laureates/2015/`>.

[63] S. Andringa et al. Current status and future prospects of the SNO+ experiment. Submitted to *Advances in High Energy Physics*, 2015.

[64] SNOLAB, 2012. https://www.snolab.ca/ Accessed 2015-06-06.

[65] A. Bialek et al. A rope-net support system for the SNO+ liquid scintillator detector. Submitted to *Nuclear Instruments and Methods in Physics Research A*, 2015.

[66] EMERSON, 2015. http://www.emerson.com/ Accessed 2015-08-26. DeltaV^{TM} is a registered trademark of Emerson Electric Co. 8000 West Florissant Avenue, P.O. Box 4100, St. Louis, MO 63136, United States.

[67] CEPSA. http://www.cepsa.ca/en/home/ Accessed 2015-06-06.

[68] C. Lan. SNO+ and Geoneutrino Physics. Master's thesis, Queen's University, 2007.

[69] SNEWS: SuperNova Early Warning System. http://snews.bnl.gov/ Accessed 2015-07-01.

[70] T. Araki et al. Search for the invisible decay of neutrons with KamLAND. *Phys. Rev. Lett.*, 96:101802, Mar 2006.

[71] S. N. Ahmed et al. Constraints on nucleon decay via invisible modes from the Sudbury Neutrino Observatory. *Phys. Rev. Lett.*, 92:102004, Mar 2004.

[72] B. Aharmim et al. Measurement of the ν_e and total ^{8}B solar neutrino fluxes with the Sudbury Neutrino Observatory phase-III data set. *Phys. Rev. C*, 87:015502, Jan 2013.

[73] B. Dasgupta and J. F. Beacom. Reconstruction of supernova ν_μ, ν_τ, $\overline{\nu}_\mu$, and $\overline{\nu}_\tau$ neutrino spectra at scintillator detectors. *Phys. Rev. D*, 83:113006, Jun 2011.

[74] T. Lund and J. P. Kneller. Combining collective, MSW, and turbulence effects in supernova neutrino flavor evolution. *Phys. Rev. D*, 88:023008, Jul 2013.

[75] LV. Krivosheina. SN 1987A – historical view about registration of the neutrino signal with BAKSAN, Kamiokande II and IMB detectors. *International Journal of Modern Physics D*, 13:685, Dec 2004.

[76] A. Gando et al. Partial radiogenic heat model for Earth revealed by geoneutrino measurements. *Nature Geoscience*, 4:647–651, 2011.

[77] G. Bellini et al. Measurement of geo-neutrinos from 1353 days of Borexino. *Physics Letters B*, 722(4–5):295 – 300, 2013.

[78] A. Mastbaum. Double-beta white paper sensitivity plots. SNO+ internal document SNO+-doc-2593-v9.

[79] J.J. Gomez-Cadenas, J. Martin-Albo, M. Mezzetto, F. Monrabal, and M. Sorel. The Search for neutrinoless double beta decay. *Riv.Nuovo Cim.*, 35:29–98, 2012.

[80] D.-M. Mei and A. Hime. Muon-induced background study for underground laboratories. *Phys. Rev. D*, 73:053004, Mar 2006.

[81] L. Segui. Background reduction in the SNO+ experiment. Submitted to *Low Radioactivity Techniques Conf. Proc.*, 2015.

[82] I. Lawson. Radon levels in the SNOLAB underground laboratory. SNOLAB, Sudbury, March 2015. SNOLAB internal document SNOLAB-STR-2014-001.

[83] V. Lozza and O. Chkvorets. Neutron sources and backgrounds in SNO+, 2015. SNO+ internal document SNO+-doc-2497-v6.

[84] P. Khaghani. Master's thesis in progress, Laurentian University, 2015.

[85] R. Ford. A scintillator purification plant and fluid handling system for SNO+. *AIP Conf. Proc.* 1672(080003), 2015.

[86] R. Ford, M. Chen, O. Chkvorets, D. Hallman, and E. Vázquez-Jáuregui. SNO+ Scintillator Purification and Assay. *AIP Conf. Proc.*, 1338(183), 2011.

[87] D. Hallman. Liquid processing & assay systems for the SNO+ experiment. CAP Congress Conference Poster, Sudbury, 2015. SNO+ internal document SNO+-doc-2547-v1.

[88] General equipment arrangement 3-D view looking northwest. Koch Modular Process Systems. RTB (2008). Drawing no D207711-13-120. Paramus, NJ.

[89] J. Benziger et al. A scintillator purification system for the borexino solar neutrino detector. *Nuclear Instruments and Methods in Physics Research Section A: Accelerators, Spectrometers, Detectors and Associated Equipment*, 587(2–3):277 – 291, 2008.

[90] K. Eguchi et al. First results from KamLAND: Evidence for reactor antineutrino disappearance. *Phys. Rev. Lett.*, 90:021802, Jan 2003.

[91] KMPS: Koch modular process systems, LLC. http://modularprocess.com/ Accessed 2015-06-09. SCHEIBEL® is a registered trademark of Koch-Glitsch, LP.

[92] P& ID Scavenger Columns. Koch Modular Process Systems. RAM, W.M. (2010).Drawing no D207711-03-145. Paramus, NJ.

[93] REAXA. http://www.reaxa.com/ Accessed 2015-06-09. QuadraSil^{TM} and QuadraPure^{TM} are registered trademarks of Reaxa LTD, Hexagon Tower, Manchester M9 8ZS, UK. In 2010 Reaxa transferred its metal scavenging technology to Johnson Matthey Plc, 25 Farringdon Street, London EC4A 4AB, UK.

[94] G. Zuzel, H. Simgen, and G. Heusser. Ar and Kr concentrations in nitrogen as a measure of the ^{39}Ar and ^{85}Kr activities in connection with the solar neutrino experiment Borexino. *Applied Radiation and Isotopes*, 61(2–3):197 – 201, 2004. Low Level Radionuclide Measurement Techniques - {ICRM}.

[95] H. F. Lucas. Improved low-level alpha-scintillation counter for radon. *Rev. Sci. Instrum.*, 28(680), 1957.

[96] B.L. Cohen, M. El Ganayni, and E.S. Cohen. Large scintillation cells for high sensitivity radon concentration measurements. *Nuclear Instruments and Methods in Physics Research*, 212(1–3):403 – 412, 1983.

[97] M. Liu. ^{222}Rn emanation into vacuum. Master's thesis, Queen's University, 1991.

[98] X. Zhu. Study of vacuum degassing for SNO water system. Master's thesis, Queen's University, 1992.

[99] PHOTONIS, 18 Avenue Pythagore, 33700 Mérignac, France. *Photomultiplier XP2262*, 2006.

[100] B. McPhail, H. Lee, and I. Levine. Calibration of two SNO Lucas Cells. Document provided by internal communication.

[101] PYLON, 2007. http://www.pylonelectronics.com/ Accessed 2015-07-18. 147 Colonnade Road, Ottawa, Ontario K2E 7L9 CANADA.

[102] I. Blevis et al. Measurement of ^{222}Rn dissolved in water at the Sudbury Neutrino Observatory. *Nuclear Instruments and Methods in Physics Research A*, 517:139–153, 2004.

[103] D. R. Grant. Process and monitor degasser system for the SNO heavy water system. Master's thesis, Carelton University, 1998.

[104] SP Industries, Inc., 935 Mearns Rd, Warminster, PA, 18974 USA. *Cold Trap Operator's Manual: FTS Titan-Trap, Refrigerated Cold Trap*, 2009.

[105] SP Scientific, 2015. http://www.spscientific.com/ Accessed 2015-07-06.

[106] A.G.M. Ferreira and L.Q. Lobo. On the vapour pressure of radon. *The Journal of Chemical Thermodynamics*, 39(10), 2007.

[107] Swagelok, 2015. http://www.swagelok.com/ Accessed 2015-06-09.

[108] Welded assembly. Swagelok Central Ontario & Atlantic Canada. (2015). ASSEMBLY-43912 Rev 2.0. Personal correspondence with Andrew Wright P.Eng, Project Manager - Custom Solutions.

[109] Eric Vazquez-Jauregui, internal communication, 2014.

[110] C. Kraus. AV cleaning report, 2011. SNO+ internal document SNO+-doc-1096-v1.

[111] M. Schumaker. AV cleaning and sanding meeting April 07 2011, 2011. SNO+ internal document SNO+-doc-921-v1.

[112] M. Schumaker. Radon-reduced air supply, 2012. SNO+ internal document SNO+-doc-1359-v1.

[113] C. Kraus. AV sanding work plans and suspended platform, 2012. SNO+ internal document SNO+-doc-1365-v1.

[114] S. Seibert et al. RAT (public version) http://rat.readthedocs.org/ Accessed 2015-09-10. The private version of RAT is still under development within the SNO+ collaboration.

[115] L. Lönnblad. CLHEP—a project for designing a C++ class library for high energy physics. *Computer Physics Communications*, 84(1–3):307 – 316, 1994. See also http://proj-clhep.web.cern.ch/proj-clhep/.

[116] S. Agostinelli et al. Geant4 – a simulation toolkit. *Nuclear Instruments and Methods in Physics Research Section A: Accelerators, Spectrometers, Detectors and Associated Equipment*, 506(3):250 – 303, 2003. See also Allison, J. et al. Geant4 developments and applications. *IEEE Transactions on Nuclear Science* 53(1):270–278 and https://geant4.web.cern.ch/geant4/.

[117] R. Brun and F. Rademakers, ROOT - An Object Oriented Data Analysis Framework, Proceedings AIHENP'96 Workshop, Lausanne, Sep. 1996, *Nucl. Inst. & Meth. in Phys. Res. A* 389 (1997) 81-86. See also http://root.cern.ch/.

[118] G. Horton-Smith et al. GLG4sim http://neutrino.phys.ksu.edu/~GLG4sim/ Accessed 2015-09-10.

[119] K. Nakajima. *Measurement of Neutrino Oscillation Parameters with Precise Calculation of Reactor Neutrino Spectrum at KamLAND*. PhD thesis, Tohoku University, 2005.

[120] E. Sanshiro. *Neutrino Geophysics and Observation of Geo-Neutrinos at KamLAND*. PhD thesis, Tohoku University, 2005.

[121] B.A. Moffat et al. Optical calibration hardware for the Sudbury Neutrino Observatory. *Nuclear Instruments and Methods in Physics Research Section A: Accelerators, Spectrometers, Detectors and Associated Equipment*, 554(1–3):255 – 265, 2005.

[122] R. Helmer. Status of UI, 2011. SNO+ internal document SNO+-doc-787-v2.

[123] VAT Vakuumventile AG, Haag, Switzerland. *Product data sheet: UHV gate valve, Series 108, DN 250 (ID 10)*, September 2013.

[124] VAT Vakuumventile AG, Haag, Switzerland. *Installation, Operating & Maintenance Instructions: UHV gate valve, Series 10.8, DN 63-200 (2 1/2" - 8").*, September 2009.

[125] National Instruments, Austin, Texas, USA. *Product data sheet: NI USB-6501 OEM User Guide and Specifications*, 2005-2006.

Appendix A

Gate Valve Monitor

A.1 Introduction

A diverse neutrino instrument, SNO+ will function as a supernova detector and study supernova neutrinos while operating within a network of neutrino detectors for the SuperNova Early Warning System (SNEWS). In the event of a core collapse supernova, neutrinos will arrive on Earth first, interacting with dedicated neutrino detectors which send alerts to SNEWS. Many of the calibration sources SNO+ will be using are capable of producing supernova-like signals, including a dedicated supernova calibration source. To ensure the SNEWS collaboration is not mistakenly alerted, SNO+ will have dedicated sensors and triggers, including a device to monitor the SNO+ gate valves required for the ingress and egress of calibration sources inside the detector (see Fig. A.1 depicting the entry of calibration sources via Umbilical Retrieval Mechanism). This SNO+ Gate Valve Monitor will determine if a calibration source is currently residing within the detector, ensuring SNEWS is not mistakenly alerted when supernova-like signals occur from the source. The monitor has been built and tested, and once installed underground, will be monitored locally and remotely.

A.2 Development

There will be 9 different gate valves (GV) within the monitoring system: 3 on the upper UI, 3 on the source storage box (SB), and 3 on the URMs. Each GV has a standard position indicator with two microswitches within (see Fig. A.2), which will complete part of a custom-designed circuit. To avoid moving large cables around while transporting a source, the gate valves on the URMs will have two sets of cables: one while at the UI and another at the SB. The naming convention chosen for the gate valve connectors follows a 6-digit alphanumeric scheme of the form GVPPNN:
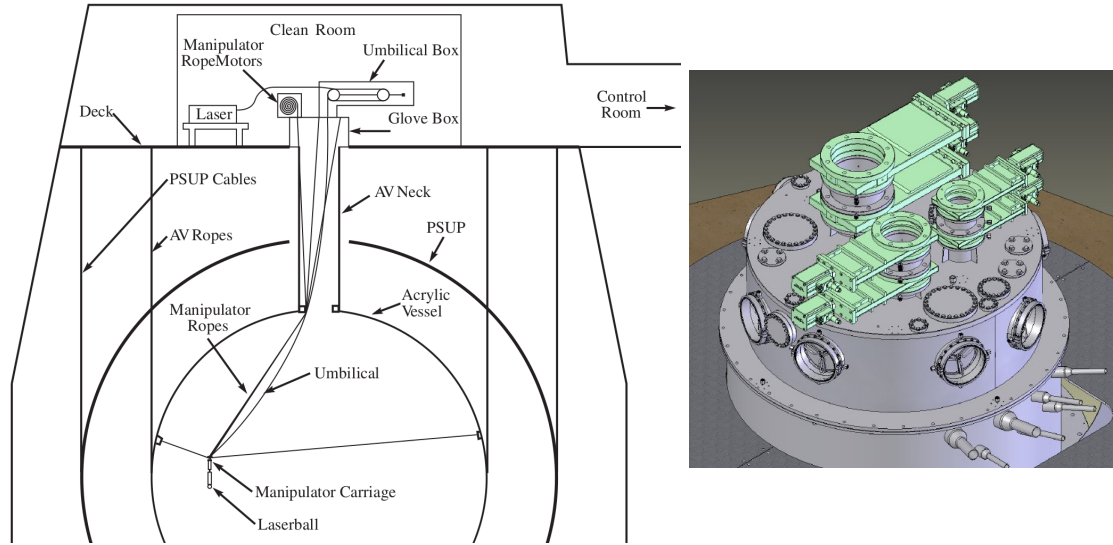
Figure A.1: Left: deployment of a laser calibration source within the SNO+ detector through the UI via URM. Figure modified from [121]. Right: Universal Interface drawing with gate valves coloured in green [122]. These gate valves are the point of entry for calibration sources entering the detector via URMs.
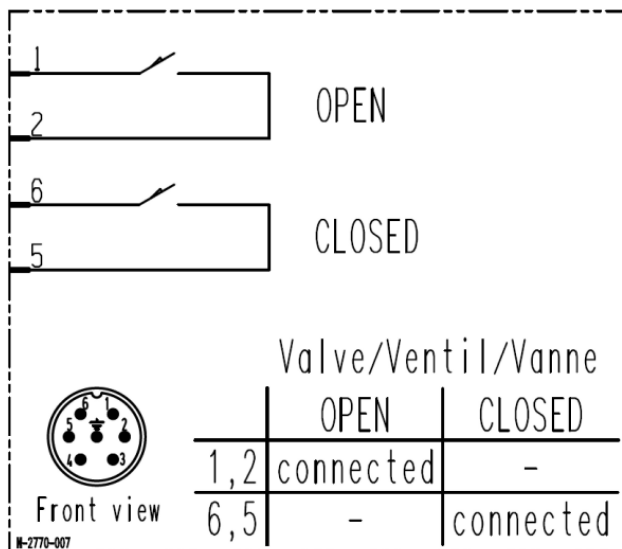
Figure A.2: Internal wiring diagram and connection arrangement of the gate valves' sensors [123, 124].

Signal	Pin	Connector	Pin	Signal
P1.0	1		2	GND
P1.1	3		4	P2.0
P1.2	5		6	GND
P1.3	7		8	P2.1
P1.4	9		10	GND
P1.5	11		12	P2.2
P1.6	13		14	GND
P1.7	15		16	P2.3
P0.0	17		18	GND
P0.1	19		20	P2.4
P0.2	21		22	GND
P0.3	23		24	P2.5
P0.4	25		26	GND
P0.5	27		28	P2.6
P0.6	29		30	GND
P0.7	31		32	P2.7
+5V	33		34	+5V

Figure A.3: Pin diagram of USB-6501 oem device [125].

- GV: All names begin with GV for Gate Valve
- PP: Position of GV, either at the UI (Universal Interface), SB (Source Box), US (URM at Source Box), or UU (URM at Universal Interface)
- NN: Number indicating the GV size, either 06 (6" flange), 08 (8" flange), or 10 (10" flange)

For example, the 6" gate valve on the UI would be called GVUI06.

Each gate valve requires 2 individual circuits, resulting in a device with 24 monitoring tools; the National Instruments USB-6501 oem digital I/O [125] was chosen as a suitable monitoring piece. In addition to 24 channels, it possesses two +5 VDC pins, at a maximum current of 230 mA, and 8 ground connections, all within a generic 34 pin connector (see Fig. A.3). This low-power device is safe for the gate valves and is self-contained, powered only via USB connection to a computer. The USB-6501 drivers require LabVIEW, or a custom ANSI C program as developed here. The USB-6501 and associated equipment was tested on a Windows 7 machine with the NI-DAQmx 9.6 driver and ANSI C language. The following National Instruments link leads to a page specifically dedicated to the USB-6501 device: `http://sine.ni.com/psp/app/doc/p/id/psp-120/lang/en`, while `http://www.ni.com/linux/` refers the reader to an online community which may help with Linux installation. The sample ANSI C code (see § A.6) follows examples downloaded along with the driver software, with additions referring to the NIDAQmx.h header and the NIDAQmx.lib library.

A Gate Valve Monitor rack enclosure 2U high and 100 mm deep was built to house the internal circuitry of the monitoring tool, and will be located on the standard 19" electronics rack inside the DCR. A hole in the center of the front panel permits the USB connection to a dedicated PC, while a nearby hole exhibits an LED
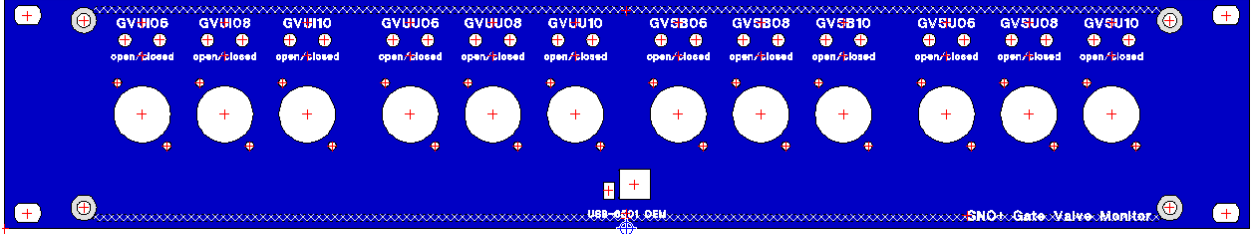
Figure A.4: Enclosure front panel, complete with system holes for components and engraved labels. Each GV will be connected to the enclosure by a long cable which connects to a mating piece on the front panel (large system holes), while two LEDs indicate the GV's status (green for open, red for closed). The USB-6501 is connected to a dedicated PC via USB connection provided by the square system hole, while a green LED beside the connection verifies PC connection.
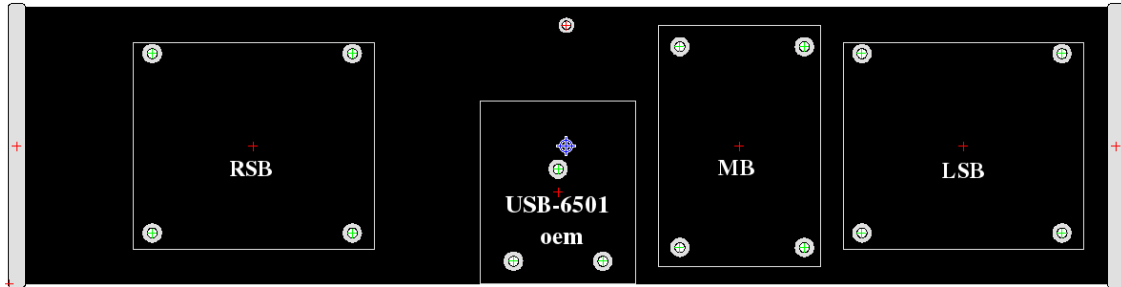
Figure A.5: Bottom-up view of enclosure bottom panel, depicting screw holes and circuit board perimeters.

indicating the USB connection (flashing if operational). 24 LEDs (12 green for open state, 12 red for closed state) are mounted to the front panel, above the outlets to connect the rack enclosure to the gate valves via cable (see Fig. A.4). For simplicity, the outlets of the enclosure are the same pieces the GVs possess, and the mating connections were purchased along with cable to connect the enclosure and GVs. Along with the USB-6501, three identical perforated prototype boards are mounted on standoffs to the bottom panel (see Fig. A.5). The prototype boards are common bus and follow an alphanumeric grid system, resulting in easy organization. A removable ribbon cable runs from the USB-6501 device to end soldered one of the perforated prototype boards, simply called the Middle Board (MB). From there, the necessary components are divided to either a left- or right-side prototype board (LSB or RSB, resp.). The rows of the RSB and LSB are junctions which connect to the objects mounted to the front panel.

Each of the USB-6501's 24 DIO lines feature a 4.7 kΩ VBus pull-up resistor, and the default state of each is high-impedance input, requiring a connection to ground to identify a change in state. Figure A.6 depicts the circuit diagram of one complete connection of a gate valve connected to the USB-6501. +5 V from the USB-6501 enters a 1.6 kΩ resistor coupled to the input of an LED rated for a 2 mA current and 1.8 forward voltage. A 3-way junction (physically a column on either the RSB or LSB) connects the low of the LED to a corresponding USB DIO line and to the front panel outlet, which connects to a cable leading
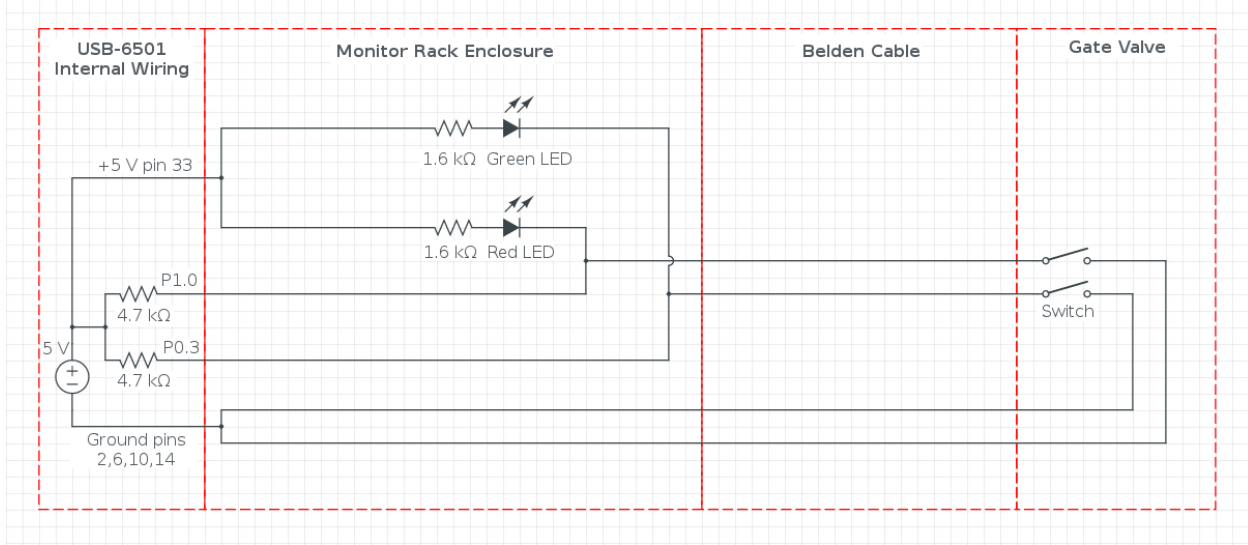
Figure A.6: A sample circuit designed to illustrate one full connection from the USB-6501 to a single gate valve (GVUI06).

to to ports 1 and 6 on a gate valve. Ports 2 and 5 connect to two other wires within the cable, which lead back to the monitor enclosure and the USB-6501's ground connections. Depending on which state the GV is in, one of the switches within the GV should engage, causing the corresponding LED to light up and the channel to report a digital low. All GV circuits are arranged in parallel, 12 powered by the USB-6501's +5V pin 33 connection on the LSB, the other 12 by the +5V source at pin 34's connection on the RSB. Table A.2 summarizes how all gate valves connect to the rows and columns of the prototype boards inside the rack enclosure, and which USB-6501 channels correspond to which gate valve.

A.3 Output and Future Work

Whereas a local observer need only examine the LEDs on the front panel to determine GV state, a remote observer requires two bits (read from the corresponding USB-6501 channels identified in table A.2) to interpret the signal from any gate valve. A 01 or 10 will be translated as "open" or "closed", depending on how the signal is inputted. For example, if the program returns that channel 0.3 is low and channel 1.0 is high (which is what was tested for and verified in Fig. A.7), then GVUI06 must be open, while the opposite indicates closed. A value of 11 is interpreted as either GV disconnected, or the GV's state is in transition. A 00 signal should not occur unless there is a malfunction, pulling both pins on the USB-6501 low. The corresponding green or red LEDs will turn on if the gate valve is connected with state open or closed, respectively. If neither light is on the GV is either disconnected or the state is in transition, while both LEDs on signifies a malfunction.

103

A short cable was manufactured to connect the GVs to the monitor, and the system has been tested and verified with the Windows computer (see Fig. A.7 for testing of GVUI06). The device must now be installed underground, and the script written to communicate with the underground computer such that the information can be recalled remotely. Once all key hardware has been established underground, the remaining cables from monitor device to GVs must be manufactured and connected.
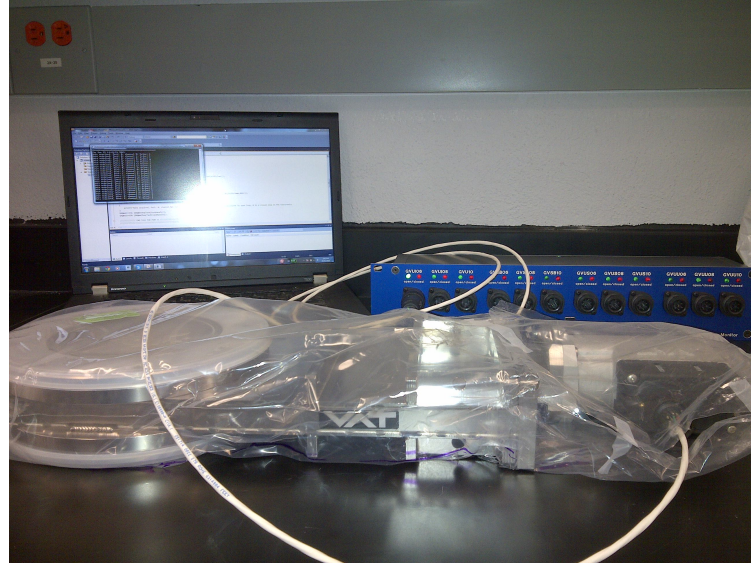
Figure A.7: Testing the GVUI06 connections in the surface lab at Laurentian University.

A.4 Parts List

Piece	P/N	Qty ordered
Vectorbord 8022 Circbord	V2018-ND	3
Green LEDs (Vf: 1.8 V, current: 2 mA)	160-1852-ND	12
Red LEDs (Vf: 1.8 V, current: 2 mA)	160-1853-ND	12
1.6 kΩ Resistors	CF14JT1K60CT-ND	24
6-32 standoffs, height.	N/A	12
6-36 nylon hex standoffs, height = 1/4"	1903AK-ND	3
Scews 6-32x1/4, black, flat head	N/A	15
Screws 6-32x3/16, black, flat head	0603MPP188B	15
Screws M3-0.5x12, black, pan head	M312MPP188B	24
M3 hex nuts	B-0934A4M3-B50	24
Binder series 692 male socket, solder termination	09-0215-00-07	12
Binder series 693 female cable connector, solder termination	99 4226 00 07	24
Belden cable, LS PVC - low smoke polyvinyl chloride	6402FE 877 (NAT)	1000 feet
Heat Shrink, 1/2" x4'	Q53X012B-ND	4 feet
USB-6501 oem	192317E-50L	1
Front Panel Custom Enclosure and assembly kit	N/A	1

Table A.1: Gate valve monitor list of parts

A.5 Gate Valve Monitor internal layout

	Open State						Closed State					
	USB-6501		LSB/RSB Connections				USB-6501		LSB/RSB Connections			
Gate Valve	Channel	MB Location	L/R Board	Junction Row	+5V	GND	Channel	MB Location	L/R Board	Row	+5V	GND
GVUI06	0.3	M-13:22	LSB	F-1:14	A(2)-19	X-19	1.0	X-13:22	LSB	F-16:29	A(2)-21	X-21
GVUI08	0.2	N-13:22	LSB	I-1:14	A(2)-23	X-23	1.1	W-13:22	LSB	I-16:29	A(2)-25	X-25
GVUI10	0.1	O-13:22	LSB	L-1:14	A(2)-27	X-27	1.2	V-13:22	LSB	L-16:29	A(2)-29	X-29
GVSB06	0.0	P-13:22	LSB	O-1:14	A(2)-9	X-9	1.4	T-13:22	LSB	O-16:29	A(2)-11	X-11
GVSB08	1.7	Q-13:22	LSB	R-1:14	A(2)-5	X-5	1.3	U-13:22	LSB	R-16:29	A(2)-7	X-7
GVSB10	1.6	R-13:22	LSB	U-1:14	A(2)-1	X-1	1.5	S-13:22	LSB	U-16:29	A(2)-3	X-3
GVUS06	0.5	K-13:22	RSB	A(2)-16:29	F-19	I-19	0.4	L-13:22	RSB	X-16:29	F-21	I-21
GVUS08	2.0	W-7:1	RSB	U-16:29	F-23	I-23	2.1	U-7:1	RSB	R-16:29	F-25	I-25
GVUS10	2.2	S-7:1	RSB	O-16:29	F-27	I-27	2.3	Q-7:1	RSB	L-16:29	F-29	I-29
GVUU06	2.4	O-7:1	RSB	L-1:14	F-9	I-9	2.5	M-7:1	RSB	O-1:14	F-11	I-11
GVUU08	2.6	K-7:1	RSB	R-1:14	F-5	I-5	2.7	I-7:1	RSB	U-1:14	F-7	I-7
GVUU10	0.6	J-13:22	RSB	X-1:14	F-1	I-1	0.7	I-13:22	RSB	A(2)-1:14	F-3	I-3

Table A.2: Gate valve monitor connections. To read the GV states with a dedicated computer, channels 0.0 through 2.7 of the USB-6501 must be read in and compared. Channels are of the format <Port>.<Line> and can all be read using the sample code provided in § A.6. Remaining connections signify positions on the prototype boards within the GV monitor enclosure if repairs must be made.

A.6 Sample Code

The following is a sample ANSI C code, written in MS Visual C++ 2010 Express, which interacts with the USB-6501 OEM device.

```
/**********************************************************************
* USB6501communication.c
* Modified ANSI C script of example: ReadDigChan.c
* Written for MS Visual C++ 2010 Express
*
* Working with USB6501 OEM for Gate Valve Monitoring:
*    - Returns the states of all channels on USB6501 as 0 or 1
*    - Outputs the states to the screen
*    - 1 second delay after each output
*    - Runs continually until user aborts
*
* Revision Author: Janet Rumleskie
* Rev. I Date: 31 Jan. 2015
*
**********************************************************************/

#include <stdio.h>
#include <time.h>
#include <Windows.h>
#include <stdlib.h>

// Needed to specify the directory for NIDAQmx.h:
#include "C:\Program Files (x86)\National Instruments\NI-DAQ\DAQmx ANSI C Dev\include\NIDAQmx.h"
// Note that we were still missing a necessary library, which was at:
//   C:\Program Files (x86)\National Instruments\NI-DAQ\DAQmx ANSI C Dev\lib\msvc\NIDAQmx\NIDAQmx.lib
// It was included (for MS Visual) by going to Project -> properties -> linker -> input -> additional dependencies
//   In the new window, typed in: NIDAQmx.lib

#define DAQmxErrChk(functionCall) if( DAQmxFailed(error=(functionCall)) ) goto Error; else

int main(void)
{

        ////////////// START THE LOOP /////////////////////////
        /////////////////////////////////////////////////////////
        int32           j;
        for(;;)
        {
        time_t          t;
        int32           error=0;
        TaskHandle      taskHandle=0;
        uInt8           data[100];
        char            errBuff[2048]={'\0'};
        int32           i;
        int32           read,bytesPerSamp;


        time(&t); // get time
        printf("%s",ctime(&t)); // print time to screen

        ////////////// START TASK FOR PORT 1 ////////////////
        /////////////////////////////////////////////////////////
        // Create the task
        DAQmxErrChk (DAQmxCreateTask("",&taskHandle));

        // Specify port 0 of USB6501, run through lines 0 to 7
        DAQmxErrChk (DAQmxCreateDIChan(taskHandle,"Dev1/port0/line0:7","",DAQmx_Val_ChanForAllLines));

        // Start the task
        DAQmxErrChk (DAQmxStartTask(taskHandle));

        // Read the data
        DAQmxErrChk (DAQmxReadDigitalLines(taskHandle,1,10.0,DAQmx_Val_GroupByChannel,data,100,&read,&bytesPerSamp,NULL));
```

106

```
        // Acquired data for the 8 channels, print them to screen
        for(i=0;i<8;++i)
        {
                printf("Data acquired, Port: 0, channel %d: Value: %X \n",(int)i,data[i]);
        }
        DAQmxErrChk (DAQmxStopTask(taskHandle));
        DAQmxErrChk (DAQmxClearTask(taskHandle));
        ////////////// END TASK FOR PORT 0 //////////////////
        //////////////////////////////////////////////////////


        //////////////////////////////////////////////////////
        ////////////// START TASK FOR PORT 1 //////////////////
        DAQmxErrChk (DAQmxCreateTask("",&taskHandle));
        DAQmxErrChk (DAQmxCreateDIChan(taskHandle,"Dev1/port1/line0:7","",DAQmx_Val_ChanForAllLines));
        DAQmxErrChk (DAQmxStartTask(taskHandle));
        DAQmxErrChk (DAQmxReadDigitalLines(taskHandle,1,10.0,DAQmx_Val_GroupByChannel,data,100,&read,&bytesPerSamp,NULL));
        for(i=0;i<8;++i) { printf("Data acquired, Port: 1, channel %d: Value: %X \n",(int)i,data[i]); }
        DAQmxErrChk (DAQmxStopTask(taskHandle));
        DAQmxErrChk (DAQmxClearTask(taskHandle));
        ////////////// END TASK FOR PORT 1 //////////////////
        //////////////////////////////////////////////////////


        ////////////// START TASK FOR PORT 2 //////////////////
        //////////////////////////////////////////////////////
        DAQmxErrChk (DAQmxCreateTask("",&taskHandle));
        DAQmxErrChk (DAQmxCreateDIChan(taskHandle,"Dev1/port2/line0:7","",DAQmx_Val_ChanForAllLines));
        DAQmxErrChk (DAQmxStartTask(taskHandle));
        DAQmxErrChk (DAQmxReadDigitalLines(taskHandle,1,10.0,DAQmx_Val_GroupByChannel,data,100,&read,&bytesPerSamp,NULL));
        for(i=0;i<8;++i) { printf("Data acquired, Port: 2, channel %d: Value: %X \n",(int)i,data[i]); }
        DAQmxErrChk (DAQmxStopTask(taskHandle));
        DAQmxErrChk (DAQmxClearTask(taskHandle));
        ////////////// END TASK FOR PORT 2 //////////////////
        //////////////////////////////////////////////////////


        ////////////// IF ERRORS HAPPEN //////////////////////
        //////////////////////////////////////////////////////
Error:
        if( DAQmxFailed(error) )
                DAQmxGetExtendedErrorInfo(errBuff,2048);
        if( taskHandle!=0 ) {
                /*********************************************/
                // DAQmx Stop Code
                /*********************************************/
                DAQmxStopTask(taskHandle);
                DAQmxClearTask(taskHandle);
        }
        if( DAQmxFailed(error) )
                printf("DAQmx Error: %s\n",errBuff);
        //////////////////////////////////////////////////////
        //////////////////////////////////////////////////////

        ////////////// MAKE THE PROGRAM PAUSE ////////////////
        //////////////////////////////////////////////////////
        Sleep(1000); // 1000 = 1 second)
        printf("********************************************* \n");

        }// END INFINITE LOOP HERE ////////////////////////
        //////////////////////////////////////////////////////
        return 0;
}
```

Appendix B

MDG Background Procedure

The monitor degasser unit for ^{222}Rn assays of H_2O within the SNO+ cavity and the SNOLAB UWP plant has been decommissioned since SNO last operated. Since then, the SNOLAB assay procedure and flowsheets have been modified, but often changes were not reflected within the existing procedure for running the monitoring system. Moreover, no simplified procedure existed for running the MDG as a standalone system, which is required for background analysis. As SNO+ requires the MDG for regular ^{222}Rn monitoring, recommissioning of the system has begun, and a modified procedure has been written and used for internal background runs. Below is the modified procedure and an accompanying flow diagram of the relevant UWP system.

	Radon Assay **MDG Background Run**	
Document Number: THIS IS A MODIFIED YET UNREVISED VERSION OF SL-OPS-PCS-30-350-P – Rev. 7 FOR THE USE IN A MDG BACKGROUND ASSAY EDITED ON JULY 15, 2015		**Revision Number: (Previously: 7)**
Document Owner: (Previously: Allan Barr)		
Reviewer: (Previously: Sanford Clark)		
Name:	**Signature:**	**Date: <YYYY-MM-DD>**
Approval Authority:		
Name:	**Signature:**	**Date: <YYYY-MM-DD>**

1. Scope

This procedure allows an assay of the H_2O Monitor Degasser (MDG) unit for background analysis. The Radon board traps radon from the vacuum degasser into Lucas cells to be taken to the surface for counting. Before assaying, the FTS water trap might need to be emptied of any residual H_2O, which is collected and the volume recorded. To supply pressure to clear the water trap, a flow of "clean" nitrogen from a gas cylinder is used to fill the trap. A checklist must be filled in when running the procedure.

2. Procedure

2.1 Authorization to Implement

One of the key changes to this procedure has been to add several places where UPWSS authorization is required. The first UPW authorization is for the tasks of draining the FTS trap and Vlad trap. This is specifically authorized even though it is a fairly benign task because it is frequently done a day or two before the actual assay, and is the only action completed that day. The second UPW authorization is for baking and pumping on the Radon board. Normally this is also an activity that does not affect the water systems, but it is normally done first thing the morning of a H_2O Rn assay, and the UPW needs to be aware of the activity taking place. The UPW may also choose to authorize both of these first two places at the beginning of the day of the assay, to allow the Assay Operator to get all of their preparations done without further interaction with the UPW required. The third UPW authorization is required before the assay proper is allowed to begin. This is the most important authorization, because it may involve water system valves.

2.2 Draining the Traps

2.2.1 UPW Authorization

See above explanation. This is more of a UPW notification than authorization.

2.2.2 Defrosting the FTS (if required)

♦ If required, the FTS can be defrosted by using the defrost function. Normally this is not required.

2.2.3 Preliminary Confirmed Closed List

♦ Follow and fill in section 2.2.3 of the checklist to confirm closed valves to prepare to drain the trap.

2.2.4 Preliminary Setup

♦ Follow and fill in section 2.2.4 to ensure the N2 gas bottle supply is connected, and the regulator and needle valve are set properly.

2.2.5 Flushing the Lines

♦ Follow and fill in section 2.2.5 to flush air out of the N2 lines

2.2.6 Valve Open List

♦ Follow and fill in section 2.2.6 to open a path from the trap to the pressure gauge.

2.2.7 Pressurizing and Draining the Trap

♦ Follow and fill in section 2.2.7 to pressurize and drain the trap

♦ Note that attention must be paid to only pressurize the trap with a slight positive pressure. There is no safety relief valve on the trap, so if it is over pressurized it would break, perhaps explosively.

2.2.8 Return System to Normal Configuration

♦ Follow and fill in section 2.2.8 to return the valves to a normal configuration. Often draining the trap is done the day before the day of the assay, but assays can be cancelled or deferred, so it is important to leave the system in a normal or standard configuration.

2.2.9 Draining the "Vlad" Trap

♦ Follow and fill in section 2.2.9 if the Vlad trap needs to be drained. This is not done as frequently as draining the Titan Trap, so is considered an optional section. If there are two people working on the Rn assay, it can also be done simultaneously with draining the Titan Trap to save time.

2.3 Pumping the Trap and Baking the Board

    2.3.1 UPW Authorization

See explanation in section 2.1. This is also more of a UPW notification than authorization, because it doesn't affect the rest of the water systems.

    2.3.2 Initial Set-up

♦ Follow and fill in section 2.3.2 of the checklist to turn on the FTS system and the vacuum pump.

    2.3.3 Cool 'Vlad' Trap

♦ Follow and fill in section 2.3.3 of the checklist to fill the Vlad trap with LN2. Note that the Assay Operator must also be authorized on the LN2 handling procedure, UPW-OP-0100-01.

    2.3.4 Pumping the Trap

♦ Follow and fill in section 2.3.4 of the checklist to confirm closed valves on the Radon board and open a path from the vacuum pump to the vapour trap.

    2.3.5 Baking the Radon Board

♦ Follow and fill in section 2.3.5 to bake the Radon board lines with a heat gun to drive off any moisture in the lines.

2.4 Main Assay

    2.4.1 UPW Authorization

See explanation in section 2.1. This is the most critical UPW authorization, because actions taken after this could affect the water systems.

    2.4.2 Confirm Closed Valves

♦ Follow and fill in section 2.4.3

    2.4.3 Confirm Open Valve

♦ Follow and fill in section 2.4.4 to confirm the valve that is normally left open.

2.5 Assay Details

    2.6.1 Recording initial Values, LC ID

    2.6.2 Opening to/running the Vacuum Degasser

♦ Follow and fill section 2.6.2 of the checklist to make final preparations before starting the extraction

2.6 Extraction from the MDG

♦ Follow and fill out section 2.6.1-2.6.4 to extract the radon from the gas coming out the vacuum degasser. Periodic checks of pressures, every 15 minutes, are to be recorded as indicated on the MDG extraction sheet and the liquid

Nitrogen filled every 30-40 minutes in the "Vlad" trap (311-VT-01). Follow and fill in section 2.6.3 of the checklist during the extraction time. At the end of the assay follow and fill in section 2.6.4 to shut off the MDG transfer and prepare for the transfer of radon.

2.7 Transfer of Radon

♦ Follow 2.7.1-2.7.5 to transfer the radon to the Lucas cell. Note that the transfer time from trap A to trap B is 15 minutes, and the transfer time from Trap B to the Lucas cell is 10 minutes. During the warming of trap B, the pressure in B may rise off scale (>700 on gauge B). If so, open to the cell immediately and record the time. Should the pressure still continue to rise too quickly, open the valve either to the next cell in line or to the small closed section of piping between where the cells should be. There is some margin of error, but at a pressure greater than 1500 or so (well off scale) the meter will be damaged.

2.8 Bake Board again

♦ To prepare for the next assay follow section 2.9 to evacuate the traps.

2.9 System Shutdown at the End of All Assays

♦ Follow and fill in section to proceed with a full shutdown of the procedure. Note that there are some valves that will already be closed. If valves are already closed, enter CC for confirm closed. If the valves require closing, enter a check mark.

2.10 Checklist Completion and Filing

♦ Follow and fill in section 2.11.1– 2.11.2 to prepare and file the checklist and complete the assay.

3.   **Potential Hazards and Risks**

The following are considered to be hazards to be aware of in the implementation of this procedure:

♦   The sample line part of this procedure draws H_2O directly from the cavity. Although previous experience has shown it does not to generate a large amount of light, the detector operator must be notified and care exercised when opening the sample line valves.

♦   Proper equipment must be used when working with and pouring liquid nitrogen. Gloves for pouring, and a protective face shield. Note also that any LN2 spills may drip through the mezzanine floor onto people below, so the utmost care must be used when pouring LN2 and if needed, the people working below should be warned and asked to move away from the area.

♦   Potential for H_2O loss which would upset the levels in the detector.

♦   Too much air entering P15 through V-544L will trip the whole H_2O recirculation system.

♦   When draining the FTS, do not over pressurize with nitrogen gas, exercise caution while working with compressed nitrogen bottle

♦   When warming the radon trap, watch the pressure rise. If it gets too high, then open the appropriate valves to relieve the pressure.

        Notes:

4.   Revision History

	ORIGINATING DATE: 2013-08-01		
REV NO.	**EFFECTIVE DATE** (YYYY-MM-DD)	**AUTHOR**	**SUMMARY OF CHANGE**
0	Unknown	H. Lee	Initial procedure development
1	Unknown	G. Carnes	Procedure revision
2	200-02	H. Lee	New plumbing between V-551L and V-255L
3	2001-02	S. Fostner, L. Wrightson	Adjusted to include board procedure, FTS drain, Record Sheet. Debugged and edited; added assay of V-535L
4	2005-09	M. Baillie, R. Rodriguez, R. Lange	Comprehensive revision. Added Henry's mark-ups on Rev. 3, the recording of vacuum values on preparation of Lucas Cell. Eliminated the need for help to open valves on deck. Added flexibility to perform loop assays as well as sample line assays
5	2005-09	M. Baillie	Incorporated mark-ups from commissioning
6	2009-07-17	J. Reynolds	Updating to the new format and from PR-140. Section 2.13.4 was added and some other changes were incorporated as per markups -Revise format to new SLOG procedure number
7	2013-08-01	S. Clark	Update to Docushare format
8**	Unrevised	J. Rumleskie	Unofficially adapted for MDG background assay

FORMERLY SL-OPS-PCS-30-350-P Rev 7
Radon Assay

ADAPTED FOR MDG
BACKGROUND RUN

Personnel: _____

_____

Day/Date: _____

Time: _____

2.1 Authorization to Implement
(Explanation)

Note: UPWSS authorization is required in **3 places** for this procedure (2.2 - Draining the Trap, 2.3 - Pumping the Trap and Baking the Board, 2.4 - Main Assay Procedure).

Sometimes the UPWSS will be asked by the assay operator for authorization for 2.2 (Draining the Traps) on the day prior to the assay.   This might be all that is done on a given day.

The day of the assay, the UPWSS may be asked for authorization for 2.2 and 2.3 together or 2.3 by itself, and then will normally wait until these sections are complete before asking for authorization to complete from 2.4 on (Main Assay Procedure).

2.2 Draining the Traps

2.2.1 Authorization to implement

UPWSS initials to implement Section 2.2 Draining the Trap	

2.2.2 Defrosting the FTS (if required)
*** OPTIONAL SECTION ***

One may melt the ice on the coils of the FTS simply by leaving it over night with the power off **OR**	
Press and hold the defrost button and wait for a click. (if not done, enter NR)	
Monitor trap when defrosting. Turn off defrost before the temp. exceeds 40 ^{O}C. (if not done, enter NR)	

2.2.3 Preliminary Confirmed Closed List

Valve on top of degasser	[Y]	V-215L	Confirm Closed	
Behind control panel	[Y]	V-189L	Confirm Closed	
Beside FTS	[Y]	V-243L	Confirm Closed	
Beside FTS	[Y]	V-224L	Confirm Closed	
Beside FTS	[Y]	V-222L	Confirm Closed	
Beside FTS – green	[Y]	V-226L	Confirm Closed	
N2 supply to vapour trap	[Y]	V-669L	Confirm Closed	
N2 flush line – behind MDG skid	[Y]	V-659L	Confirm Closed	
N2 line	[Y]	V-668L	Confirm Closed	

2.2.3 Preliminary Confirmed Open List

Formerly actuated valve (normally left open)	[Y]	V-537L	Confirm Open	

2.2.4 Preliminary Setup

Connect the hose from the N2 regulator in the chem. lab to the line leading to the degasser skid			
Main N2 bottle supply valve (N2 cylinder - beside fume hood)	[Y]	OPEN ¼ Turn	
Regulator diaphragm valve (N2 cylinder - beside fume hood)	[Y]	OPEN P ~ 5 psi	
Needle valve on regulator	[Y] V-660L	OPEN 1 Turn	

2.2.5 Flushing the Lines

Back of MDG Skid, N2 Flush valve	[Y]	V-659L	OPEN
Open V-745L	[Y]	V-745L	OPEN
Flush the line for 20 seconds.			
Close V-745L	[Y]	V-745L	CLOSE
Back of MDG Skid	[Y]	V-659L	CLOSE

2.2.6 Valve Open List   NOTE: Be sure to open the valves slowly

N2 PP Isolation valve (upstairs, backside of skid)	[Y]	V-225L	OPEN slowly
MDG Vapour Trap N2 inlet (backside of skid)	[Y]	V-222L	OPEN slowly
N2 SS supply line (backside of skid)	[Y]	V-579L	OPEN slowly
Note: Pressure gauge along the line should drop to −30 inches of Hg (red scale) if FTS is under vacuum.			

2.2.7 Pressurizing and Draining the Trap

Important Note: The Vapour Trap must not be over-pressurized (>2 psi) or it will break.				
Watch PI 647 during the next two steps to pressurize the trap to 0.5 psi				
N2 supply valve (backside of skid)	[Y]	V-669L	OPEN Slowly	
Watch PI 647 carefully, close V-669 when P~0.5 psi				
N2 supply valve (backside of skid)	[Y]	V-669L	CLOSE P~ 0.5	
Record pressure	[Y]	PI-647	Pressure:	
Place a bucket below the outlet drain pipe			Bucket Placed	
FTS Drain	[Y]	V-226L	OPEN	
Drain water only to a level just above the outlet tube				
Drain of FTS	[Y]	V-226L	CLOSE	
Record pressure	[Y]	PI-647	Pressure:	
NOTE: If the gauge indicates that the pressure has fallen below atmosphere, repeat the above steps				

2.2.8 Return System to Normal Configuration

N2 PP Isolation valve (upstairs, backside of skid)	[Y]	V-225L	CLOSE
MDG Vapour Trap N2 inlet (backside of skid)	[Y]	V-222L	CLOSE
N2 SS supply line (backside of skid)	[Y]	V-579L	CLOSE
Drain of FTS	[Y]	V-226L	Confirm Closed
N2 Supply Valve (behind MDG)	[Y]	V-669L	Confirm Closed
Measure the amount of water taken from the FTS, Record this number in the MDG log book & here:			
Main N2 bottle supply valve (in chem. lab)	[Y]		CLOSE
Regulator diaphragm valve (in chem. lab)	[Y]		BACK OFF
Needle valve on regulator (in chem. lab)	[Y]	V-660L	CLOSE
Disconnect the hose leading to the degasser skid			

2.2.9 Draining "Vlad" Trap (321-VT-01)
*** OPTIONAL SECTION, May be Done in Parallel With Draining the FTS Trap***

Inlet to Vlad Trap (near VP02, Alcatel pump)	[Y]	V-539L	Confirm Closed
Outlet of Vlad Trap (near VP02, Alcatel pump)	[Y]	V-247L	Confirm Closed
Loosen one clamp (NW vacuum fitting style) and vent the vacuum			
Reconnect / tighten clamp once vented			
Remove top section of Vlad trap			
Use syringe to draw water out of Vlad trap			
Measure the amount of water in Vlad trap and record amount in MDG log book & here:			

Notes:

2.3 Pumping the Trap and Baking the Radon Board

2.3.1 Authorization to implement

UPWSS initials to implement Section 2.3 Pumping the Trap and Baking the Radon Board	

2.3.2 Initial Setup

Turn on FTS main power and activate the cooling cycle by depressing the Start/Stop button			
Record Time:		hh:mm	
Inlet to Vlad Trap (near VP02, Alcatel pump)	[Y]	V-539L	Confirm Closed
Outlet of Vlad Trap (near VP02, Alcatel pump)	[Y]	V-247L	Confirm Closed
Outlet of Alcatel pump	[Y]	V_exhaust	Confirm Open
Confirm oil in U-trap for Alcatel pump exhaust			
Start the Alcatel vacuum pump. The switch is on the control panel (labeled "Vacuum pump").			

2.3.3 Cool "Vlad" Trap (321-VT-01)

Confirm Vlad trap is connected	
Obtain Liquid N$_2$ according to SNOLAB-SOP-022 (LN2 handling procedure)	
Cool "Vlad" trap by filling with liquid N$_2$.	
NOTE: do not overfill as O-ring will freeze and trap will begin leaking	

2.3.4 Pumping Trap

Drain of FTS	[Y]	V-226L	Confirm Closed	
Rn Board (Radon Trap bypass)	[Y]	V-258L	Confirm Closed	
Rn Board (3-way valve after Radon Trap)	[Y]	V-245L	Confirm Closed	
Rn Board (outlet of last Lucas Cell)	[Y]	V-262L	Confirm Closed	
Rn Board (capped)	[Y]	V-256L	Confirm Closed	
Rn Board (inlet to Radon trap)	[Y]	V-244L	Confirm Closed	
Rn Board (secondary isolation from FTS)	[Y]	V-243L	Confirm Closed	
Radon Board bypass to Vlad Trap and vacuum pump	[Y]	V-242L	Confirm Closed	
Valve on top of degasser	[Y]	V-215L	Confirm Closed	
N2 PP Isolation valve (backside of skid)	[Y]	V-225L	Confirm Closed	
Rn Board, valve **normally left open**	[Y]	V-257L	Confirm Open	
Rn Board, valve **normally left open**	[Y]	V-538L	Confirm Open	
Formerly actuated valve (**normally left open**)	[Y]	V-537L	Confirm Open	
* Outlet of Vlad Trap (near VP02, Alcatel pump)	[Y]	V-247L	OPEN Slowly	
* Inlet to Vlad Trap (near VP02, Alcatel pump)	[Y]	V-539L	OPEN Slowly	
* Watch pressure on FTS panel, make sure it is going down or else check for leaks before continuing.				
Confirm pressure is below 20 mTorr before proceeding.				
Record pressure reading (PT 007, display on FTS panel)		mTorr		
Confirm FTS has cooled for 10 minutes before pumping on it				
Record Time:		hh:mm		
Vapour Trap inlet, beside FTS	[Y]	V-222L	OPEN	
Vapour Trap outlet, beside FTS	[Y]	V-224L	OPEN	
* Radon Board bypass to Vlad trap and vacuum pump	[Y]	V-242L	OPEN Slowly	
Note: Open V-242L in small stages, not letting the Alcatel pump to strain too much from the gas load.				
Check and Fill "Vlad" trap when needed (~ every 30-40 min)				
Confirm pressure is below 50 mTorr before proceeding.				
Record pressure reading (PT 007, display on FTS panel)		mTorr		
Radon Board bypass to Vlad Trap and vacuum pump	[Y]	V-242L	CLOSE	
Plug in trap/MDG pressure gauges (2 plugs) and heat gun (120 VAC)				

2.3.5 Baking the Radon Board

Use heat gun to bake the two radon traps (311-CT01, 311-RTR02). Take care not to point heat gun at FTS chamber or wiring for pressure gauges A and B. Traps should be heated until they are hot to touch (approx. 40°C)				
Radon Board bypass to Vlad Trap and vacuum pump	[Y]	V-242L	Confirm Closed	
Radon Board (isolation from N2 supply)	[Y]	V-243L	Confirm Closed	
Radon Board (Radon Trap inlet)	[Y]	V-244L	Confirm Closed	
Radon Board (outlet from last Lucas Cell)	[Y]	V-262L	OPEN	
Radon Board (between Lucas Cells)	[Y]	V-261L	OPEN	
Radon Board (inlet to first Lucas Cell)	[Y]	V-260L	OPEN	
Radon Board (inlet to Secondary Radon Trap)	[Y]	V-259L	OPEN	
Heat Trap B (311-RTR-02)				
Close when PT 007 < 15 mTorr	[Y]	V-259L	CLOSE	
Record pressure reading (PT 007, display on FTS panel, and PT-B)	PT-007:		PT-B:	
Radon Board (inlet to first Lucas Cell)	[Y]	V-260L	CLOSE	
Radon Board (between Lucas Cells)	[Y]	V-261L	CLOSE	
Radon Board (outlet from last Lucas Cell)	[Y]	V-262L	CLOSE	
Radon Board (3-way valve after Radon Trap)	[Y]	V-245L	OPEN Down	
Heat Trap A (311-CT01)				
Close when PT 007 < 15 mTorr	[Y]	V-245L	CLOSE	
Record pressure reading (PT 007, display on FTS panel, and PT-A)	PT-007:		PT-A:	

Notes:

_____

_____

_____

_____

_____

_____

_____

_____

_____

2.4 Main Assay

      2.4.1 Authorization to Implement

UPWSS initials to implement Section 2.4 – Main Assay	

      2.4.2 Confirm Closed Valves

Above FTS, back	[Y]	V-550L	Confirm Closed	
On side of degasser	[Y]	V-208L	Confirm Closed	
MDG Skid, back near P26	[Y]	V-168L	Confirm Closed	
MDG Skid, by P26 (P26 outlet valve)	[Y]	V-285L	Confirm Closed	
Near Dummy Column	[Y]	V-232L	Confirm Closed	
Near Dummy Column	[Y]	V-234L	Confirm Closed	
MDG Skid, above P26	[Y]	V-255L	Confirm Closed	
MDG Skid, above P26	[Y]	V-254L	Confirm Closed	
MDG Skid, above P26	[Y]	V-467L	Confirm Closed	
MDG Skid, above P26	[Y]	V-479L	Confirm Closed	
MDG Skid, by UF (Injection Port)	[Y]	V-641L	Confirm Closed	
On side of Degasser	[Y]	V-228L	Confirm Closed	
Top of Degasser	[Y]	V-189L	Confirm Closed	
Top of Degasser	[Y]	V-215L	Confirm Closed	
Inlet to Degasser	[Y]	V-248L	Confirm Closed	
Beside Degasser (Capped)	[Y]	V-576L	Confirm Closed	
Bottom of Degasser	[Y]	V-294L	Confirm Closed	
UFR06 permeate	[Y]	V-302L	Confirm Closed	
UFR06 permeate	[Y]	V-303L	Confirm Closed	
MDG skid	[Y]	V-209L	Confirm Closed	
Above FTS	[Y]	V-551L	Confirm Closed	
Loop sample valve after PDG (by UV skid)	[V]	V-535L	Confirm Closed	
P15 inlet loop sample and return line (downstairs)	[V]	V-544L	Confirm Closed	
To Forced Drain (downstairs)	[V]	V-558L	Confirm Closed	
Loop sample valve after HX01 and new RO (downstairs)	[V]	V-229L	Confirm Closed	
P15 outlet return line (downstairs, PDG pit)	[V]	V-470L	Confirm Closed	
To drain (downstairs, PDG pit)	[V]	V-471L	Confirm Closed	
PDG pit	[Y]	V-171L	Confirm Closed	
PDG pit	[Y]	V-252L	Confirm Closed	
PDG pit	[Y]	V-540L	Confirm Closed	

      2.4.3 Confirm Open Valve

Above Degasser, by PT-004 (normally left open)	[Y]	V-241L	Confirm Open	

Notes:

_____

_____

_____

_____

_____

_____

_____

_____

Note:
This procedure has been re-designed so that it is only for a background run of the isolated MDG skid. For water assays of cavity water or for loop sample lines, refer to SL-OPS-PCS-30-350-P Rev. 7.

Other permutations and combinations are possible, but should be planned in advance with Richard Ford.

2.5 Assay Details
2.5.1 Recording initial values, LC ID

Lucas Cell Number LC #	**LC ID:**	
Record baseline values on extraction sheet (PT-007, PT-A, PT-B, MDG temperature)		

2.5.2 Opening to/running the MDG (311-DG01)

Confirm closed V-242L	[Y]	V-242L	Confirm Closed	
Gradually open to MDG	[Y]	V-215L	Slowly Open	
Start time of water flow			Time:	
Establish connection to MDG	[Y]	V-258L	Open SLOWLY	
Wait at least **25 minutes** for an accurate measurement				

2.6 Extraction from the Water
2.6.1 Radon Trap Setup

Fill the large Dewar with LN2 and place it around the Trap A (311-CT01). Use the support elevator to lift the Dewar until the top is even with the Swagelok elbow at the top of the trap.	

2.6.2 Trap A Extraction

CLOSE **V-258L**, quickly open **V-244L**, turn **V-245L** downward		
Record Start Time: run for **~30 min, or as required** (At this point the gas flow is into the board through V-257L, through the primary trap, and out V-245L) **Meanwhile**, perform section 2.6.3	Time:	

Trap A = Primary Radon Trap = 311-CT01 ; Trap B = Secondary Radon Trap = 311-RTR-02

2.6.3 Extraction Monitoring

Record initial values of extraction on log sheet: Start time, MDG temp, PT-007, PT-A			
Fill out the Rn extraction log sheet every **15 min** **and** check Vlad trap periodically, fill with LN$_2$ as req'd (**every 30-40 min**)			

2.6.4 Water Extraction Completion [PROCEED QUICKLY]

Radon Board	[Y]	V-244L	CLOSE	
Rn Board, close when P<100	[Y]	V-245L	CLOSE	
Record Time **Immediately (time of V-244L closure)**, then fill out log sheet for extraction values		Time :		

2.7 Transfer of Radon
2.7.1 Preparing Trap A and Trap B

Remove Dewar from **Trap A**.		
Cool **Trap B** with LN2 using the smaller Dewar supported with scissors jack(s)		
Heat trap A to approx. room temp		
Record pressure of gauge A on the Radon extraction sheet	PT-A:	
NOTE: If pressure on trap A exceeds +200, abort by opening V-245L into the down position		

2.7.2 Transfer from Trap A to Trap B

Radon Board	[Y]	V-259L	OPEN	

Radon Board (**start of transfer**)	[Y]	V-245L	OPEN Upwards	
Record time (**start of transfer**)			Time:	
Allow the transfer to continue for **15 minutes** (meanwhile continue with 2.7.3)				

2.7.3 Preparing the Lucas Cell

Remove the blue plastic protective cap from the Lucas cell and nozzle, secure one Lucas cell to the left quick connect port				
Record Lucas Cell #			LC #	
Radon Board	[Y]	V-261L	OPEN	
Radon Board (Note: watch PT-007 closely during this step)	[Y]	V-262L	OPEN	
Cell normally jumps to 20-30 mTorr on FTS and drops to stable pressure <2 mTorr				
Record maximum pressure		PT-007	Pmax: mTorr	
Record low stable pressure		PT-007	Pstable: mTorr	
Radon	[Y]	V-261L	CLOSE	
Radon	[Y]	V-262L	CLOSE	

2.7.4 End of Transfer from Trap A to Trap B

Radon Board – close V-259L at 15 min mark (**end of transfer**)	[Y]	V-259L	CLOSE	
Record time (**end of transfer**)			Time:	
Record Pressures PT-007 and **A** and **B** on Rn Extraction Sheet				
Radon Board - V-245L Turn to downward position to pump trap A	[Y]	V-245L	OPEN Down	

2.7.5 Transfer from Trap B to the Lucas Cell

Remove the liquid Nitrogen from **Trap B**				
Heat Trap B until it is warm (approx. room temp).				
If pressure on gauge **B** goes above +**600**, open **V-260L** to relieve the pressure and allow the radon to flow into the Lucas cell.				
Record Pressure **B** on Extraction Sheet			PT-B:	
Start Transfer to Lucas Cell	[Y]	V-260L	OPEN	
Record Pressure **B** immediately after start of transfer on Extraction Sheet			PT-B:	
Note transfer start time (or use stop watch):			Time:	
Bake **Trap A** for ~ 5 min (start of bake)			Bake	
Close when PT-007 < 15 mTorr	[Y]	V-245L	CLOSE	
Note time: (having allowed transfer to take place for 10 minutes)			Time:	
Before removing Lucas cell, note Pressure B	[Y]	PT006	mTorr	
Remove the Lucas cell and re-attach the blue caps				
Note Pressure B again	[Y]	PT006	mTorr	
Close (end of transfer)	[Y]	V-260L	CLOSE	
==**Extraction is now complete**.==				

2.8 Bake Trap B

Use the heat gun to bake Trap B (311-RTR-02). Take care not to point the heat gun at the FTS chamber or the wiring for the pressure gauges A and B. Trap B should be heated until hot to touch (approx. 80°C)				
Radon Board	[Y]	V-262L	OPEN	
Radon Board	[Y]	V-261L	OPEN	
Radon Board	[Y]	V-260L	OPEN	
Radon Board	[Y]	V-259L	OPEN	
Heat Trap B (~ 3 min)				
Rn Board Close when PT-007 <15	[Y]	V-259L	CLOSE	
Radon Board	[Y]	V-260L	CLOSE	

Radon Board		[Y]	V-261L	CLOSE	
Radon Board		[Y]	V-262L	CLOSE	

2.9 System Shutdown at the End of All Assays
    2.9.1 Degasser Shutdown

Valve on top of degasser	[Y]	V-215L	CLOSE	
Record Time		Time		hh:mm

    2.9.2 Valve Close List

Confirm close or close	[Y]	V-550L	CLOSE	
Confirm close or close	[Y]	V-551L	CLOSE	
Confirm close or close skid inlet	[Y]	V-255L	CLOSE	
Confirm close or close skid inlet	[Y]	V-254L	CLOSE	

    2.9.3 FTS and Radon Board

FTS, inlet valve		[Y]	V-222L	CLOSE	
FTS, outlet valve		[Y]	V-224L	CLOSE	
Shut off Cooling Switch on FTS	FTS Panel, **(on/off)**			OFF	
Turn off FTS	FTS Panel, **(0/l)**				
Near Vlad Trap		[Y]	V-539L	CLOSE	
Shut off vacuum pump	Control Panel			OFF	
Vent vacuum pump, at Vlad trap				Vent	
Near Vlad Trap		[Y]	V-247L	CLOSE	
Unplug heat gun, meter for A/B and meter for MDG				Unplug	
Store liquid N2 (fill XRF detector in the junction if needed)				Store	

2.10 Checklist Completion and Filing

    2.10.1 Ultrapure Water Systems Supervisors Review and Sign-off

Signature of the Ultrapure Water System Shift Supervisor	

    2.10.2 Copy and File Checklist, Report

* Xerox checklist pages and send the copy to surface with the cell(s)
* Fill in the "Shift Report"

Notes:

2.11 MDG Extraction Experiment Record Sheet

DATE _____/_____/200____   Operators: _____   Lucas cell # _____

EXTRACTION DETAILS

Step	Time	PT-007 (mTorr)	PT-A	PT-B	MDG Temp (C)	Comment
2.5.1.2						Baseline Values
2.5.2.3						Start MDG flow to vacuum pump
2.6.3.1						Start of Assay
2.6.3.2						15 min in
						30 min in
						45 min in
						1 hour in
2.6.4.3						End MDG extraction
2.7.1.4						Trap A pressure when finished heating
2.7.2.3						Start A->B transfer
2.7.3.6						Attach LC, PT-007 high pressure
2.7.4.2						End A->B trans, LC stable pressure
2.7.5.4						Trap B when finished warming
2.7.5.6						Start B->LC trans, baking A
2.7.5.10						End B->LC trans, end baking A
2.7.5.13						PT-B at LC removal
2.8.6						End of baking B
2.9.2						System shutdown time & states

MDG EXTRACTION EXPERIMENT

Rn extraction is made from the monitor degasser. On surface the Lucas cell is put onto the appropriate PMT and counted to determine number of Rn atoms extracted.

DESCRIPTION of the EXPERIMENT:_____

COUNTING of the LUCAS CELL

    Lucas cell # _____   LC Bkg (cpd): _____   Counter/PMT #_____

    Start: _____/_____/20 ___, _____
           m   d   time

    Stop: _____/_____/20 ___, _____   File Name: _____
         m   d   time

Counts/ Live time: _____

COMMENTS:_____

_____
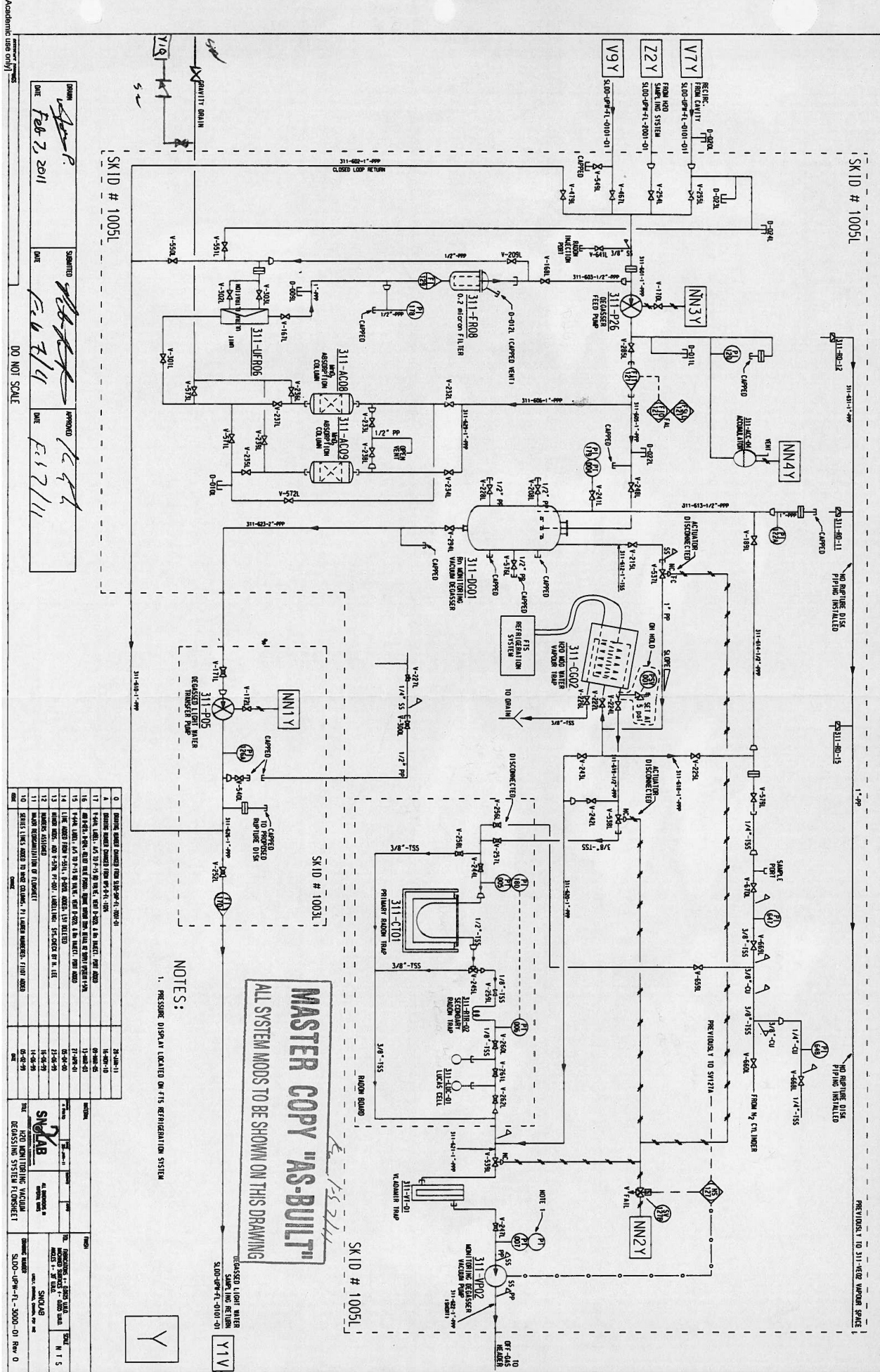
Figure B.1: Flowsheet Y depicting MDG and accompanying assay system (Skid # 1005L).

Appendix C

Mobile Assay System Procedure

In certain cases pieces placed in or near the SNO+ detector must undergo tests to determine if they will meet the SNO+ radon budget. One such test is performed with a ^{222}Rn assay system built completely on a movable cart. No well-written procedure dictated how the extraction of radon should occur from a sample emanating within a stainless steel chamber on the cart, so the following procedure has been written and used during the extraction of samples mention in Ch. 4 § 4.9. Additionally, Lucas cell preparation (for LC background runs, leak-testing, or in preparation for use with the assay systems) was also performed on this skid, by following sections 1.0, 1.1, 1.2, 3.3, 3.4, and 3.5.

Date: _____   Shift: _____   Operator: _____   Start Time: _____   Sample Extracted: _____

Note: There is an entirely unconnected system on the mobile cart which will have no impact on the assay. The components of this system include: V2, V3, VC, VD, and both flowmeters mounted to the top left side of the front panel.

1.   Preparation for Extraction

1.0   Initial State

Action	Instrument	Comment/Description	Check/Notes
Confirm Closed	V-Chamber		
Confirm Closed	V4		
Confirm Closed	V-Input		
Confirm Closed	V-N2		
Confirm Closed	VP		
Confirm Closed	V5		
Confirm Closed	V6		
Confirm Closed	VH		
Confirm Closed	V9		
Confirm Closed	V-A1		
Confirm Closed	V-A2		
Confirm Closed	V10		
Confirm Closed	V11		
Confirm Closed	V12		
Confirm Closed	V13		
Confirm Closed	V14		
Confirm Closed	Unmarked valve parallel to V4	If open, the entire system will no longer be sealed as this leads to an open port!	
Plug in	Power Bar		
Plug in	Pump Gauge		
Plug in	Trap A/B Gauge		
Plug in	Flow Meter		
Plug in	Heat Gun		
Confirm	Oil in pig tail		

1.1   Pump Down

Confirm Closed	Vp		
Confirm Closed	V-vent	Green handle on brass connection, leads to a bleeding (open) end	
Confirm Open	V-1021H	Large black valve above pump	
Confirm Open	V-1023H	Green valve to pig tail exhaust	
Start Pump			
Open Slowly	VP	Do not want to overload and stall pump. Can watch PT 'Pump' gauge drop	
Open	V5	Bypass to vacuum	
Open	V6	Near PT-A	
Open	V4	Flow meter to PT-A	
Open	V-Input	Near chamber and N2 inlet	

Open down	V-10	Trap A to vacuum	
Open	V-A2	Trap A outlet	
Open	V-A1	Trap A inlet	
Open	V9	Trap A bypass	
Open	VH	PT-A to Trap A	
Remove blue plastic caps and record LC IDs	LC1 and Lucas cell	**LC ID 1 (sample):** **LC ID 2 (control):**	
Attach Lucas cell to connect port	LC1		
Open	V14	Outlet from last LC	
Open	V13	Between LCs	
Open	V12	Inlet to first LC	
Open	V11	Trap B inlet	

1.2   Lucas Cell Flushing with N2

Close	V6	Not want to flush traps	
Close	V12	Not want to flush traps	
Close	V10	Not want to flush traps	
Close	V11	Not want to flush traps	
Connect	N2 bottle		
Ensure N2 bottle is isolated and closed	N2 bottle	Red "switch" is down; nothing connected	
Ensure regulator's outlet valve is closed	(black circular valve)		
Ensure regulator's control valve is decreased a lot (note rotation)			
Connect regulator to N2 tank		Use 1 1/8" wrench	
Ensure tubing connects regulator to port at VN2 on Rn board			
Open	N2 bottle valve/switch	Red switch on bottle	
Turn regulator's control valve to increase flow just so that the needle starts moving on outlet pressure gauge (Note: can skip this step)			
Close	V-input		
Open	Outlet valve on regulator		
Open	VN2		
"Increase" flow on N2 regulator until pressure gauge at VN2/Vinput (called PT-Chamber) intersection reads 5-10 psi		**PT-Chamber Pressure:**	
Close	Vp		
Open	V-input		
Close	V-input	When PT-Chamber value returns to recorded pressure	

Allow flush		30 sec	
SLOWLY Open	VP	Watch oil in pig tail and listen to pump for stress	
Wait until pressure reaches <100 militorr	PT 'PUMP'	**PT-'PUMP' pressure:**	
Close	VP		
Open, then close	Vinput	Close when pressure returns to	

		initial value	
Allow flush		30 sec	
Slowly open	VP		
Wait until pressure reaches <100 militorr	PT-01	**PT-'PUMP' pressure:**	
Close	VP		
Open	VInput		
Close (once pressure returns to initial value)	VN2	Allows for evacuation of tubing leading to chamber	
Allow flush		30 sec	
Slowly open	VP		
Wait until PT-Pump pressure reaches <100 miltorr	PT-01	Most important evacuation **PT-'PUMP' pressure:**	
Open	V6		
Open	V12		
Open down	V10		
Open	V11		

1.3

Bake	Trap A		
Bake	Trap B		
Continue baking until PT-01 reads ~60 mTorr		**PT-'PUMP' pressure:**	
Close	V-Input		
Close	V5		
Record pressure	PT-A	**Pressure in Trap A:**	
Close	V-A1		
Close	V-A2		
Close	V9		
Close	V10		
Record Pressure	PT-B	**Pressure in Trap B:**	
Close	V11		
Close	V12		
Close	V13		
Close	V14		

2. Assay
2.1 Capture in Trap A

Important: If the flowrate of gas through Trap A is greater than 1 lpm, its trapping efficiency will be less than unity. The last closed valve between the chamber and Trap A must be opened very slowly while monitoring the gas flow. Keeping the reading on the flow meter between 0.8 lpm is recommended. Watching the oil in the pig-tail and the reading on PT-A are secondary means of judging the flow rate.

Place dewar around Trap A and raise with support elevator			
Obtain Liquid Nitrogen and fill dewar	Fill 2 red dewars	Use 7/8" wrench, face shield, gloves	
Open down	V10	Trap A to vacuum	
Open	V-A2	Trap A outlet	
Open	V-A1	Trap A inlet	
Open	V-Chamber		
Record Pressure of Chamber	PT-Chamber	**Pressure PT-Chamber:**	

Record Pressure	PT-'PUMP'	**Pressure PT-'PUMP':**	
Record Flow Rate	FI-01	**'zero' at:**	
Record Time		**Start time of transfer to Trap A:**	
Very Slowly Open	V-Input	Extraction begins Watch flow rate stays under 1 lpm	
Run for at least an hour (including time spent opening V-Input).		Top up LN2 dewar as necessary	
Record Pressure	PT-'PUMP'	**Pressure PT-'PUMP':**	
Close	V-A1	Extraction Ends	
Record Time		**End time of transfer to Trap A:**	
Close	V-A2		
Close	V10		
Close	V-Chamber		

2.2 Transfer to Trap B

Record Pressure	PT-A	**Pressure PT-A:**	
Open	V11	Inlet to Trap B	
Open Up	V10	Trap A to Trap B	
Open	V-A2		
Record Pressure	PT-B	**Pressure PT-B:**	
Raise small dewar around Trap B			
Remove large dewar from Trap A			
Fill small dewar with LN2 from large dewar			
Heat Trap A with heat gun		Continue until all condensation is evaporated, then proceed	
Record Time		**Start time of transfer to Trap B:**	
Run for 15 minutes, heating Trap A throughout transfer **(meanwhile, proceed to 2.1.3)**			

2.3 Additional Preparation of Lucas Cell

Open	V14		
Open	V13		
Allow LC to evacuate until transfer from Trap A to B is complete			
Close	V13		
Close	V14		

2.4 End of Transfer to Trap B

Close	V11		
Record Time		**End time of transfer to Trap B:**	
Record Pressure	PT-A	**Pressure PT-A:**	
Open Down	V10		
Remove LN2 dewar from Trap B			
Heat Trap B to **room temperature**		Evaporate all condensation, but if tubing is too hot to touch, wait until it cools	
Record Pressure	PT-B	**Pressure PT-B:**	

2.5 Transfer to Lucas Cell

Open	V12		
Record Time		**Start time LC fill:**	
Transfer for 15 min. Meanwhile, open/confirm open Bake Trap A	V-A1 V9 V5 V6		
Close	V12		
Record Time		**End time LC fill:**	
Record Pressure	PT-B	**Pressure PT-B:**	
Disconnect LC from port			
Reattach blue plastic caps	LC1 and Lucas Cell		

3.   End of Assay

3.0   Bake Trap B

Open	V14		
Open	V13		
Open	V12		
Open	V11		
Bake Trap B			

3.1   Changing Samples

Close	V6		
Close	V10		
Close	VInput		
Confirm Closed	VChamber		
Open	Downstream outlet valve at regulator		
Open	VN2		
Set N2 regulator to 15-20 psi	Best to read from PT-Chamber gauge	**Pressure: PT-Chamber:**	
Open	V-Chamber	Allow gas to enter	
Close	V-Chamber		
Close	VN2		
Close	Outlet valve at regulator		
Disconnect	Emanation Chamber	Best done at the brass Swagelok connection	
Remove bolts on chamber, swap samples, replace bolts		Two 7/16" wrenches to remove bolts Wear gloves to avoid contamination of samples **Sample out:** **Sample in:**	
Re-connect	Emanation Chamber		

3.2   Flusing Emanation Chamber

Close/Ensure Closed:	V6, VH, VA1, VA2, V9, V10, V11, V12, V13, V14	Want to avoid contaminating and flushing board system	
Ensure Open:	V4, V5, VP, V-1021H, V-1023H		
Open	V-Chamber		
SLOWLY Open	V-Input	Do not want to stall pump	
Allow drain	Wait until PT-'PUMP' <100 mTorr	**Pressure PT-'PUMP':**	
Close	V-Input		
Open	VN2	First flush of chamber	

Open, then close	Regulator outlet valve	Once pressure at PT-Chamber returns to 15-20 psi	
Close	VN2	Then wait: Allow flush 30 sec.	
Slowly Open	V-Input		
Watch pressure decrease	PT-'PUMP' <100 mTorr	**Pressure PT-'PUMP':**	
Close	V-Input		
Open	VN2		
Open, then close	Regulator outlet valve		
Close	VN2	Allow flush 30 sec.	
Slowly Open	V-Input		
Allow pressure to drop	PT-'PUMP' <100 mTorr	**Pressure PT-'PUMP':**	
Close	V-Input		
Open	VN2		
Open, then close	Regulator outlet valve		
Close	VN2	Allow flush 30 sec.	
Slowly Open	V-Input		
Wait for maximal pressure drop	PT-'PUMP'	**Pressure PT-'PUMP':**	
Close	V-Chamber		
Close	V-Input		

3.3   Valve Off

Record Pressure:	PT-'PUMP'	**Pressure PT-'PUMP':**	
Confirm Closed	V-Chamber		
Confirm Closed	V-Input		
Close	V4		
Confirm Closed	V9		
Confirm Closed	V10		
Confirm Closed	VH		
Confirm Closed	V6		
Close	V5		
Close	VP		

3.4 Shutdown

Turn off Pressure Gauges and flowmeter			
Unplug Heat Gun			
Turn off Vacuum Pump			
Vent Vacuum Pump	V-Bypass	Open, then close the green valve upstream of V-1021H	

3.5 Disconnect N2 Cylinder

Close	N2 cylinder valve/switch		
Close	Regulator outlet valve		
Close/dial down	Regulator control valve: dial down to "decrease"		
Disconnect regulator	Use 1 1/8" wrench		

On Surface:

LC ID 1 (sample): _____ Filename: _____ Date/time initiated: _____
LC ID 2 (control): _____ Filename: _____ Date/time initiated: _____